UNIVERSITY OF ALBERTA

PARTICLE PACKING, COMPACTION AND SINTERING IN POWDER METALLURGY

by

Xiaolin Chen ©

A thesis submitted to the Faculty of Graduate Studies and Research in partial fulfillment of the requirements for the Degree of DOCTOR OF PHILOSOPHY

in

MATERIALS ENGINEERING

DEPARTMENT OF CHEMICAL AND MATERIALS ENGINEERING

EDMONTON, ALBERTA, CANADA

Fall, 1998

National Library
of Canada

Acquisitions and
Bibliographic Services

395 Wellington Street
Ottawa ON K1A 0N4
Canada

Bibliothèque nationale
du Canada

Acquisitions et
services bibliographiques

395, rue Wellington
Ottawa ON K1A 0N4
Canada

Your file Votre référence

Our file Notre référence

The author has granted a non-exclusive licence allowing the National Library of Canada to reproduce, loan, distribute or sell copies of this thesis in microform, paper or electronic formats.

L'auteur a accordé une licence non exclusive permettant à la Bibliothèque nationale du Canada de reproduire, prêter, distribuer ou vendre des copies de cette thèse sous la forme de microfiche/film, de reproduction sur papier ou sur format électronique.

The author retains ownership of the copyright in this thesis. Neither the thesis nor substantial extracts from it may be printed or otherwise reproduced without the author's permission.

L'auteur conserve la propriété du droit d'auteur qui protège cette thèse. Ni la thèse ni des extraits substantiels de celle-ci ne doivent être imprimés ou autrement reproduits sans son autorisation.

0-612-34746-X

Canada

UNIVERSITY OF ALBERTA

Library Release Form

NAME OF AUTHER: **XIAOLIN CHEN**
TITLE OF THESIS: **Particle Packing, Compaction And Sintering In Powder Metallurgy**
DEGREE: **Doctor of Philosophy**
YEAR THIS DEGREE GRANTED: **1998**

Permission is hereby granted to the University of Alberta Library to reproduce single copies of this thesis, and to lend or sell such copies for private, scholarly or scientific research purposes only.

The author reserves all other publication and other rights in association with the copyright in the thesis, and except as hereinbefore provided neither the thesis nor any substantial portion thereof may be printed or otherwise reproduced in any material form whatever without the author's prior written permission.

Xiaolin Chen
c/o Dr. R. L. Eadie
CME 536, University of Alberta
Edmonton, AB T6G 2G6
Canada

Date: Sept. 21, 1998

University of Alberta

Faculty of Graduate Studies and Research

The undersigned certify that they have read, and recommend to the faculty of Graduate Studies and Research for acceptance, a thesis **ENTITLED PARTICLE PACKING, COMPACTION AND SINTERING IN POWDER METALLURGY** submitted by Xiaolin Chen in partial fulfillment of the requirements for the degree of **DOCTOR OF PHILOSOPHY** in **MATERIALS ENGINEERING**.

Ray Eadie

Dr. R. L. Eadie, Supervisor

D. Ghosh

Dr. D. Ghosh, Co-supervisor

A. Bhattacharyya

Dr. A. Bhattacharyya

Dr. H. Henein

S.E. Wanke

Dr. S. E. Wanke

Dr. Z. Xu

G.C. Weatherly

Dr. G. C. Weatherly

Date: Aug. 20, 1998

ABSTRACT

This thesis focuses on the improvement of density based on the controlling of particle packing and the subsequent densification processes. First, the two-sphere model for monosized powder to determine the lattice diffusion contribution in sintering is considered. Based on Eadie's model, two new solutions are developed and presented, an upper limit solution with surface curvature at a maximum all along the neck and a more accurate solution in which the form of the surface curvature at the neck can be varied as appropriate. Producing bimodal powder distribution powder metallurgy (P/M) parts is next considered. It is shown that this technique is capable of producing parts with excellent final densities and mechanical properties. In order to explain the above experimental results, theoretical research about bimodal powder is focused on particle packing. The first theoretical tool is the coordination number of the particles and the second theoretical tool is the concept of percolation. A bridge is established between packing density, microstructure and leading eventually to macroscopic properties by using coordination number and percolation. A new model (modified saturated model) for coordination number in bimodal packing is developed and presented. It is concluded that the structures that arise in bimodal powder distributions lie somewhere between the previously proposed random structure and the saturated structure. The important role of the coarse particle network which can shield fine particles from the compaction forces is emphasised. Some comments about parameters influencing sintering and suggestions for future work are included.

ACKNOWLEDGEMENTS

First of all, I am very grateful to my supervisor Dr. R.L. Eadie and co-supervisor, Dr. D. Ghosh whose insight, guidance, encouragement are invaluable to me. I feel very lucky to have had the opportunity to be associated with them over this time. I am indebted to them for their immeasurable help and financial assistance; and for suffering through the many drafts of this thesis, and tirelessly telling me to be confident. Their efforts made this work possible.

I would also like to thank the other members of my committee: Dr. A. Bhattacharjee, Dr. H. Heinen, Dr. S.E. Wanke, Dr. G.C. Weatherly and Dr. Z. Xu for their evaluation of this thesis and helpful suggestions and comments. My colleagues at Dr. Eadie's Lab., M. Anderson, Dr. M. Jovanovic, G. Lin, S. McFarland, Dr.S. Sun and D. Yan, G. Reomer at Alberta Research Council deserve a special note of recognition. Their helpful suggestions and patience with my countless questions are greatly appreciated. The contributions of Dr. J. Luo and Dr. R.L. Plitt in helpful discussions are appreciated. The contribution of the excellent technical staff of the department is acknowledged - in particular Mrs. T. Barker and J. Gibeau.

I dedicate this thesis to my father C. Chen and my mother H. Du and my sister Qun, for their love and support, their constant pride in me, and for staying so close to me.

Special thanks to my wife Zhoulin Yan for her endless love.

TABLE OF CONTENTS

1. Introduction 1

1.1. Powder Metallurgy: Theory & Practice 1

1.2. References 6

2. Lattice Diffusion from the Grain Boundary in the Sintering of Metal Powders -- Contribution to the Theory of Sintering 8

2.1. Introduction 8

2.2. Published Models for Lattice Diffusion from the Grain Boundary in Sintering 10

2.2.1. Nomenclature and Symbols 10

2.2.2. The Models 11

2.2.3. Interaction Between Mechanisms 13

2.3. New Model for Lattice Diffusion from the Grain Boundary 13

2.4. Discussion 17

2.5. Conclusions 19

2.6. References 19

2.7. Appendices 21

2.7.1. Appendix A 21

2.7.2. Appendix B 24

2.7.3. Appendix C 27

3. Bimodal Powder Distributions in P/M -- Literature Survey 39

3.1. Improving Densities -- Practical Significance of Using Bimodal 39

Powder Distributions

3.2. Particle Packing in Bimodal Powder Distributions 40

3.3. Percolation 50

3.4. Compaction of Bimodal Powder Distributions 53

3.5. Sintering of Bimodal Powder Distributions 61

3.6. References 64

4. Improving P/M Parts by Bimodal Powder Distributions—Experimental 84

4.1. Testing Materials 86

4.1.1. Chemical Composition 86

4.1.2. Size Distribution 86

4.1.3. Particle Shape 87

4.1.4. Particle Cross-Section and Grain Structure 88

4.1.5. Flow Rate, Apparent Density and Tap Density 88

4.2. Testing Procedure 89

4.3. Compaction of Bimodal Powder Distributions 90

4.3.1. Green Compact's Characteristics 90

4.3.2. Green Density 91

4.4. Sintering of Bimodal Powder Distributions 92

4.4.1. Sintered Density for Bimodal Powder Distributions 92

4.4.2. Grain Structure of Sintered Samples 93

4.4.3. Influence of Temperature 94

4.5. Mechanical Properties 95

4.6. References 96

5. Packing Models In Random Close Packed Bimodal Powder Distributions 119

5.1. Background For Packing Models 120

5.1.1. Packing Behaviour in Bimodal Powder Distributions 120

5.1.2. Networks and Percolation 121

5.1.3. Suzuki and Oshima's Model for Coordination Number 122

5.1.4. The Experimental Packing and Calculated Coordination Numbers 123

5.1.5. Contacts, Saturated Structures and Percolation Thresholds. 124

5.2. New Models for Bimodal Particle Packing 126

5.2.1. Saturated Model 126

5.2.2. Modified Saturated Model -- The Perturbation of the Ideal Saturation Concept 130

5.3. Discussion 135

5.4. References 136

5.5. Appendix 139

6. Discussion: The Influence of Network Structure on the Compaction of Bimodal Powder Distribution 159

6.1. Discussion 159

6.2. References 170

6.3. Appendix 172

7. Summary and Conclusions 186

7.1. Experimental Results 186

7.2. Theoretical Models 187

  7.2.1. Packing Models 187

  7.2.2. Compaction Models 189

  7.2.3. Sintering Models 191

7.3. Future Work 193

7.4. References 194

LIST OF TABLES

Table 2-1 Geometric parameters used in calculations (silver spheres, 100 μm radius) [Nicolls and Mullins] 32

Table 2-2 Fractional shrinkage rates (sec^{-1}) based on various models for lattice diffusion from grain boundary (siler spheres, 100 μm radius, sintering in air) 32

Table 2-3 Fractional shrinkage rates (sec^{-1}) caused by lattice diffusion and grain boundary diffusion (silver spheres, 100 μum radius, sintering in air) 33

Table 4-1 Compositions of the 17-4 PH powders 98

Table 4-2 Flow rates of bimodal powder mixtures 99

Table 4-3 Porosities for different coarse-fine composition 100

Table 4-4 The coarse-fine composition versus UTS and hardness 101

LIST OF FIGURES

Figure 2-1	The mechanisms of sintering	34
Figure 2-2	The row of spheres used in the calculation of the shrinkage rates	35
Figure 2-3	Annular ring of grain boundary at the neck used to calculate the uniform shrinkage condition	36
Figure 2-4	$\mu(x, z)$ versus the distance z/ρ for three values of the constant F_2	37
Figure 2-5	Boundary between lattice and grain boundary diffusion regions calculated from different models	38
Figure 3-1	The relative cost and density ranges for various P/M processes. [Rutz and Hanejke, 1995]	69
Figure 3-2	Schematic illustration of the packing density variation with composition for a bimodal powder distribution. [German, 1992]	70
Figure 3-3	The specific volume versus composition for bimodal powder distributions with perfect homogeneity and infinitely particle size ratio. [German and Bulger, 1992]	71
Figure 3-4	The specific volume versus composition for bimodal powder distributions with less than ideal homogeneity and a finite particle size ratio.[German and Bulger, 1992]	72
Figure 3-5	Schematic diagram showing the disruption in powder packing around isolated coarse particles. [Zok, et al., 1991]	73
Figure 3-6	Schematic diagram showing the disruption in particle packing at a coarse-coarse particle contact point [Zok, *et al.*, 1991]	74
Figure 3-7	The randomly cut network as an example of percolation [Zallen, 1985]	75
Figure 3-8	Simplified illustrations of clusters of particles held together by bonds formed through application of uniaxial pressure on powders in a rigid die	76
Figure 3-9	Compact density versus log (pressure) of blends of the coarse and fine alumnus, X_f is the volume fraction of the fines.[Zheng, *et*	77

al.,1995]
Figure 3-10 Correlation between coordination and pressure transmission in a percolating cluster [Bouvard and Lange,1991] 78
Figure 3-11 Fraction of inclusions in a percolating cluster vs volume fraction of inclusions relative to solid volume 79
Figure 3-12 Correlation between the percolation parameter and the coordination number for inclusions touching one another. [Bouvard and Lange,1991] 80
Figure 3-13 Two-dimensional schematic of the division of the powder bed into Voronoi cells [Arzt, 1982] 81
Figure 3-14 Sketches of the densification behaviour [German, 1992a] 82
Figure 3-15 The change in specific volume during sintering as a function of the bimodal powder composition. [German, 1992a] 83
Figure 4-1 Size distribution of 100% coarse powder 102
Figure 4-2 Size distribution of 100% fine powder 103
Figure 4-3 . Size distribution of 90% coarse powder + 10% fine powder 104
Figure 4-4 Size distribution of 75% coarse powder + 25% fine powder 105
Figure 4-5 Size distribution of 60% coarse powder + 40% fine powder 106
Figure 4-6 . Size distribution of 45% coarse powder + 55% fine powder 107
Figure 4-7 SEM micrograph of coarse 4-7 (a) and fine 4-7 (b) powders 108
Figure 4-8 Optical micrograph of cross-section of the powders 109
Figure 4-9 Optical micrograph of etched cross-section of the powders 110
Figure 4-10 Densities versus mass fraction for bimodal powder distributions 111
Figure 4-11 Fracture surface of green compacts for different coarse-fine mass fractions. 112
Figure 4-12 Green densities versus mass % of fine powder 113
Figure 4-13 Final densities versus mass % of fine powder 114
Figure 4-14 Specific volume change versus mass % of fine powder during sintering 115
Figure 4-15 Grain structures for sintered samples (1300 °C 2 hrs) 720X 116

Figure 4-16 Pore structures of sintered samples for different coarse-fine mass fractions. 117
Figure 4-17 Final densities versus mass % of fine powder (Sintered at 1250°C for 2 hours) 118
Figure 5-1 Fractional density versus particle size ratio in bimodal powder distributions (the experimental results of McGeary) [McGeary, 1961] 140
Figure 5-2 Tap densities of different compositions of blends of bimodal powders [Holman, 1991] 140
Figure 5-3 Tap densities versus mass % of fine powder 141
Figure 5-4 Coordination numbers in coarse powder of figure 4-1 142
Figure 5-5 Coordination numbers in fine powder of figure 4-2 143
Figure 5-6 N_{ff} versus mass % of fine powder (Based on Suzuki and Oshima's model) 144
Figure 5-7 N_{cc} versus mass % of fine powder 145
Figure 5-8 N_{cf} versus mass % of fine powder (Based on Suzuki and Oshima's model) 149
Figure 5-9 N_{fc} versus mass % of fine powder (Based on Suzuki and Oshima's model) 150
Figure 5-10 N versus mass % of fine powder 151
Figure 5-11 The scheme of pure coarse particle packing 154
Figure 5-12 Volume versus mass % of fine powder (total mass of powders is 1 gram) 157
Figure 5-13 M_f , M_{f-1} , M_{f-2} versus mass % of fine powder (total mass of powders is 1 gram) 158
Figure 6-1 Compactibility versus mass % of Fine Powder 176
Figure 6-2 Apparent, Tap and Green Densities versus mass % of fine Powder 177
Figure 6-3 Density Change by Rearrangement versus mass % of Fine Powder 178
Figure 6-4 Compactibility versus mass % of Fine Powder (Calculation Without Structure Factor) 179

Figure 6-5 Network Structure Factor (Structure Influence in Compaction) 180

Figure 6-6 N_{cc} versus mass % of Fine Powder (Before and After Compaction) 181

Figure 6-7 N_{ff} versus mass % of Fine Powder (After Compaction) 182

Figure 6-8 N_{cf} versus mass % of Fine Powder (After Compaction) 183

Figure 6-9 N_{fc} versus mass % of Fine Powder (After Compaction) 184

Figure 6-10 Coordination Number N versus mass % of Fine Powder (After Compaction) 185

CHAPTER 1.

Introduction

1.1. Powder Metallurgy: Theory & Practice

Powder metallurgy is the science and the technique of producing articles from metallic powders. Sometimes non-metals, metallic compounds or chemical additions in various proportions are added into the metallic powders to get desired properties. Usually the process consists of pressing the powder within dies followed by heating or sintering of the powder compact, usually under controlled atmosphere, at a temperature below the melting point of the metal or alloy. By this means a porous to dense product is obtained which has the required shape and size and the mechanical properties necessary to fulfil the article's function. Where such a basic process does not produce the required characteristics, various special processes or modifications may be introduced [Yarnton and Argyle, 1962].

Powder processing of metals is widely used for the manufacture of automotive components, electronic packaging and in aerospace technology. From 1991 to 1995 the North American powder metallurgy market grew at a average annual rate of 14.5% [White, 1996]. This method has become increasingly popular not only because of its ability to impart a unique combination of properties and microstructures, but also because of a significant reduction in costs associated with the conversion of raw materials to finished products. Furthermore, the key processing steps can be modified with relative ease to obtain properties that are tailored to specific applications.

For powder metallurgy to realize its full potential and compete with wrought products, it has to face the challenge of meeting more stringent quality demands, such as higher density, better dimensional control, better and more uniform mechanical properties and lower cost. Density is a predominant factor in the performance of powder metallurgy components. Residual porosity is a common feature of the microstructures of sintered materials. Thus the control of the final properties of sintered materials requires the control of final density. Generally, as density is increased, almost all properties, including hardness, strength, fatigue life, toughness, ductility, electrical conductivity, magnetic saturation, and corrosion resistance, are improved [German, 1984; Hirschhorn, 1969]. This thesis will focus on controlling the density of powder metallurgy products.

A generation of scientists has attempted to derive a unified and generalized picture of powder metallurgy including densification on the basis of theoretical and experimental investigation. Nevertheless, the understanding of the fundamental mechanisms is still a matter of controversy [Exner, 1990]. Basically, there still are two separate directions (theory and practice) in powder metallurgy studies. Each of them has its merits and its limitations. The experimental studies often give empirical equations and can be applied directly in practice. These empirical relations often do not contribute to the understanding of processes. The parameters in the equations sometimes lack reasonable physical meanings. On the other hand, there is no doubt that many of the theoretical models opened the way for a quantitative description of powder metallurgy processes and has led to a good insight into the fundamental mechanisms and the effect of various parameters of influence (*e.g.* particle size, temperature, *etc.*). However, the extrapolation of these results, especially the application of equations derived for idealized models to actual powder compacts, has not provided a significant insight into actual practical processes [Exner, 1990]. But both theory and practice are of significance and necessary. Even though the bridge between theory and practice studies in powder metallurgy is still under construction, further studies in both areas would contribute to better understanding of powder metallurgy processes. This is the reason that this thesis discusses both theory and practice.

The first part of this thesis (Chapter Two) is a theoretical contribution. It considers a two-sphere model for monosized powder to determine the lattice diffusion contribution in sintering. This analysis differs from previous ones in that the surface curvature is treated in a more quantitative way. Thus a detailed understanding of the sintering process and the associated shrinkage can be derived. The model also establishes with more rigour the approximations used previously for the construction of sintering diagrams.

The second part of this thesis (Chapter Three to Six) addresses the effects of bimodal powder distributions on powder packing, compaction and sintering. It includes both experimental and theoretical studies. Bimodal powder distributions are distributions of coarse and fine powders. The powder in the bimodal powder distributions are randomly packed rather than orderly packed. The random packing is the real situation in powder metallurgy processing. Analysis of the current state of model investigations in powder metallurgy reveals that there is a distinct tendency for the properties of materials to be described on the basis of models of random particle packings [Nikolenko and Koval'chenko, 1984].

This research starts from a very simple idea: maximizing space-filled by varying sphere sizes. If coarse or large powders randomly pack, there are lots of voids or empty space among them. If the fine or small powders are added into coarse powders, the fine powder will fill in the voids among the coarse powders, therefore increasing the packing density [Furnas, 1931]. In powder metallurgy, the green density and final density of the products are very important. It is well known that bimodal powder distributions improve the packing density. Mixtures of coarse and fine powders are commonly used for processing ceramics and powder injection molding [German, 1992a]. However, they are not often used in traditional metal powder compaction and sintering since it is commonly considered that a high compaction force could be applied to the powder to overcome poor packing, and that only in cases of relatively low sintering temperatures or short sintering times is the sintered density highest in bimodal powder distributions.

Using bimodal powder distributions, could the green density after compaction and the final density after sintering be improved? If it does improve, how much does it improve? How many percent of fine powders should be added to coarse powders to get the optimal green density and final density? This experimental test program tries to answer these questions. Very high sintered densities (97.7% relative density) and mechanical properties (comparable to wrought products) were achieved using the conventional P/M processes of single compaction and single sintering for bimodal powder distributions of precipitation hardening stainless steel powders. The medians of the two sizes were in the size ratio of about 5:1. A 2% increase of final density is achieved by adding only 25% fine powders and the final density of the bimodal powders reached the same value as 100% fine powders. Using bimodal powders has practical significance in reducing cost and achieving better dimensional control (lower shrinkage) with a high final density.

The theoretical research about bimodal powder was focused on particle packing (or tap density) because all the consolidation process, such as, compaction and sintering, start from the particle packing. That greater effort should be expended on research in studies for clarifying and quantifying the influence of contact geometry was singled out by Exner [Exner, 1990]. In order to understand and model the packing in a random packing there must be a means of characterising the packing and of evaluating hypotheses about the packing. The first tool that will be used is the coordination number of the particles. Coordination number increases with the fractional density and fairly detailed models have been developed by a number of researchers. The second tool that will be used is the concept of percolation or the interconnection of the different particle types as their density and number are varied. The concept of percolation has been used by researchers like Holman to successfully explain macroscopic behaviour changes in particle compaction [Holman, 1990,1991]. Using coordination number and percolation it will be shown that a bridge can be established between packing density, microstructure and leading eventually to macroscopic properties. The models for coordination number in bimodal packings will be utilised to show that there is a significant discrepancy between the random space filling models used in computer generated packings and the saturated model of German [German, 1992b]. Neither model satisfactorily agrees with experimental observations. Some attempt will be made to resolve these discrepancies by modifying the saturated model so that the experimental observations are explained.

1.2. References

Exner, H.E., "Solid-State Sintering: Critical Assessment of Theoretical Concepts and Experimental Methods," Sintering Key Papers, Editors: Somiya, S. And Moriyoshi, Y., Elsevier Applied Science, London and New York, pp. 87 - 100, 1990.

Furnas, C.C., "Grading Aggregates I - Mathematical Relations for Beds of Broken Solids", Ind. Eng. Chem., Vol. 23, 1931, pp. 1052-1058.

German, R.M., "Powder Metallurgy Science," Metal Powder Industries Federation, Princeton, NJ, 1984, p.175.

German ,R.M., "The Role of Particle Parking Density in Powder Injection Molding", Reviews on Powder Metallurgy and Physical Ceramics, Vol. 5, No. 2, 1992a, pp. 81-110.

German, R.M., "The Prediction of Packing and Sintering Density for Bimodal Powder Mixtures", Advances in Powder Metallurgy & Particulate Materials - 1992, Compiled by J.M. Capus and R.M. German, Metal Powder Industries Federation, New Jersey, Vol. 3, pp. 1-15, 1992b.

Hirschhorn, J.S., "Introduction to Powder Metallurgy," American Powder Metallurgy Institute, New York, 1969.

Holman, L.E. and **Leuenberger**, H., "The Effect of Varying the Composition of Binary Powder Mixtures and Compacts on Their Properties: A Percolation Phenomenon", Powder Technology, Vol. 60,1990, pp. 249-258.

Holman, L.E., "The Compaction Behaviour of Particulate Materials. An Elucidation Based on Percolation Theory", Powder Technology, Vol. 66, 1991, pp. 265-280.

Nikolenko, A.N. and **Koval'chenko**, M.S., "Analysis of the Random Packing of Identical Particles. I. General Theory," Poroshkovaya Metallurgiya, Vol.275, No.11, pp. 38-41, 1984.

Yarnton, D. and **Argyle,** M., "Practical Course in Powder Metallurgy," Cassell, London, p.4, 1962.

White, D.G., "P/M in North America", International Journal of Powder Metallurgy, Vol. 32, No. 3, 1996, pp. 221-228.

CHAPTER 2.

Lattice Diffusion From The Grain Boundary In The Sintering Of Metal Powders – Contribution To The Theory Of Sintering*

2.1. Introduction

The ability to achieve dimensional tolerances in powder metallurgy parts arises directly from the control of the sintering process and in particular shrinkage. Thus a detailed understanding of the sintering process and the associated shrinkage is of considerable importance. Sintering behaviour has been very capably summarised in the review papers of Ashby [Ashby, 1974] and Swinkels and Ashby [Swinkels and Ashby, 1981]. The morphological development is defined in three stages in the following way. The first stage begins with the particles adhering to one another and there is growth in the size of the neck. It ends when the pores have become more or less cylindrical. The second stage consists of shrinkage of the cylindrical pores and ends when these pores pinch off. The third stage consists of the rounding and shrinkage of these isolated pores. Based on this topological description, the driving force for sintering can be quantified by the relationship between the surface curvature and μ, the chemical potential (free energy) of the atoms. This solution was first presented by C. Herring [Herring, 1951]. The relationship, assuming isotropy of the specific surface free energy, γ, is given as:

---

* A version of this chapter has been published as "Lattice Diffusion from the Grain Boundary in the Sintering of Metal Powders," R.L. Eadie and X.L. Chen, in International Journal of Powder Metallurgy, Vol.32, No.3, pp.265-275, 1996.

$$\mu = \mu_0 + \gamma\left(\frac{1}{R_1} + \frac{1}{R_2}\right)\Omega \qquad (2\text{-}1)$$

where μ_o is the chemical potential under a flat surface, R_1 and R_2 are the principal radii of curvature of the surface and Ω is the atomic volume. It is the surface curvature that provides the driving force for sintering. Six atomic transport mechanisms responding to this driving force can contribute to neck growth. These, as shown in Figure 2-1, are: 1. lattice and 2. surface diffusion from the surface of the particles to the neck surface; 3. grain boundary and 4. lattice diffusion from the grain boundary between the two particles to the neck, 5. evaporation and condensation at the surface (where the vapour pressure of the solid is appreciable); and 6. dislocation climb. Mechanisms 4 and 5 will contribute to both neck growth and compact densification in all three stages and will be present as long as the grain boundary remains attached to the pore. The six different atomistic transport phenomena can occur simultaneously. But when the contribution of each mechanism is compared it is found that it is often possible to describe the process quite accurately with one equation or perhaps with two. Ashby showed the regions of applicability for the mechanisms using sintering diagrams. These diagrams have homologous temperature ($T(K)/T_{mp}$) along the vertical axis and a morphological parameter like the neck radius along the horizontal axis [Ashby, 1974]. The sintering diagram shows regions where a mechanism is dominant in neck growth, with equal contributions along the boundaries of each region. Grain boundary diffusion, surface diffusion or lattice diffusion from the grain boundary are the mechanisms that usually dominate sintering - with the lattice diffusion dominating at the highest temperatures and largest neck sizes. Of course the diagrams depend for their accuracy and usefulness on the accuracy of the models used for each of the processes. These concepts and diagrams have been used since 1974, but there has been up to the present day no definitive analysis to describe lattice diffusion from the grain boundary to the neck surface. This issue will be addressed here.

2.2. Published Models for Lattice Diffusion from the Grain Boundary in Sintering

2.2.1. Nomenclature and Symbols

To describe these equations, it is necessary to define the geometry and transport constants symbols (see Figure 2). The symbols used in this chapter are nearly the same as those used by Ashby and co-workers [Ashby, 1974; Swinkels and Ashby, 1981]

a -- particle radius

C -- a constant equal to $\pi\gamma_s / kT$

D_B -- grain boundary diffusion coefficient

D_L -- lattice diffusion coefficient

D_S -- surface diffusion coefficient

J_t -- the flux of atoms to the neck per unit area per unit time

k -- Boltzmann's constant

r -- the radial direction for a cylindrical co-ordinate system perpendicular to the plane of the grain boundary

$\dot{V}$ -- volume of atoms flowing per unit time into the neck region

x -- radius of the circle of contact of the particles

$\dot{x}$ -- the neck growth-rate

z -- the direction perpendicular to the grain boundary

δ_B -- grain boundary thickness

γ_s -- surface free energy

θ -- the contained angle in radians at a point in the plane of the grain boundary and $x + \rho$ from the center of the grain boundary between lines drawn to the center of the grain boundary and the center of the particle. The value gradually decreases from about 1.5 as sintering proceeds, the minimum value depends on packing, but is usually more than 0.5.

μ_i -- chemical potential of the i^th^ species

ρ -- radius of curvature perpendicular to the grain boundary

Ω -- the atomic volume

2.2.2. The Models

Several models for mechanism 5 (lattice diffusion from the grain boundary) are in the literature and must be discussed:

2.2.2.1. The model used in Ashby's first paper on sintering maps [Ashby, 1974] was:

$$J_t = 8CD_L\left(1+\frac{x}{\rho}\right) \qquad (2\text{-}2)$$

This is based on the equation of D. Johnson [Johnson, 1969], but modified in the manner of Wilson and Shewmon [Wilson and Shewmon, 1966] to reflect the larger area over which the lattice diffusion flows (πx^2 versus $\pi x \delta_B$).

2.2.2.2. A model developed by D. Johnson [Johnson, 1969] based on his grain boundary diffusion model:

$$J_t = 16\, C D_L \frac{x+\rho}{x} \tag{2-3}$$

This model is flawed by the assumption made in its development that the shrinkage rate (divergence of the flux) throughout the volume under consideration is a constant . This means that the lattice is shrinking and acting as the source of matter arriving at the neck surface. It has been shown experimentally that the atoms for the neck come from the grain boundary since shrinkage stops when the grain boundary migrates from the neck [Alexander and Balluffi, 1957]. The divergence of the flux is zero in the lattice, this being the underlying assumption for the application of Laplace's equation, which is normally associated with steady state diffusion.

2.2.2.3. An upper limit model developed by R. Eadie for the case [Eadie 1976] where μ is constant at its maximum value all along the surface (solution is detailed in Appendix A):

$$J_t = 6\, C D_L \left(1 + \frac{x}{\rho}\right) \tag{2-4}$$

Observe that the first model of Ashby is exactly one third larger than this. Hence it can be concluded that Ashby's Equation (2-2) [Ashby, 1974] overestimates the sintering rate.

2.2.2.4. The model used in the second paper on sintering maps [Swinkels and Ashby, 1981]:

$$J_t = 16\,CD_L\frac{x+\rho}{x}\theta \tag{2-5}$$

This model was based on grain boundary diffusion model, but with the source term modified by the ratio $2\theta\rho/\delta_B$ rather than $\pi x^2/\pi x\delta_B$. Its form is the same as (2-3) with the additional term θ which is not very different from unity. One should therefore consider the comments that were applied to (2-3) *i.e.* that it is based on a non-zero divergence throughout the volume.

2.2.3. Interaction Between Mechanisms

The different phenomena may also interact with each other. In particular Eadie *et al.* have treated the uniform shrinkage condition at the grain boundary by coupled boundary and lattice fluxes [Eadie, 1976; Eadie, *et al.*, 1974; Eadie and Weatherly, 1975; Eadie, *et al.*, 1978] since the shrinkage at the grain boundary must be uniform to maintain continuity. This coupling becomes less important if one of the mechanisms is significantly smaller than the other. The coupled and uncoupled solutions will be compared in this chapter.

2.3. New Model For Lattice Diffusion From The Grain Boundary

The sintering of pure metals in the absence of applied stress is considered in this model. The initial stage of sintering for a row of spheres is considered for geometric preciseness. This analysis differs from previous ones in that the surface curvature and its variation are treated in a more quantitative way. This is significant since this curvature is the driving force for the process. Thus the model can have considerable generality since the description of the driving force on the surface can be modified as appropriate. The predictions of this new model will be compared with those of equations (2-3 to 2-5). The new equation will also be examined to determine its effect on sintering diagrams. Although spheres in a row are being considered, this geometry can often represent the more general situation of powders in a compact because the gradients in chemical potential are concentrated near the neck region. The row geometry can be approximated by a cylinder as shown in Figure 2-2. The annular ring of grain boundary at the neck used to calculate the uniform shrinkage condition is shown in Figure 2-3. The equation for lattice diffusion is :

$$J = \frac{-D_L}{\Omega kT} \nabla(\mu) \tag{2-6}$$

Surface curvature is inserted in functional form, (*i.e.* the surface curvature was allowed to vary along the surface of the neck). In principle the shrinkage solution can thus be made as accurate as curvature profile can be measured. This also permits the form of the surface curvature to be varied in a way that is appropriate for the different stages of sintering.

At steady state, div J = 0, as required by the conservation of matter and Laplace's equation results:

$$\nabla^2 \mu(r,z) = 0 \tag{2-7}$$

From symmetry the lower and the upper half of the cylinder are the same, only the upper half is treated. From cylindrical symmetry there is no angular variation around the cylinder. In order to employ this equation it is necessary to assume a quasi steady-state ; *i.e.* that the geometry is changing only slowly compared to the rate of atom migration to the neck. This is a good approximation for diffusion rates encountered in sintering. For the sake of convenience $\mu - \mu_V$ as used by Herring has been replaced by μ, and it is assumed that the concentration of vacancies is at equilibrium. It should be remembered that this is a necessary condition and that if it does not apply the concentration and chemical potential of vacancies must be considered explicitly. Solutions to (2-7) in cylindrical co-ordinates are the products of hyperbolic functions and Bessel functions. The coefficients are determined by the boundary conditions which apply. This solution is then used in conjunction with the diffusion equation (2-6) to calculate the flux to the neck and hence the shrinkage rate. The boundary conditions may be summarised as follows. Since the flux from the grain boundary must be uniform (to maintain continuity), the following equation must hold :

$$D_L(\partial\mu/\partial z) = K\,, \quad z = 0 \tag{2-8}$$

A further condition is required to evaluate K. This is the condition for mechanical equilibrium at the grain boundary:

$$\int \mu\,(r,0)ds \quad = \; 2\pi x\,\gamma_s\,\Omega \tag{2-9}$$

At the mid-point of spheres, from symmetry:

$$\partial\mu/\partial z = 0\,, \quad r = a \tag{2-10}$$

The chemical potential along the surface (r=x) can be appropriately expressed as:

$$\mu\,(x,\,z) = F_1 \exp\,(-\,F_2\,z) + \frac{2\gamma\Omega}{a} \tag{2-11}$$

where $F_1 = -\,\gamma\Omega/\rho$ and F_2 is of order $1/\rho$. F_2 will be allowed to vary around this value. Figure 4 shows $\mu(x,\,z)$ versus the dimensionless distance z/ρ measured from the grain boundary for three values of the constant F_2. This constant determines how rapidly μ decays as z increases.

Because the sum of two harmonic functions is also harmonic, a two-fold boundary value problem such as this can be reduced to two separate and simpler boundary value problems. This is the basis for the solution to this problem as outlined in Appendices B and C. In Appendix B, the boundary condition (2-11) is replaced by $\mu(x, z) = 0$ and as a result (2-9) becomes:

$$\int \mu_A(r,0)ds = 2\pi\gamma\Omega - \int \mu_B\, ds \tag{2-12}$$

(where the A and B subscripts refer to the two simpler boundary value solutions covered in Appendices B and C respectively). In Appendix B the other boundary conditions are unchanged. In Appendix C the simplest homogeneous boundary condition compatible with the problem is applied along the grain boundary:

$$2\, D_L \frac{\partial \mu}{\partial z} = 0 \tag{2-13}$$

This implies no net flux from the grain boundary and hence no shrinkage. From the solution $\mu_B(r, z)$ the value of $\int\mu_B\,(r,0)ds$ can be found and consequently (2-12) can be solved for K. Since no shrinkage occurs from μ_B, its only effect is to redistribute the flux paths according to the actual surface curvature values $\mu(x, z)$.

The solution to these separate boundary value problems as given in the appendices are:

$$\mu_A(r,z) = \frac{2Kx}{D_L}\Sigma\left\{[\sinh(\frac{X_n z}{x}) - \coth(\frac{X_n a}{x})\cosh(\frac{X_n z}{x})]\times\frac{J_0(\frac{x_n r}{x})}{X_n^2 J_1(X_n)}\right\} \qquad (2\text{-}14)$$

$$\int\mu_B(r,0)ds = 2\pi\,\Sigma\frac{\alpha_n x^2}{X_n}J_1(X_n) + 4\pi\,F_2^2 F_1 x^2\,\Sigma\frac{1}{X_n^2(\frac{X_n^2}{x^2} - F_2^2)} + \pi\,F_1 x^2 + \frac{2\pi\gamma\Omega\,x^2}{a}$$

(2-15)

where J_0 and J_1 denote Bessel functions of order zero and one respectively, x_n is the nth lowest zero of J_0, and α_n and β_n are defined via variation of parameters in Appendix C. K can be evaluated from (1-12) as :

$$K = \frac{D_L(2\pi x\gamma\Omega - \int\mu_B\,ds)}{4\pi\,x^3}\left\{\Sigma\frac{\frac{\coth(X_n a)}{x}}{x_n^3}\right\} \qquad (2\text{-}16)$$

The shrinkage rate is :

$$dL/dt = 2K/kT \qquad (2\text{-}17)$$

The flux of atoms is :

$$J_t = -\frac{2\pi\,x^2 K}{\Omega\,kT} \qquad (2\text{-}18)$$

2.4. Discussion

The present model differs from the upper limit of lattice diffusion in that this model treats the surface curvature in a more quantitative way. In order to evaluate this model, numerical comparison was made for the second stage of sintering of silver spheres in air to the upper limit model, Johnson's Model and the model currently used in sintering maps by Swinkels and Ashby. The geometrical parameters [Berrin and Johnson, 1967; Nicholls and Mullins, 1963] used in the calculations are given in Table 2-1 and the other parameters used are: $D_L = 4.4*10^{-5}\exp(-1.854*10^{5}/RT)$ (m^2/sec), $D_B = 1.2*10^{-5}\exp(-9.0*10^{4}/RT)$ (m^2/sec), $\Omega = 1.71*10^{-29}$ m^3, $\gamma_s = 0.4$ J/m^2 and $\delta_B = 5.0*10^{-10}$m. In Table 2-1, the values for x/a and ρ/a were calculated on the basis that only shrinkage mechanisms contribute to neck growth [Eadie, Wilkinson and Weatherly, 1974] and the experimental values were those measured by Eadie for silver [Eadie, 1976] after about 3% linear shrinkage of a random close packed compact . Using equations (2-3) to (2-5) and equation (2-18), the results are obtained and shown in Table 2-2. As predicted the upper limit is just that, an upper limit for all the solutions. It is approached by the more detailed solution as the values of x and ρ increase as would be expected. The maximum difference between the proposed model and that used by Swinkels and Ashby is about 40% for the numerical data examined.

A comparison of the fractional shrinkage rates calculated using the coupled solution [Eadie, *et al.*, 1974; Eadie, 1974] and that calculated as the sum of the uncoupled grain boundary [Johnson, 1969] and the present lattice diffusion models is given in Table 2-3 for 900 °C and 950°C. It is clear that in the region where lattice diffusion is most significant i.e. x/a > 0.3 and homologous T > 0.8 the uncoupled solution is quite close to the coupled solution (within 10%). This suggests that the new equations can be confidently used in the construction of sintering maps. What remains to be done however is an experimental evaluation of the surface curvature variation along the surface during the sintering process to determine which value of F_2 is appropriate at each stage of sintering. Such an evaluation would permit a more accurate application of the new solution to real sintering problems.

This F_2 factor affects the shrinkage rate by about 50% as F_2 varies by a factor of 4.

Figure 2-5 shows the boundary between lattice and grain boundary regimes for the Swinkels and Ashby model and the proposed model with $F_2 = 1/\rho$ and $F_2 = 2/\rho$. Above the field boundaries the volume diffusion is the dominant mechanism. At the field boundaries $J_L = J_g$. Although the changes are not large the lattice diffusion is somewhat restored by the more precise model with F_2 equal to $1/\rho$.

2.5. Conclusions

A new method has been presented to determine the lattice diffusion contribution in sintering. This analysis differs from previous ones in that the surface curvature was treated in a more quantitative way. The present model modifies somewhat the approximation used previously. The model also establishes with more rigour the approximations used previously for the construction of sintering diagrams.

2.6. References

Alexander, B.H. and **Balluffi**, R.W., "The Mechanism of Sintering of Copper," Acta metallurgica, 1957, Vol.5, p666.

Ashby, M.F., "A First Report on Sintering Diagrams," Acta Metallurgica, 1974, Vol.22, p.275.

Berrin, L. and **Johnson**, D.L., "Precise Diffusion Sintering Models for Initial Shrinkage and Neck Growth," Sintering and Related Phenomena, Gordon and Breach, 1967, p369.

Eadie, R.L., "Densification during the First Two Stages of Sintering of Spherical Metal

Powders," Ph. D. Thesis, University of Toronto, 1976, p44.

Eadie, R.L., **Wilkinson**, D.S. and **Weatherly**, G.C., "The Rate of Shrinkage during the Initial Stage of Sintering," Acta Metallurgica, 1974, Vol.22, p1185.

Eadie, R.L. and **Weatherly**, G.C., "Solutions for the Shrinkage Rate in the Intermediate Stage of Sintering," Scripta Metallurgica et Materialia, 1975, Vol.9, p 285.

Eadie, R.L., **Weatherly**, G.C. and **Aust**, K.T., "A Study of Sintering of Spherical Silver Powder - I. The Intermediate Stage," Acta Metallurgica, 1978, Vol.26, p759.

Herring, C., *The Physics of Powder Metallurgy*, Chap.8, McGraw-Hill, 1951.

Johnson, D.L., "New Method of Obtaining Volume, Grain-boundary, and Surface Diffusion Coefficients from Sintering Data," Journal of Applied Physics, 1969, Vol.40, No.1, p192.

Nicholls, F.A. and **Mullins**, W.W., "Morphological Changes of a Surface of Revolution Due to Capillarity Induced Surface Diffusion," Journal of Applied Physics, Vol. 16, No. 1, 1963, p. 1826.

Swinkels, F.B. and **Ashby**, M.F., "A Second Report on Sintering Diagrams," Acta Metallurgica, 1981, Vol.29, p259.

Wilson, T.L. and **Shewmon**, P.G., "The Role of Interfacial Diffusion in the Sintering of Copper," Transactions of the Metallurgical Society of AIME, 1966, Vol.236, p48.

2.7. Appendices

2.7.1. Appendix A – Upper Limit For Volume Diffusion

Problem:

$$D_L \frac{\partial \mu}{\partial z} = k \qquad at \quad z = 0 \qquad [A\text{-}1]$$

$$\mu(x, z) = \gamma\Omega\left(\frac{1}{x} - \frac{1}{\rho}\right) \qquad [A\text{-}2]$$

$$\int \mu(r, 0)\, ds = 2\pi x \gamma\Omega \qquad [A\text{-}3]$$

$$\frac{\partial \mu(r, a)}{\partial z} = 0 \qquad [A\text{-}4]$$

$$\nabla^2 \mu(r, z) = 0 \qquad [A\text{-}5]$$

In order to employ the known zeros of Bessel functions the solution will be obtained with:

$$\mu(x, z) = 0 \qquad [A\text{-}6]$$

The constant $\gamma\Omega\left(\frac{1}{x} - \frac{1}{\rho}\right)$ is then added to this solution. The equation [A-3] must be altered to:

$$\int \mu_A\, ds + \int \gamma\Omega\left(\frac{1}{x} - \frac{1}{\rho}\right) ds = 2\pi x \gamma\Omega \qquad [A\text{-}7]$$

The solution must be of the form:

$$\mu(r, z) = \sum_n \{C_n \cosh(k_n z) + D_n \sinh(k_n z)\} J_0(k_n r)$$

from [A-6]

$$k_n = X_n / x$$

and from [A-4]

$$C_n = -D_n \coth(\frac{X_n a}{x})$$

from [A-2]

$$D_L \sum_n \frac{X_n}{x} D_n J_0(\frac{X_n r}{x}) = K$$

Applying Fourier-Bessel analysis:

$$\int_0^x K r J_0(\frac{X_n r}{x}) dr = \sum_n t_n \int_0^x r J_0(\frac{X_n r}{x}) J_0(\frac{X_m r}{x}) dr$$

where $t_n = \frac{2\pi D_n X_n}{x}$. Solving we get:

$$D_n = \frac{2Kx}{D_L X_n^2 J_1(X_n)}$$

Hence

$$\mu(r,z) = \sum_n \frac{2Kx}{D_L X_n^2 J_1(X_n)} \left\{ \sinh\left(\frac{X_n z}{x}\right) - \coth\left(\frac{X_n a}{x}\right) \cosh\left(\frac{X_n z}{x}\right) \right\} J_0\left(\frac{X_n r}{x}\right)$$

Employing [A-7] and with $\coth\left(\frac{X_n a}{x}\right) = 1$ and $\left\{\sum_n \frac{1}{X_n^3}\right\}^{-1} = 12$

$$K = \frac{3D_L \gamma\Omega}{x}\left(-\frac{1}{x} - \frac{1}{\rho}\right) \qquad \text{[A-8]}$$

Now $\frac{dL}{dt} = \frac{-J_t \Omega}{\pi x^2}$, $J_t = j2\pi x^2$, $j = \frac{-D_L}{\Omega kT}\frac{\partial\mu}{\partial z}$ *and* $K = \frac{\partial\mu}{\partial z}$, so

$$J_t = \frac{K 2\pi x^2}{\Omega kT}$$

Hence $dL/dt = 2K/kT$. From [A-8]

$$\frac{dL}{dt} = -\frac{6D_L\gamma\Omega}{kTx}\left(\frac{1}{x}+\frac{1}{\rho}\right) \quad \text{[A-9]}$$

and

$$J_t = \frac{6\pi D_L\gamma}{kT}\left(1+\frac{x}{\rho}\right) \quad \text{[A-10]}$$

2.7.2. Appendix B –

Solution To Laplace's Equation For Boundary Value – Problem B

Problem:

$$\nabla^2\mu_A = 0 \qquad \text{[B-1]}$$

$$\mu_A(x,z) = 0 \qquad \text{[B-2]}$$

$$\frac{\partial \mu_A(r,a)}{\partial z} = 0 \qquad \text{[B-3]}$$

$$D_L \frac{\partial \mu_A}{\partial z} = k \quad \text{at } z=0 \qquad \text{[B-4]}$$

$$\int \mu_A \, ds = 2\pi x \gamma \Omega - \int \mu_B \, ds \qquad \text{[B-5]}$$

Solution:

From separation of variables the solution is of the form:

$$\mu_A(r,z) = \sum_n \{C_n \cosh(k_n z) + D_n \sinh(k_n z)\} J_0(k_n r) \qquad \text{[B-6]}$$

where C_n and D_n are coefficients to be determined from the boundary conditions and k_n are the separations constants.

From [B-2], $\mu_A(r,z) = 0 = \sum_n \{C_n \cosh(k_n z) + D_n \sinh(k_n z)\} J_0(k_n r)$ for all z.

Hence $J_0(k_n x) = 0$, so

$$k_n = X_n / x \qquad \text{[B-7]}$$

From [B-3], at any value of

$$r\frac{\partial \mu_A(r,a)}{\partial z} = 0 = \sum_n \frac{X_n}{x}\left\{C_n \sinh\left(\frac{X_n a}{x}\right) + D_n \cosh\left(\frac{X_n a}{x}\right)\right\} J_0\left(\frac{X_n r}{x}\right)$$

$$C_n = -D_n \coth\left(\frac{X_n a}{x}\right) \qquad \text{[B-8]}$$

Hence

$$\frac{\partial \mu_A}{\partial z} = \sum_n \frac{X_n}{x} D_n \left\{ -\coth\left(\frac{-X_n a}{x}\right)\sinh\left(\frac{X_n z}{x}\right) + \cosh\left(\frac{X_n z}{x}\right)\right\} J_0\left(\frac{X\,r}{x}\right)$$

So from [B-4]

$$D_L \sum_n \frac{X_n}{x} D_n J_0\left(\frac{X_n r}{x}\right) = K \qquad \text{[B-9]}$$

put $t_n = D_L \frac{D_n X_n}{x}$ and

$$\sum_n t_n J_0\left(\frac{X_n r}{x}\right) = K \qquad \text{[B-10]}$$

$$R.H.S. = \int_0^x K r J_0\left(\frac{X_m r}{x}\right) dr = K \frac{x^2}{X_n} J_1(X_n)$$

L.H.S. (from orthogonal property of Bessel functions) =

$$\sum_n t_n \int_0^x r J_0\left(\frac{X_n r}{x}\right) J_0\left(\frac{X_m r}{x}\right) dr = t_m \frac{x^2}{2} J_1^2(X_m)$$

Equating these and transposing:

$$t_n = \frac{2K}{X_n J_1(X_n)} \qquad \text{[B-11]}$$

and from [B-9]

$$D_n = \frac{2Kx}{D_L X_n^2 J_1(X_n)} \qquad \text{[B-12]}$$

Hence from [B-6], [B-7], [B-8] and [B-12]:

$$\mu_A(r,z) = \frac{2Kx}{D_L}\sum_n \left\{ \left[\sinh\left(\frac{X_n z}{x}\right) - \coth\left(\frac{X_n a}{x}\right)\cosh\left(\frac{X_n z}{x}\right)\right] \frac{J_0\left(\frac{X_n r}{x}\right)}{X_n^2 J_1(X_n)} \right\}$$

[B-13]

To solve for K, $\mu_A(r,0) = \frac{2Kx}{D_L}\sum_n \frac{\coth\left(\frac{X_n a}{x}\right)}{X_n^2 J_1(X_n)} J_0\left(\frac{X_n r}{x}\right)$

Now $\int ds = \int_0^x 2\pi r dr$

so $\int \mu_A(r,0)ds = -4\pi K x^3 \sum_n \frac{1}{D_L X_n^3 \tanh\left(\frac{X a}{x}\right)}$

Substituting from [B-5]

$$K = \frac{D_L(2\pi x\gamma\Omega - \int \mu_B ds)}{4\pi x^3}\left\{\sum_n \frac{\coth(X_n a)}{X_n^3}\right\}^{-1} \qquad \text{[B-14]}$$

Substituting for K in [B-13] from [B-14] completes the solution once $\int \mu_B ds$ is known.

2.7.3. Appendix C --

Solution To Laplace's Equation For Boundary Value – Problem B

Problem:

$$\nabla^2 \mu_B = 0 \qquad \text{[C-1]}$$

$$\mu_B(x, z) = F_1 \exp(-F_2 z) + \frac{2\gamma\Omega}{a} \qquad \text{[C-2]}$$

$$\frac{\partial \mu_B(r, a)}{\partial z} = 0 \qquad \text{[C-3]}$$

$$\frac{\partial \mu_B}{\partial z} = 0 \quad \text{at } z=0 \qquad \text{[C-4]}$$

Solution:

In order to use the same functions we used for μ_A we transform to a function *w(r, z)* defined by:

$$\mu_B(r, z) = w(r, z) + f(z) \qquad \text{[C-5]}$$

Apply Fourier-Bessel analysis, multiply each side by $rJ_0(\frac{X_m r}{x})dr$ and integrate from 0 to x, where $f(z) = F_1 \exp(-F_2 z) + 2r\Omega / a$.

Using this definition and the above equations in order we obtain:

$$\nabla^2 w = f''(z) \qquad \text{[C-6]}$$

$$w(r, z) = 0 \qquad \text{[C-7]}$$

$$\partial w(r, z)/\partial z = 0 \qquad \text{[C-8]}$$

$$\text{at Z=0} \quad \partial w/\partial z = -f'(z) \qquad \text{[C-9]}$$

By separation of variables:

$$w(r,z) = \sum_n m_n(z) J_0\left(\frac{X_n r}{x}\right) \qquad [C\text{-}10]$$

Where $m_n(z)$ is a hyperbolic function to be determined.

From [C-8]:

$$m_n'(a) = 0 \qquad [C\text{-}11]$$

From [C-9]:

$$\sum_n m_n'(0) J_0\left(\frac{X_n r}{x}\right) = -f'(0) \qquad [C\text{-}12]$$

From [C-6]:

$$\sum_n \left\{ m_n''(z) - \frac{X_n^2}{x^2} m_n(z) \right\} J_0\left(\frac{X_n r}{x}\right) = -f''(0)$$

If

$$h_n(z) = m_n''(z) - \frac{X_n^2}{x^2} m_n(z) \qquad [C\text{-}13]$$

Then

$$\sum_n h_n(z) J_0\left(\frac{X_n r}{x}\right) = -f''(z) \qquad [C\text{-}14]$$

Applying Fourier-Bessel analysis:

$$h_n \frac{x^2}{2} J_1^2(X_n) = -f''(z) \frac{x^2}{X_n} J_1(X_n)$$

So

$$h_n(z) = -2f''(z) / X_n J_1(X_n) \qquad [C\text{-}15]$$

Applying Fourier-Bessel analysis to [C-12] we get:

$$m_n'(0) = h_n(0) \qquad [C\text{-}16]$$

where

$$h_n(0) = -2f''(0)/X_n J_1(X_n) \qquad \text{[C-17]}$$

Equation [C-13], [C-15], [C-16], [C-17] and [C-11] now define a problem in $m_n(z)$. We can find a particular solution (m_{np}) to this problem by applying variation of parameters to the homogeneous solution (m_{nh}). The homogeneous solution is:

$$m_{nh}(z) = \alpha_n \cosh(\frac{X_n z}{x}) + \beta_n \sinh(\frac{X_n z}{x})$$

So $m_{np}(z) = C_{n1}(z)m_{n1}(z) + C_{n2}(z)m_{n2}(z)$ with $C_{n1}(z) = -\dfrac{\int m_{n2}(z)h_n(z)dz}{w_r(m_{n1}, m_{n2}, z)}$ and, similarly $C_{n2}(z)$. But $w_r(m_{n1}, m_{n2}, z) = X_n / x$ so $m_n(z) = m_{nh}(z) + m_{np}(z)$. Hence

$$m_n(z) = \alpha_n \cosh(\frac{X_n z}{x}) + \beta_n \sinh(\frac{X_n z}{x}) - \frac{\cosh(\frac{X_n z}{x})}{X_n / x}\int h_n(z)\sinh(\frac{X_n z}{x})dz$$
$$+\frac{\sinh(\frac{X_n z}{x})}{X_n / x}\int h_n(z)\cosh(\frac{X_n z}{x})dz \qquad \text{[C-18]}$$

We determine α_n and β_n from the boundary conditions [C-17] and [C-11] and substitute back in [C-5] to determine $w(r, z)$. Equation [C-18] is solved as follows:

$$h_n(z) = -2F_1F_2^2 \exp(-F_2 z)/X_n J_1(X_n)$$

$$\int h_n(z)\sinh(\frac{X_n z}{x})dz = -\frac{F_2^2 F_1}{X_n J_1(X_n)}\left\{\frac{\exp\left[(\frac{X_n}{x} - F_2)z\right]}{\frac{X_n}{x} - F_2} + \frac{\exp\left[(\frac{-X_n}{x} - F_2)z\right]}{\frac{X_n}{x} + F_2}\right\}$$

$$\int h_n(z)\cosh(\frac{X_n z}{x})dz = -\frac{F_2^2 F_1}{X_n J_1(X_n)}\left\{\frac{\exp\left[(\frac{X_n}{x} - F_2)z\right]}{\frac{X_n}{x} - F_2} + \frac{\exp\left[(\frac{-X_n}{x} - F_2)z\right]}{\frac{X_n}{x} + F_2}\right\}$$

Hence by substituting in [C-18] and simplifying:

$$m_n(z) = \alpha_n \cosh(\frac{X_n z}{x}) + \beta_n \sinh(\frac{X_n z}{x}) + \frac{2F_2^2 F_1 \exp(-F_2 z)}{X_n J_1(X_n)(\frac{X_n{}^2}{x^2} - F_2^2)} \qquad [C\text{-}19]$$

From [C-11] taking derivatives:

$$\alpha_n \frac{X_n}{x} \sinh(\frac{X_n a}{x}) + \beta_n \frac{X_n}{x} \cosh(\frac{X_n a}{x}) = \frac{2F_2^3 F_1 \exp(-F_2 a)}{X_n J_1(X_n)(\frac{X_n{}^2}{x^2} - F_2^2)} \qquad [C\text{-}20]$$

From [C-16] and [C-17]

$$\frac{X_n}{x} \beta_n = \frac{2F_2 F_1}{X_n J_1(X_n)} + \frac{2F_2^3 F_1}{X_n J_1(X_n)(\frac{X_n{}^2}{x^2} - F_2^2)} \qquad [C\text{-}21]$$

Solving simultaneous equations [C-19] and [C-20]

$$\alpha_n = \frac{2xF_2 F_1}{X_n{}^2 J_1(X_n) \sinh(\frac{X_n a}{x})} \left\{ \frac{F_2^3 \exp(-F_2 a)}{(\frac{X_n{}^2}{x^2} - F_2^2)} - \cosh(\frac{X_n a}{x})[1 + \frac{F_2^3}{(\frac{X_n{}^2}{x^2} - F_2^2)}] \right\} \qquad [C\text{-}22]$$

$$\beta_n = \frac{2xF_2 F_1}{X_n{}^2 J_1(X_n)} [1 + \frac{F_2^3}{(\frac{X_n{}^2}{x^2} - F_2^2)}] \qquad [C\text{-}23]$$

From [C-10] and [C-19]

$$w(r,z) = \sum_n^{\infty} \left\{ \alpha_n \cosh(\frac{X_n z}{x}) + \beta_n \sinh(\frac{X_n z}{x}) + \frac{2F_2^2 F_1 \exp(-F_2 z)}{X_n J_1(X_n)(\frac{X_n{}^2}{x^2} - F_2^2)} \right\} J_0(\frac{X_n r}{x}) \qquad [C\text{-}24]$$

with α_n and β_n defined by [C-22] and [C-23].

Having obtained $w(r, z)$, $\mu_B(r, z)$ is obtained from [C-5]. The final step is to determine

$\int \mu_B(r,0)ds$. This is done by substitution and integration:

$$\int \mu_B(r,0)ds = 2\pi \sum_{n=1}^{\infty} \frac{\alpha_n x^2}{X_n} J_1(X_n) + 4\pi F_2^2 F_1 x^2 \sum_{n=1}^{\infty} \frac{1}{X_n{}^2 (\frac{X_n{}^2}{x^2} - F_2^2)} + \pi F_1 x^2 + \frac{2\pi\gamma\Omega x^2}{a}$$

[C-25]

This completes the solution when it is substituted into [B-14].

Table 2-1. Geometric parameters used in calculations

(Silver spheres, 100 μm radius) [Nicolls and Mullins]

Shrinkage %	x/a	ρ/a
1	0.198	0.0117
3	0.338	0.0415
3*	0.45	0.144
6	0.47	0.113

*Value measured by Eadie for Silver [Eadie, 1976]

Table 2-2. Fractional shrinkage rates (sec^{-1}) based on various models for lattice diffusion from grain boundary

(Silver spheres, 100 μm radius, sintering in air)

*S	Eadie	Ashby I	Johnson	Ashby II		This Model	
%	(Upper Limit)				$F_2=2/\rho$	$F_2=1/\rho$	$F_2=1/2\rho$
			Temperature : 700°C				
1	3.1E-9	4.1E-9	5.2E-10	7.1E-10	7.5E-10	1.0E-9	1.4E-9
3	5.4E-10	7.2E-10	1.8E-10	2.2E-10	2.1E-10	2.7E-10	3.5E-10
*3	1.7E-10	2.2E-10	1.2E-10	1.5E-10	8.7E-11	1.1E-10	1.2E-10
6	1.4E-10	1.9E-10	9E-11	9.4E-11	8.4E-11	1.0E-10	1.3E-10
			Temperature : 900°C				
1	1.3E-7	1.7E-7	2.1E-8	2.9E-8	3.1E-8	4.2E-8	5.7E-8
3	2.3E-8	3.0E-8	7.2E-9	8.7E-9	8.6E-9	1.1E-8	1.4E-8
*3	6.8E-9	9.0E-9	5.8E-9	6.0E-9	3.6E-9	4.4E-9	5.1E-9
6	5.9E-9	7.8E-9	3.7E-9	3.8E-9	3.5E-9	4.3E-9	5.3E-9
			Temperature : 950°C				
1	2.6E-7	3.5E-7	4.3E-8	5.8E-8	6.5E-8	8.8E-8	1.2E-7
3	4.7E-8	6.2E-8	1.5E-8	1.8E-8	1.8E-8	2.3E-8	3.0E-8
*3	1.4E-8	1.9E-8	1.2E-8	1.2E-8	7.5E-9	9.1E-9	1.1E-8
6	1.2E-8	1.6E-8	7.7E-9	8.0E-9	7.3E-9	9.1E-9	1.1E-8

*S : Shrinkage

*3 : Calculation based on the measured geometric value [Eadie, 1976]

Table 2-3. Fractional shrinkage rates (sec^{-1}) caused by lattice diffusion and grain boundary diffusion

(Silver spheres, 100 μm radius, sintering in air)

*S %	Coupled Model			This Model + Johnson's g.b. Model		
	$F_2=2/\rho$	$F_2=1/\rho$	$F_2=1/2\rho$	$F_2=2/\rho$	$F_2=1/\rho$	$F_2=1/2\rho$
			Temperature : 900°C			
1	6.3E-8	7.3E-8	8.7E-8	5.4E-8	6.5E-8	8.0E-8
3	1.2E-8	1.4E-8	1.7E-8	1.1E-8	1.3E-8	1.6E-8
6	4.1E-9	5.0E-9	5.9E-9	4.0E-9	4.8E-9	5.8E-9
			Temperature : 950°C			
1	1.1E-7	1.3E-7	1.6E-7	9.7E-8	1.2E-7	1.2E-7
3	2.3E-8	2.8E-8	3.5E-8	2.1E-8	2.6E-8	3.3E-8
6	8.2E-9	1.0E-8	1.2E-8	8.0E-9	9.8E-9	1.2E-8

*S : Shrinkage

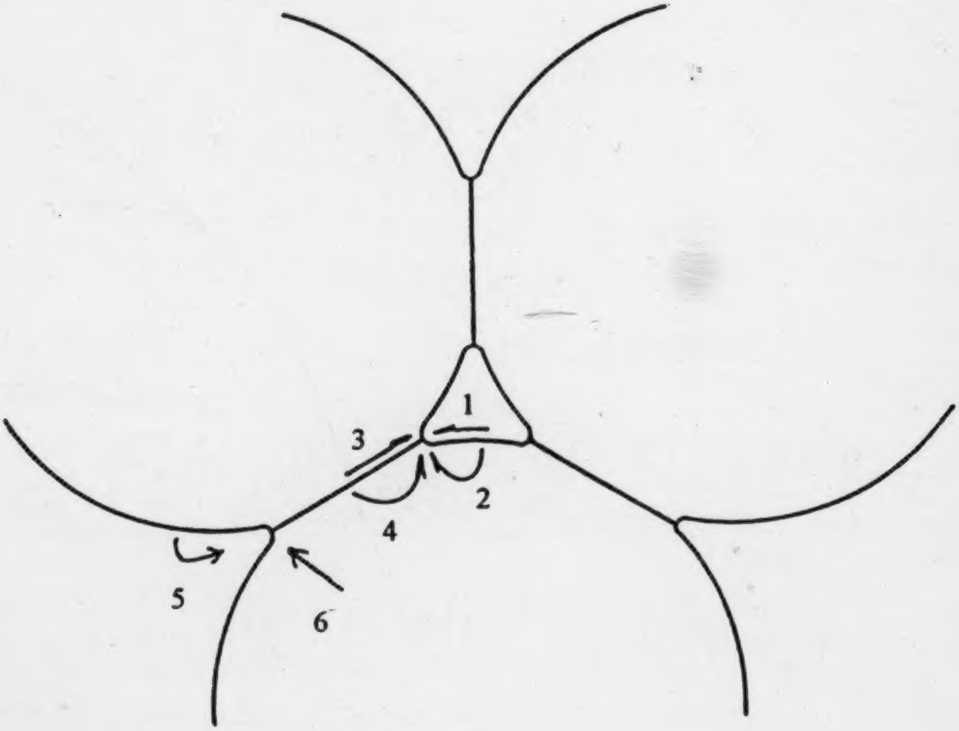

Figure 2-1. The mechanisms of sintering.

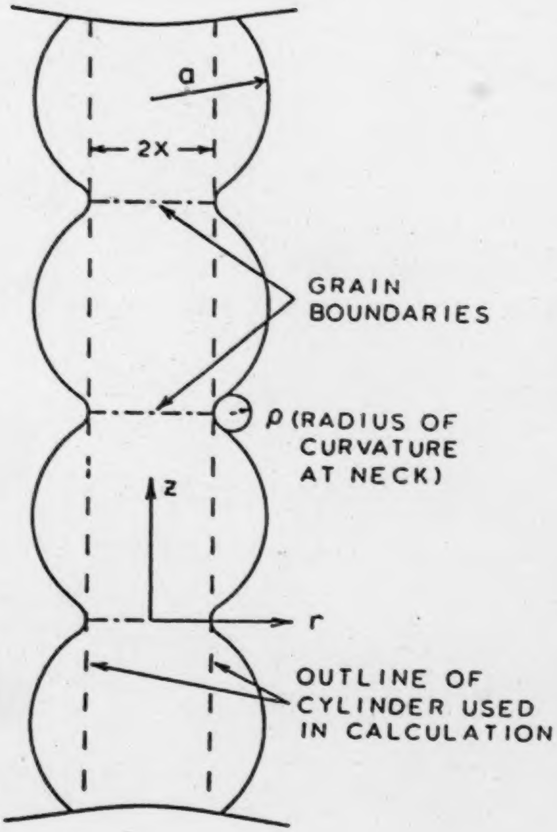
a
2X
GRAIN BOUNDARIES
ρ (RADIUS OF CURVATURE AT NECK)
z
r
OUTLINE OF CYLINDER USED IN CALCULATION

Figure 2-2. The row of spheres used in the calculation of the shrinkage rates.

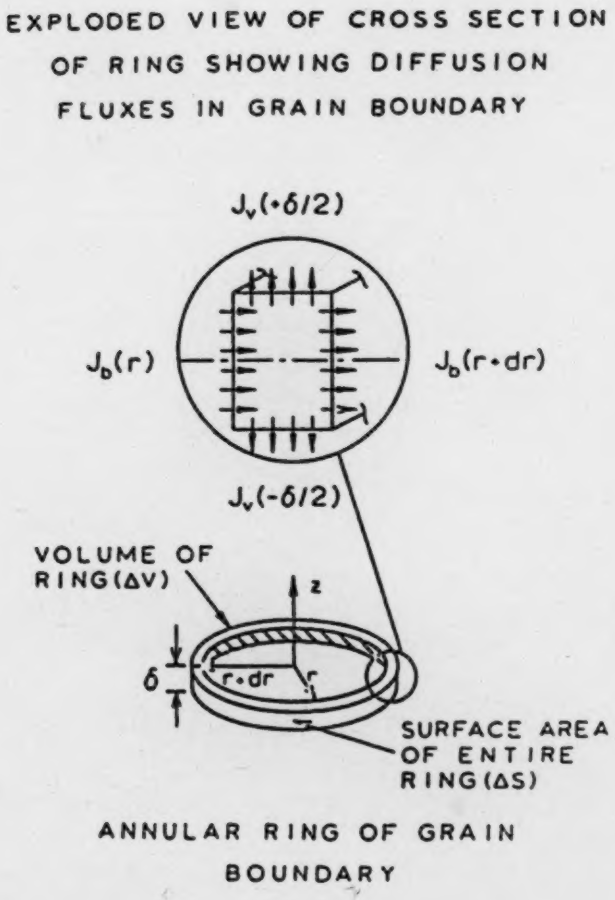
EXPLODED VIEW OF CROSS SECTION OF RING SHOWING DIFFUSION FLUXES IN GRAIN BOUNDARY
$J_v(+\delta/2)$
$J_b(r)$
$J_b(r+dr)$
$J_v(-\delta/2)$
VOLUME OF RING(ΔV)
z
δ
r+dr
r
SURFACE AREA OF ENTIRE RING(ΔS)
ANNULAR RING OF GRAIN BOUNDARY

Figure 2-3. Annular ring of grain boundary at the neck used to calculate the uniform shrinkage condition.

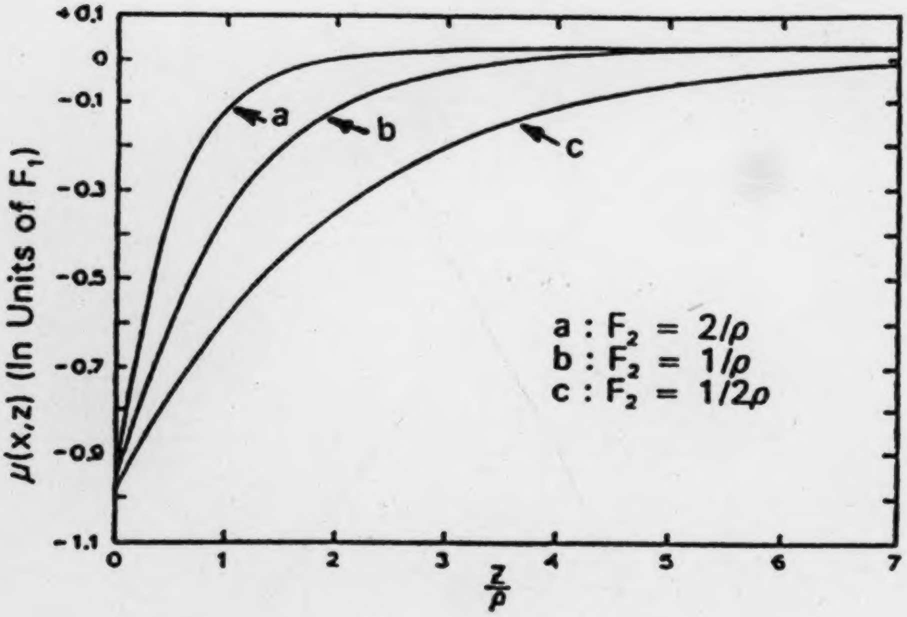

Figure 2-4. μ (x, z) versus the distance z / ρ for three values of the constant F_2

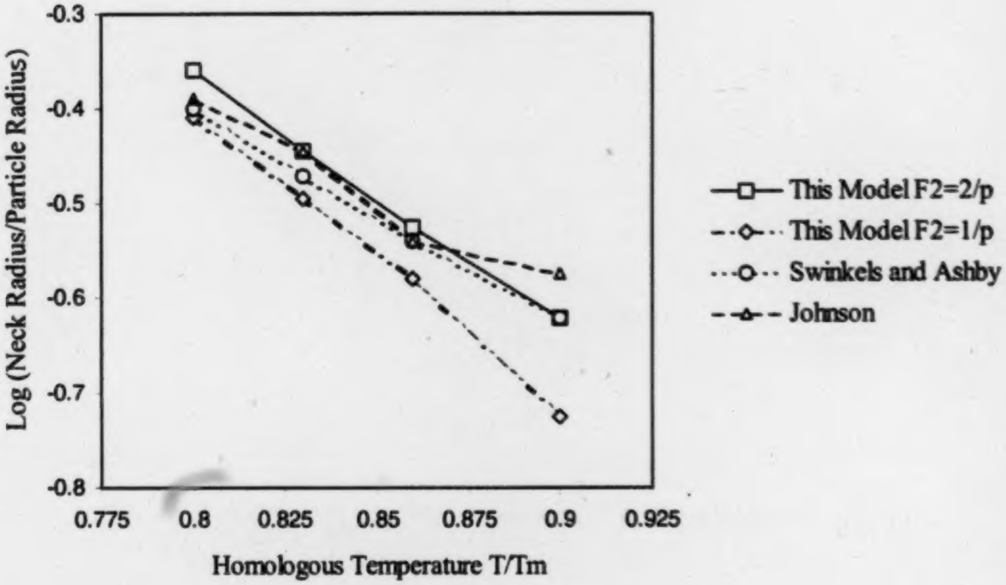

Figure 2-5. Boundary between lattice and grain boundary diffusion regions calculated from different models.

CHAPTER 3.

Bimodal Powder Distributions In P/M

-- Literature Survey

3.1. Improving Densities

-- Practical Significance of Using Bimodal Powder Distributions

For P/M to realize its full potential and compete with wrought products, it has to face the challenge of meeting more stringent quality demands, such as higher density, better dimensional control, better and more uniform mechanical properties and lower cost. Density is a predominant factor in the performance of powder metallurgy components. Generally, as density is increased almost all properties increase. Methods such as double press/double sinter, copper infiltration and powder forging have been employed to provide higher densities than traditional single press and sinter operations; however, their wide spread use is constrained by cost and geometry considerations. As illustrated in Figure 3-1, increasing the density of powder metallurgy components is typically accompanied by a significant increase in part cost [Rutz and Hanejko, 1995].

With unimodal size distributions, higher density can be achieved by using finer powders but this has detrimental effects on dimensional control. The inherent advantage of powder metallurgy is that the finished shape can be made almost directly and hence dimensional control during sintering is a significant concern during component fabrication. The less the sintering shrinkage, the better the dimensional control. There are other disadvantages to using fine powders, including : higher powder costs, lower green strength, higher fabricating and handling costs, and increased risk of oxidation.

The purpose of this part of the thesis is to develop a better understanding of the structure in bimodal packings, which is fundamental to the density of the packing and to coordination number, but also affects the subsequent operations of compaction and sintering. The model will be focused on the coarse /fine size ratio around 5 :1 and for volume fractions of coarse particle > 50%. This situation has not been studied and has yielded industrially important results. The relevant literature for this problem will be reviewed.

3.2. Particle Packing in Bimodal Powder Distributions

An understanding of particle packing characteristics is important in many diverse fields of technology, such as, solid state fuel packing for rockets and missiles in aeronautics; water seepage and drying of soils in agriculture; cellular structure of plants and animals in biology; powder synthesis and agglomeration in ceramics and flow characteristics through packed particles for polymer orientation in chemical engineering [German, 1989a]. In powder metallurgy, a major concern is the influence of the particle packing characteristics on the consolidation process and subsequent sintering behaviour. Packing density and coordination number are the two most important parameters used to represent the characteristics of particle packing. For monosized spheres, depending on the packing type (ordered, random loose, or random dense) the fractional packing density can range up to a maximum value of 0.7405. This density limit is rarely observed with powders. Rather, random structures are more common with fractional densities between approximately 0.60 and 0.64. The random loose packing roughly corresponds to the apparent density while the random dense packing roughly corresponds to the tap density. The accepted fractional density for the random dense packing and random loose packing of monosized spheres are 0.637 and 0.6, respectively [German, 1989a]. For bimodal powder distributions, an ideal distribution with infinitely different particle sizes, with a distribution of approximately 70% large and 30% small particles will give a fractional tap density approaching 0.86. The greater the size difference, the closer the packing density of the distribution will approach this limiting value [Fedors and Lanel, 1979].

The packing density of bimodal powder distributions was first analyzed theoretically by Furnas [Furnas, 1931], who derived a relation between the specific volume of a distribution and its weight fraction using simple space-filling concepts. Based on Furnas's model, bimodal powder distributions improve the packing density. Distributions of powders with different sizes give improved packing densities over that available from either powder by itself. Figure 3-2 [German, 1992a] schematically illustrates the variation in packing density f with composition X (measured by the percentage of large particles, assuming here that both powders are of the same alloy) for a bimodal distribution. The packing density improves in the terminal region rich in small particles, because the addition of large particles substitutes dense regions for porous clusters of small particles. Alternatively, for regions rich in large particles, the density improves because the small particles are able to fill the interstices between the large particles. The packing density peaks at X*, which corresponds to a dense packing of large particles with small particles in all of the interstices.

A significant concept about bimodal packings proposed by Furnas [Frunas,1931] is that saturated structures should develop which maximize the density of the packings. The tacit assumption here is that these packings are the most thermodynamically stable because they occupy the least volume (minimum potential energy relative to the gravitational field). For an ideal distribution consisting of infinitely different particle sizes, it is possible to accurately predict the packing density (actually apparent densities) versus composition for bimodal powder distributions if certain characteristics are known [German, 1992a]. German and Bulger expressed Furnas's model in the following way [German and Bulger 1992].

As shown in Figure 3-3 [German and Bulger 1992], the packing behaviour is linear with composition when viewed in terms of the nondimensional specific volume (normalised by the theoretical value corresponding to 100% density), which is the inverse of the fractional density f. The composition is measured in terms of the large particle content X. For 100% of the small powder (X= 0%), the specific volume V_S is given as the inverse of the small particle fractional packing density f_S :

$$V_S = 1 / f_S \tag{3-1}$$

Likewise, for 100% of the large powder (X= 100%) the specific volume V_L is given as:

$$V_L = 1 / f_L \tag{3-2}$$

where f_L is the large particle fractional packing density. With no interaction between the powders, the distribution specific volume would vary with composition as the rule of distributions V_r:

$$V_r = V_S - X(V_S - V_L) \tag{3-3}$$

However, as noted above, large-small powder distributions exhibit behaviour that improves the packing density. As a consequence, for the composition rich in large particles:

$$V = XV_L \qquad for\ X > X^* \tag{3-4}$$

and for the compositions rich in small particles :

$$V = V_S - X(V_S - 1) \ \ for\ X < X^* \tag{3-5}$$

For an ideal distribution, maximum packing occurs at X*, giving a specific volume of

$$V^* = V_S V_L / (V_S + V_L - 1) \tag{3-6}$$

where

$$X^* = V_S / (V_S + V_L - 1) \tag{3-7}$$

In the real situation, mixed powders have less than the ideal packing due to interference between the large and small particles. One of the factors which affects the packing density is the particle size ratio [Gray, 1968]. The relative improvement of packing density depends on the particle size ratio of the large and small particles. Within a limited range, the greater the size ratio, the higher the maximum packing density. This is true up to a limiting size ratio of approximately 20:1, but requires at least a 20% difference in particle sizes to occur [Ridgway and Tarbuck, 1968]. Another factor that impacts on packing is the homogeneity of mixed powders [Onoda and Messing, 1978; Messing and Onoda, 1978]. There are many factors, such as particle shape and mixing technique, which influence the overall homogeneity of bimodal powder distributions. Since the actual packing density may be less than the ideal value, to account for such behaviour a correction is needed. A simple homogeneity parameter H is introduced in German's work [German and Bulger, 1992]. Figure 3-4 indicates the specific volume versus composition for bimodal powder distributions with less than ideal homogeneity and a finite difference in particle sizes [German and Bulger 1992].

Because it is so important, coordination number has been widely discussed and investigated by many workers. For randomly packed monosized spheres, approximately six contacts per sphere represents the stable assembly [Suzuki, *et al*., 1981; German, 1989a]. For a system of particles with a continuous distribution, typically, the mean coordination number for the distribution is near six [German, 1989b]. However, the distribution in coordination number varies with the spread in the particle size distribution. The large particles have a greater number of contacts than the small particles [Ouchiyama and Tanaka, 1980]. For bimodal powders mixed from two monosized powders, the result of computer simulations is that the overall average coordination number remains nearly constant at 6.0 for all particle size ratios [Suzuki and Oshima, 1983; German, 1989c].

For a system of particles with a continuous distribution, the large particles have a greater number of contacts than the small particles, as indicated in the following equation

[Ouchiyama and Tanaka, 1980; German, 1989b]:

$$\frac{N}{\overline{N}} = \left(\frac{D + \overline{D}}{2\overline{D}}\right)^2 \tag{3-8}$$

where D is the particle diameter and $\overline{D}$ is the average diameter of the powders, N is the coordination number for the powder which has diameter of D and $\overline{N}$ is the average coordination number.

In most of the coordination number studies, however, the authors have concentrated mainly on the limiting case of monosized spherical particles and there are few reports concerning particle size distribution. There has been an attempt to understand the effect of bimodal particles on the nature of the packing through modelling of co-ordination number by Suzuki and Oshima [Suzuki and Oshima, 1983].

Considering a two component distribution comprising coarse and fine particles, four cases of contacts could be considered. They are [Nair *et al.*, 1986; Suzuki and Oshima, 1983]:

a. Coarse particles contact with a reference coarse particle;

b. Fine particles contact with a reference coarse particle;

c. Coarse particles contact with a reference fine particle;

d. Fine particles contact with a reference fine particle.

If $N_{1\text{-}2}$ is defined as the coordination number of a coarse particle when there is only a single coarse powder added into fine powders, it can be calculated from the following equation [Suzuki and Oshima, 1983]:

$$N_{1\text{-}2} = \frac{2\alpha\left(\frac{D_c}{D_f} + 1\right)}{1 + \frac{D_c}{D_f} - \left[\frac{D_c}{D_f}\left(\frac{D_c}{D_f} + 2\right)\right]^{1/2}} \tag{3-9}$$

where D_c is the average diameter of the coarse powder and D_f is the average diameter of the fine powders. The constant α is 0.4221 based on α = 0.067N [Suzuki and Oshima, 1983], where N, is the coordination number for the monosized spherical particles in random close packing.

There are two cases described in a and b above by which particles can contact with a reference coarse particle. If $N_{1\text{-}1}$ is defined as the coordination number of the coarse particle when a coarse particle is in the pure coarse powder bed, the coordination number N_c (average contact number of coarse powders in coarse-fine powder distribution) can be expressed by the summation of the products of $N_{1\text{-}1}$ and $(1\text{-}S_a)$ and of $N_{1\text{-}2}$ and S_a (the surface area fraction for fine powders in the powder distribution). If it is assumed that no agglomeration of fine particles occurs, the coordination number N_c is then [Suzuki and Oshima, 1983]:

$$N_c = S_a N_{1\text{-}2} + (1\text{-}S_a)N_{1\text{-}1} \tag{3-10}$$

where S_a can be calculated from the following equation [Suzuki and Oshima, 1983]:

$$S_a = \frac{S_p}{S_p + \left(\frac{D_c}{D_f}\right)^2 (1 - S_p)} \tag{3-11}$$

S_p is the particle number fraction for fine particles in the powder distribution. In Equation (3-10), a mixing ratio measured in the ratio of the surface areas is used in place of the number fraction. This is because the number fraction of the contact particles on the reference particle is related to the surface area shielded by the individual contact particle.

In equation (3-10), the product of $N_{1\text{-}1}$ and $(1\text{-}S_a)$ represents the average coarse-coarse contact number in the powder distribution ($N_{c\text{-}c}$) and the product of $N_{1\text{-}2}$ and S_a represents the average coarse-fine contact number of the coarse particles in the powder distribution ($N_{c\text{-}f}$).

Applying similar considerations to cases c and d, the coordination number of fine particles N_f in the powder distribution can be determined from [Suzuki and Oshima, 1983]:

$$N_f = S_a N_{2\text{-}2} + (1\text{-}S_a) N_{2\text{-}1} \tag{3-12}$$

where $N_{2\text{-}2}$ is the coordination number of the fine particles when a fine particle is in a pure fine particle bed, $N_{2\text{-}1}$ is the coordination number of a fine particle when there is only a single fine powder particle added into coarse powders, and S_a is defined through equation (3-11) as before. $N_{2\text{-}1}$ can be calculated from equation (3-9) by changing $N_{1\text{-}2}$ to $N_{2\text{-}1}$, D_c to D_f, and D_f to D_c :

$$N_{2\text{-}1} = \frac{2\alpha\left(\frac{D_f}{D_c} + 1\right)}{1 + \frac{D_f}{D_c} - \left[\frac{D_f}{D_c}\left(\frac{D_f}{D_c} + 2\right)\right]^{1/2}} \tag{3-13}$$

From [Suzuki and Oshima, 1983; Suzuki and Oshima, 1985], the average coordination number N in bimodal powder distributions is calculated by:

$$N = \Sigma S_{(i)} N_i \tag{3-14}$$

where S_j in equation (3-14) is the particle number fraction of particle j size range, and can be obtained from the particle size distribution functions. This was verified with computer simulations [Suzuki and Oshima, 1985].

Based on equations (3-9) to (3-14), the co-ordination numbers or four types of contact numbers for bimodal particle distributions can be estimated from the fraction of coarse (or fine) particles and the coarse / fine particle size ratio. The limitation of Suzuki and Oshima's model is that the model works when the coarse/fine particle size ratio is less than 3:1.

Zok *et al.* have developed a model for the particle packing in the bimodal system in which the large to fine particle size ratio is larger than 10 and the volume percent of the coarse particle is less than 70% [Zok, *et al.* 1991]. In Zok's model, the discrepancy between the idealised densities (Furnas' model) and the measured packing densities is due in part to the disruption in powder packing at the coarse particle surface, as shown schematically in Figure 3-5. It is convenient to idealise the problem by a periodic array of spherical particles situated against a flat surface (Figure 3-5b). The author neglected both the curvature of the coarse particles and the disruption in powder packing at distances greater than one monolayer from the coarse particle surface. In this model, the reduction of packing density is attributed to the spherical caps of fine powder which would otherwise be present at the surface in the absence of the coarse particles (Figure 3-5b). The disruption in packing is similar to that which occurs at the container walls and is consequently referred to as the "wall effect." The additional void volume, v_w, per unit volume of powder distribution associated with the wall effect is [Zok, *et. al.* 1991]:

$$v_w = N_s V_s N_i \tag{3-15}$$

where N_s is the number of such sites per coarse particle, V_s is the void volume associated with one site, and N_i is the number of coarse particles per unit volume of powder distributions. In the model, the assumption that the curvature of the coarse particle does not influence the packing density limits the use of the model to coarse particle / fine particle size ratio larger than 10.

An additional void volume is created when coarse particles contact one another. The way in which fine particles fit into the void space created by touching coarse particles is thus a major concern to packing efficiency [Zok, *et al.* 1991]. The void volume at a contact is in the form of a pendular ring, as shown schematically in Figure 3-6 [Zok, *et al.* 1991]. Since fine particles can not be packed into the ring, the associated void volume v_e is referred to as an "excluded volume." It has a magnitude [Zok, et al. 1991]:

$$v_e = N_c V_e N_i \tag{3-16}$$

where N_c is the number of contact points per coarse particle, V_e is the excluded volume per contact point, and N_i is the number of coarse particles per unit volume of powder distributions. Thus, v_e is additional void volume per unit volume of powder distributions. It should be noted that N_c is equal to one half of the average coarse-coarse coordination number, since each contact point is associated with two coarse spheres. Because of the method used in the calculation, the model is expected to be valid only in the regime where the volume fraction of coarse particles < 74%, *i.e.*, where coarse particles are added to fine particles.

The combined effects of coarse particle surfaces and coarse particle contacts on packing density can be described by [Zok, *et al.* 1991]:

$$\rho_c = \rho_c^F - v_e - v_w \qquad (3\text{-}17)$$

where ρ_c is the relative packing density of the powder distributions and ρ_c^F is the relative packing density of the powder distributions according to ideal distribution structure (Furnas or German's model).

3.3. Percolation

In addition to coordination number, a further tool is needed to build the bridge between the macro properties and microstructure. Percolation theory could be used for this purpose. Percolation theory describes a phenomena whereby a property of a system as a function of a continuously varying parameter diverges, vanishes or just begins to manifest itself at one sharply defined point. This point (transition) is characterized by a percolation threshold at which a three-dimensional continuous network of bonds is just formed throughout the particulate system [Stauffer, 1985]. The percolation probability P is defined either as the fraction of sites in a network occupied (site percolation) or the fraction of bonds formed between sites which are all regarded as filled (bond percolation). As an introductory example of a percolation process and the qualitative event called the percolation threshold, consider the experiment illustrated in Figure 3-7 [Zallen, 1985]. A communication network, represented by a very large square-lattice network of interconnections, is attacked by a crazed saboteur who, armed with wire cutters, proceeds to cut the connecting links at random. His aim is to break contact between two well-separated but well-connected communication centers or command posts, represented by the heavy bars which, in Figure 3-7, form the left and right boundaries of the network. Question: What fraction of the links (or bonds) must be cut in order to isolate the command posts from each other? This question, which can be given a definite answer by percolation theory, illustrates the central issue at the heart of the percolation model: the existence of a sharp transition at which the long-range connectivity of the system disappears (or, going the other way, appears). This basic transition, which occurs abruptly as the composition of the system - or some generalized density - is varied, constitutes the percolation threshold. At the percolation threshold, significant properties may change qualitatively in an off / on manner. In the context of the present example, certainly the question of whether the joint command posts can communicate is a yes - or - no matter of some importance.

For the bimodal powder distributions, at a critical threshold of connections, the cluster becomes infinite or percolates the system. In this case, the networks considered are those of the large particles and those of the fine particles and the probabilities are considered relative to the percentage of coarse powder which is represented by X (per cent of mass of large particles). Above the threshold X_c, the infinite coarse network percolates the structure. Below the threshold X_f, the infinite fine network percolates the structure. Between X_c and X_f, the infinite coarse and fine networks coexist. The threshold X_c is important because a network of large particles with its large contact area and rigid framework might dominate the compaction or sintering behavior of the distribution.

Percolation theory is a useful approach to elucidate the compaction behaviour of the powders. During the compaction, the transitions from one state to another are signified by percolation thresholds which include particulate bond percolation threshold, rigidity threshold and pore percolation threshold. Holman has developed this theory in his studies on pharmaceutical powders [Holman, 1991].

Holman and Leuenberger first used percolation theory in the compaction of powders [Holman and Leuenberger 1990]. The approach was based on percolation theory and the principles of mechanics and has been used to elucidate the relationship between the normalised solid fraction (fraction of solid) D of compacts and the compressive pressure p during compaction. The series of linear regions comprising the $D = f(\ln p)$ relationship has been shown to be a manifestation of the different stages, namely, powder --> flexible compact --> rigid compact --> continuum solid body. The transitions from one state to another are signified by percolation thresholds which occur in crossover regions. Near the percolation thresholds, there is a deviation in the $D = f(\ln p)$ relationship. Thus, different relationships exist between D and ln p in the different regions.

More importantly percolation theory offers a method to directly link the compaction phenomena to the microstructure of the compacts. Figure 3-8 [Holman, 1990] illustrates, in a simplified way, the clusters of particles held together by bonds formed through application of uniaxial pressure on powders in a rigid die. When pressure is below the particulate bond percolation threshold D_{CS}, where D_{CS} is identified as the point at which a continuous interparticle network of bonds spanning the system is formed , a large number of the particles do not transmit forces and do not feel the applied stress. As illustrated in

Figure 3-8(a), these columns of particles transmitting forces are not connected and are separated by several particles. It can therefore be said that the powder system at this stage of consolidation consists of isolated clusters of bonded particles. The heterogeneity in the transmission of forces in the powder bed has been attributed to different geometric properties (size or shape) of the particles. For example, in a powder system exhibiting a bimodal size distribution of particles, the stresses are preferentially transmitted through the larger particles. In the region $D < D_{CS}$, D increases linearly with a unit increase in ln p , reflecting an increase in the number of contact points and the area of each. Near the particulate bond percolation threshold D_{CS} , a cluster spanning the whole structure in all three dimensions begins to form. As illustrated in Figure 3-8(b), the continuous network of interparticulate bonds comprising the infinite cluster is just formed above the threshold D_{CS}. Above D_{CS}, although D increases linearly with a linear increase in ln p, the slope is different from that at D - values below D_{CS}. This is because the underlying structures which confer on the particulate body the ability to resist deformation are different on either side of D_{CS}.

There is no published paper that focuses on elucidating the compaction and sintering behaviour of binary metal distribution based on percolation theory. An effort will be made to connect the percolation threshold phenomenon with the microstructural geometry of pressed bimodal powder distributions.

3.4. Compaction of Bimodal Powder Distributions

The changes during compaction are complicated. Usually, there are three stages in the compaction procedure. The first is packing during which there is a rapid decrease in porosity with increasing pressure. The particles are brought closer together without undergoing deformation since individual particle movement, rearrangement and bridge collapse occurs before interparticle deformation becomes appreciable. The second stage is plastic compression attributed to deformation of the powders or fracture. The third stage pertains to elastic compression under very high pressures.

One of the most important aspects of compaction is the equation of compaction which describes the relationship between green density and the applied external pressure. Ge mentioned that from an analysis of the various compaction equations, it could be shown that most of the equations were derived from the differential equation [Ge, 1991] :

$$dD/dp = K_1 \times D^{a}/p^{b} \tag{3-18}$$

where p is compaction pressure, D is relative density and K_1, a and b are constants.

According to Shapiro, the general compaction equation can be expressed by the following equation [Shapiro 1994; Shapiro 1993; Shapiro 1992] :

$$P = P_0 \exp\{-kp - bp^{0.5}\} \tag{3-19}$$

where P and P_0 are apparent porosity and porosity at zero external pressure respectively, k and b are constants.

But there are no clear meanings related to material properties or compaction conditions for all the constants in these equations. There are several variables influencing the properties of powder metallurgy parts. Among them, particle size has a strong effect on the interparticle friction, packing density, green strength, the pore size, shrinkage (or densification) during sintering and sintered density. As mentioned in section 3.1, the effect of particle size distribution on the consolidation processes, such as compaction and sintering, is an area of surprisingly little research and understanding. There are just some qualitative analysis and a few experimental equations. The finer particle sizes are more difficult to press, since large pores collapse under lower pressures than fine pores and there is higher interparticle friction for compacting finer powders.

Among the few researchers who have studied the influence of powder size distribution on compaction, Zheng *et al.* described in detail the experimental compaction of bimodal powder distributions [Zheng, *et al.*, 1995; Zheng and Reed, 1990]. In the pressing of powders, the packing efficiency is a function of forming pressure. Generally, the compact density versus the log of pressure curves are approximately linear over certain pressure ranges. There is a change of slope for some curves which have the same nominal composition. This change is attributed to a difference of the particle-size distribution or the shape of the particles in the powder. Zheng and Reed defined the slope of the density curve versus log of pressure as the compaction efficiency [Zheng, *et al.*, 1995; Zheng and Reed, 1990]. The compact densities for blends of the coarse (mean particle size: 111 μm) and fine (mean particle size: 0.64 μm) powders at different forming pressures are plotted in Figure 3-9. It is seen that the density-log of pressure curves for all of the blends are approximately linear. It is also seen from Figure 3-9 that not only the compact densities but also the compaction efficiencies are different for different compositions. The highest compaction efficiency is achieved around 25% fine + 75% coarse powder distribution composition. [Zheng, *et al.*, 1995].

Using networks (percolation theory) as a tool has been a successful method in composite materials studies. Lange *et al.* [Lange *et al.*, 1991] have studied the plastic consolidation of metal powders containing different volume fractions of spherical, non-deformable inclusions. Their results show that the connective network of inclusions supports an increasing fraction of the applied pressure as the volume fraction of inclusions exceeds ≈ 0.2. In effect, they argue that since the applied pressure is not totally supported by the deformable metal matrix powder, a higher applied pressure must be exerted on the composite powder to obtain the same matrix density obtained without inclusions. [Lange *et al.*, 1991].

Research concerning the connectivity of spherical inclusions has received considerable attention with regard to the percolation threshold. At the percolation threshold, a critical volume fraction (relative to all space, ϕ_p) exists to form an infinite connective cluster of inclusions that completely spans the volume of the container. For identical spheres, ϕ_p ranges between 0.146 (diamond lattice) to 0.167 (body centered cubic lattice) [Zallen, 1983] for periodic particle packing, and from about 0.16 for dense random packing [Fitzpatrick, *et al.*, 1974] to 0.183 for a computer simulated random packing [Powell, 1979]. Oger *et al.* [Oger et al., 1986] have also numerically determined ϕ_p, when the matrix particles have a different size relative to the inclusions. Once ϕ_i (the volume fraction of inclusions relative to the total volume) is greater than ϕ_p (the percolation threshold), P_c (the fraction of inclusions within an infinite connective cluster) has the functional form [Zallen, 1983]:

$$P_c = A\,(\phi_i - \phi_p)^{\beta} \tag{3-20}$$

where A is a dimensionless constant and $\beta = 0.4$. $P_c = 0$ when $\phi_i \leq \phi_p$, and quickly increases as ϕ_i exceeds ϕ_p .

For the deformation processing of composites, the value of the percolation threshold is not as important as the value of ϕ_i where the network formed by the inclusion cluster can begin to support a portion of the applied pressure. Figure 3-10 [Bouvard and Lange, 1991] illustrates five touching inclusions within three different clusters, where the number of inclusions touching any other inclusion, Z_{ii} , increases from 2 to 4. When $\phi_i = \phi_p$, where the infinite network just starts to span the volume, Z_{ii} is expected to have an average value of 2. For this case, the inclusions within the cluster do not form a supporting, three-dimensional network, and the path for transmitting force would be very tenuous. On the other hand, when $Z_{ii} = 3$, every inclusion within the percolating cluster is part of a three dimensional network with some capability of supporting load and transmitting force as shown in two-dimensions in Figure 3-10. When $Z_{ii} = 4$, the apparent "strength" of the network increases by both the increased density of supporting paths, and the formation of some triangular and tetrahedral supports between 3 and 4 touching inclusions, which increase their number density as Z_{ii} becomes greater than 4. Thus, a relation between ϕ_i , P_c and $Z_{ii} \geq 4$ appears to be of great interest for correlating the effect of inclusions on the deformation processing of composite systems. In the compaction of bimodal powder distributions, it is reasonable to choose $Z_{ii} = 4$ as the percolation threshold.

Bouvard and Lange used computer simulations to get the following results [Bouvard and Lange, 1991]. Figure 3-11a illustrates the results expressed as a fraction of inclusions (P_c)

in the percolative clusters vs the volume fraction of inclusions relative to total solids f_i (function of the volume fraction of inclusions, f_i, relative to the total volume of matrix particles and inclusions ($f_i + f_m = 1$)), for $0.33 \leq R \leq 3$ (size ratio $R = r_m / r_i$). Since the relative packing density is also determined for these systems, P_c can be plotted as a function of ϕ_i as shown in Figure 3-11b (If the relative density of the binary distribution, ρ, is known, then ϕ_i can be related to f_i with the relation: $\phi_i = f_i \rho$). It appears that the percolation threshold (f_p or ϕ_p) depends on R as also observed by Malliaris and Turner [Malliaris and Turner, 1971] and Oger *et al.*[Oger *et al.*, 1986]. ϕ_p ranges between 0.081 for R=3 to 0.223 for R=0.5. These data also show that small particles percolate more easily than larger ones in mixed random packing. When R=0.33 significant scattering is observed around the percolation threshold ($\phi_p \cong 0.219 \pm 0.01$). This larger scatter is probably caused by the large radius of the inclusion relative to the cube edge (0.066), and thus relatively few inclusions at the percolation threshold. A similar effect was found by Powell [Powell, 1979]. For inclusion volume fractions greater than the threshold value ($f_i > f_p$ or $\phi_i > \phi_p$), P_c dramatically increases until all inclusions are part of the same cluster ($P_c = 1$) [Bouvard and Lange, 1991].

In a more interesting way of representing the data, P_c is plotted as a function of inclusion connectivity expressed as Z_{ii} (the average coordination number for inclusions touching one another as determined through numerical simulation). As shown in Figure 3-12 [Bouvard and Lange, 1991], a plot of P_c vs Z_{ii} reduces all data to one single curve independent of size ratio (R). The percolation threshold corresponds to $Z_{ii} \cong 2$, and $Z_{ii} \cong 4$ characterises the complete connectivity of all inclusions (P_c=1). These data show that the fraction of inclusions within a percolating cluster is simply a function of the inclusion-inclusion coordination number. Since Z_{ii} is proportional to f_i or ϕ_i, it seems reasonable to use a functional form similar to Equation (3-20) around the percolation threshold, to describe P_c as a function of Z_{ii}. The following relation is proposed [Bouvard and Lange, 1991]:

$$P_c = (1-(\frac{4-Z_{ii}}{2})^{2.5})^{0.4} \qquad (3\text{-}21)$$

which satisfactorily describes the results in the whole range of volume fraction, as shown by the solid line in Figure 3-12. The scatter around the percolation threshold is probably due to the suddenness of the percolation process, which is difficult to catch with precision using numerically simulated samples of limited size.

Among the shortcomings of this approach, that may limit its practical application, are the restricted range in size ratio used in this study due to computing capability (0.33 < R < 3).

It is worth mentioning Arzt's model [Arzt, 1982] about the influence of an increasing particle coordination on the compaction process even though this model is only used for monosized powder. It is believed that this model can be used in more complicated particle size distribution situations if the compaction is homogeneous. Most theories of the densification behaviour of powders subjected to high temperature (as in sintering) and/or pressure (as in hot and cold compaction) deduce the shrinkage from the linear densification between two spherical particles in a regular packing. This approach neglects the peculiarities arising from the fact that the particle structure is never regular and changes continually during densification. As the average particle distance decreases, the particles are squeezed together and form new contact areas. During this process the coordination number increases steadily. This implies that in pressing operations the forces acting on the individual particle contacts decrease continuously as a fraction of the external load, because the external pressure is shared among an increasing number of contacts. The geometry of the particle packing may therefore influence the densification; but to what extent remains to be seen [Arzt, 1982].

In a packing without rearrangement, densification can be brought about only by centre-to - centre approach of particles. During shrinkage new particle pairs will be brought close enough to form additional contacts. A study of the geometrical changes during cold compaction of a spherical powder [Fischmeister, *et al.*, 1978] has shown this to be a continuous process: the coordination number increases steadily as densification proceeds. A regular lattice-type packing cannot account for this behaviour. A continuous increase in coordination can be modelled by assuming a 'random' particle structure with a continuous distribution of centre-to-centre distances. Whether a particular sphere of the packing is likely to form a new contact at a certain stage of densification depends upon the distribution of particles in its immediate vicinity. The arrangement of near-neighbours of a representative reference sphere can be characterised by the distribution of centre distances ('radial density function', RDF), or by its integral, the cumulative radial distribution function, G(r). G(r) represents the number of particle centres within a fictitious sphere of radius r around the reference sphere [Arzt, 1982].

During densification each particle changes its shape by forming contact areas with its neighbours. The sphere packing has been converted into a space-filling stack of irregular polyhedra. If it is assumed that the densification has been homogeneous, then these polyhedra are identical in shape with the Voronoi polyhedra of the original packing (Figure 3-13) [Arzt, 1982]. The Voronoi polyhedron of a particle in a packing is the set of all points in space which are closer to its centre than to any other particle centre. The boundaries of this polyhedron are obtained by placing perpendicular bisecting planes on all centre-to-centre connections. The bisection is of the distance between particle surfaces of course. The faces of the Voronoi polyhedra contain all the contact areas and potential contacts. Densification can be visualised as the shrinkage of these polyhedra; the deformation of the particles can be regarded as being imposed by the walls of the shrinking cells.

Using the concepts of radial density function and Voronoi polyhedra, Arzt modelled the particle geometry during compaction based on the initial particle packing. Simple equations can be deduced to relate the fractional density D to the mean coordination number (obtained for $Z_0 = 7.3$ and $D_0 = 0.64$)[Arzt, 1982]:

$$Z = Z_0 + 9.5(D - D_0) \text{ for } D < 0.85 \tag{3-22}$$

$$Z = Z_0 + 2 + 9.5(D - 0.85) + 881(D - 0.85)^3 \quad \text{for } D > 0.85 \tag{3-23}$$

where Z and Z_0 are the coordination number at the compacted relative density D and initial relative density D_0 respectively.

3.5. Sintering of Bimodal Powder Distributions

The sintered density for a bimodal distribution is less predictable and requires experimentation [German, 1992a]. Most of the studies on the effects of bimodal mixing on sintering were focussed on ceramic systems without large particle deformation before sintering. Most recently, German has studied the prediction of sintered density for both ceramic and metal bimodal powder distributions in powder injection molding [German, 1992a]. As sketched in Figure 3-14, the shrinkage of the small particles is constrained by the full density large particle. This results in stresses that can reduce the shrinkage and open cracks in the matrix.

Based on Onoda and German [Onoda and Messing, 1987; German, 1992a], sintered density prediction could be explained by an idealised model as in Figure 3-15. H is a homogeneity parameter. At the composition consisting of pure small particles, the volume change during sintering is ΔV_S, and at the composition consisting of pure large particles, the volume change during sintering is ΔV_L. These two terminal values can be measured for any bimodal powder system.

During sintering, compositions above X* (the composition at the packing density peak) will be constrained by the rigid skeleton of large particles (Fig. 3-4). Alternatively, at the end of sintering, there will be a new composition X_t that is constricted in densification by the large particles (Fig. 3-5). Typically, $X_t > X^*$, but they are usually close together.

As shown in Figure 3-15, when H=1 (perfect mixing), the change in specific value on sintering will consist of two straight line segments connecting the behaviour of the pure small and pure large powders with a change in slope at the transition composition X_t. At compositions over the transition composition, $X > X_t$, the change in specific volume for the distribution ΔV is just ΔV_L :

$$\Delta V = \Delta V_L \quad X > X_t \tag{3-24}$$

The sintering of the small particles located in the voids between the large particles will not alter the bulk volume change. On the other hand, at compositions rich in small particles ($X < X_t$), the sintering volume change will decrease as large particles are added, since the regions occupied by large particles are already dense. Accordingly, the volume change on sintering will be linearly dependent on the small particle content :

$$\Delta V = \Delta V_S - (X/X_t)(\Delta V_S - \Delta V_L) \quad X < X_t \tag{3-25}$$

where ΔV_S and ΔV_L are the changes in specific volume for the small and large powders, respectively. If a powder is separated into regions of large and small particles with a homogeneity of zero (H=0), then the change in specific volume will follow the rule of distributions.

German's model is an idealised model. There is no connection between the macro-properties and the microstructure of the powder system or the physical characteristics of the powders.

There is no theoretical model in the literature for sintering of bimodal powder distribution. The influence of an increasing particle coordination on the sintering of monosized powder was discussed by Arzt [Arzt, 1982; Arzt *et al.*, 1983] and the relationship between coordination number and fractional density during sintering was given as equation (3-26)

[Arzt, 1982]:

$$Z = Z_0 + C[\frac{D - D_0}{3D_0} - (\frac{D - D_0}{3D_0})^2 + ...] \tag{3-26}$$

where C is a constant, Z and Z_0 are the coordination number when sintered density is D and initial density is D_0 respectively. This model may be useful in the study of bimodal powder sintering when the coarse powder network dominates the sintering of the powder distribution.

As a summary of the literature survey, the effect of particle size distribution on P/M processes is an area of surprisingly little research and understanding [Ting and Lin, 1994; Patterson, *et al.*,1987]. Studying the effects of bimodal powder distributions with size distributions on P/M processes has both theoretical and practical significance.

3.6. References

Arzt, E., " The Influence of an Increasing Particle Coordination on the Densification of Spherical Powders," Acta Metall. Vol. 30, pp. 1883-1890, 1982.

Arzt, E., **Ashby**, M.F. and **Easterling**, K.E., " Practical Applications of Hot-Isostatic Pressing Diagrams: Four Case Studies," Metallurgical Transactions A, Vol. 14A, No. 2, pp. 211-221, 1983.

Bouvard, D. And **Lange**, F.F. , " Relation Between Percolation and Particle Coordination in Binary Powder Mixtures," Acta Metall. Mater. , Vol. 39, No. 12, pp. 3083-3090, 1991.

Fedors, R. F., and **Landel**, R. F., "An empirical Method of Estimating the Void Fraction in

Mixtures of Uniform Particles of Different Size," Powder Technology, Vol. 23, pp 225-231, 1979.

Fischmeister, H.F., **Arzt**, E. and **Olsson**, L.R., "Particle Deformation and Sliding During Compaction of Spherical Powders: A Study by Quantitative Metallography," Powder Metallurgy, Vol. 21, pp. 179-187, 1978.

Fitzpatrick, J.P., **Malt**, R.B. and **Spaepen**, F. , " Percolation Theory and the Conductivity of Random Close Packed Mixtures of Hard Spheres," Physics Letters, Vol. 47A, No. 3, pp.207-208, 1974.

Furnas, C.C., "Grading Aggregates I - Mathematical Relations for Beds of Broken Solids", Ind. Eng. Chem., Vol. 23, pp. 1052-1058, 1931.

German, R.M., "Particle Packing Characteristics," Metal Powder Industries Federation, Princeton, New Jersey, chapter four, 1989a.

German, R.M., "Particle Packing Characteristics," Metal Powder Industries Federation, Princeton, New Jersey, chapter eight, 1989b.

German, R.M., "Particle Packing Characteristics," Metal Powder Industries Federation, Princeton, New Jersey, chapter six, 1989c.

German, R.M., "Prediction of Sintered Density for Bimodal Powder Mixtures", Metallurgical Transactions A, Vol. 23A, No. 5, pp. 1455-1465, 1992a.

German, R.M., "The Prediction of Packing and Sintering Density for Bimodal Powder Mixtures", Advances in Powder Metallurgy & Particulate Materials - 1992, Compiled by J.M. Capus and R.M. German, Metal Powder Industries Federation, New Jersey, Vol. 3, pp. 1-15, 1992b.

German, R.M. and **Bulger**, M., "A Model for Densification by Sintering of Bimodal Particle

Size Distributions," International Journal of Powder Metallurgy, Vol. 28, No. 3, pp. 301-310, 1992.

Ge, R. D., "A New Powder Compaction Equation," The International J. of Powder Metallurgy, Vol. 27, No. 3, pp 211 - 216, 1991.

Gray, W., " The Packing of Solid Particles," Chapman and Hall, London, UK, 1968.

Holman, L.E., "The Compaction Behaviour of Particulate Materials. An Elucidation Based on Percolation Theory", Powder Technology, Vol. 66, pp. 265-280, 1991.

Holman, L.E. and **Leuenberger**, H., "The Effect of Varying the Composition of Binary Powder Mixtures and Compacts on Their Properties: A Percolation Phenomenon", Powder Technology, Vol. 60, pp. 249-258, 1990.

Lange, F.F., **Atteraas**, L. and **Zok**, F. , "Deformation Consolidation of Metal powders Containing Steel Inclusions," Acta metall. Mater. Vol.39, No.2, pp. 209-219, 1991.

Malliaris, A. and **Turner**, A.T., "Influence of Particle Size on the Electrical Resistivity of Compacted Mixtures of Polymeric and Metallic Powders," Journal of Applied Physics, Vol.42, No. 2, pp. 614-618, 1971.

Messing, G.L. and **Onoda**, G.Y. , "Inhomogeneity-Packing Density Relations in Binary Powders", Journal of American Ceramics Society, Vol. 61, p. 1, 1978.

Nair, S.V., **Hendrix**, B.C. and **Tien**, J.K., "Obtaining the Radial Distribution of Random Dense Packed Hard Spheres," Acta Metallurgica, Vol. 34, pp. 1599-1605, 1986.

Oger, L., **Troadec**, J.P., **Bideau**, D., **Dodds**, J.A. and **Powell**, M.J., "Properties of Disordered Sphere Packings II. Electrical Properties of Conducting and Insulating Spheres of Different Sizes," Powder Technology, Vol. 46, pp.133-140, 1986.

Onoda, G.Y. and **Messing**, G.L., "Packing and Sintering Relations for Binary Powders", Materials Science Research, Compiled by H. Palmour, R.F. Davis and T.M. Hare, Plenum Press, New York, pp. 99-112, 1978.

Ouchiyama, N. and **Tanaka**, T., "Estimation of the Average Number of Contacts Between Randomly Mixed Solid Particles," Industrial and Engineering Chemistry Fundamentals, Vol. 19, pp. 338-340, 1980.

Patterson, B.R., **Parkhe**, V.D. and **Griffin**, J.A., "Effect of Particle Size Distribution on Sintering", Sintering '85, Compiled by G.C. Kuczynski, D.P. Uskokovic, H. Palmour III and M.M. Ristic, Plenum Press, New York and London, pp. 43-51, 1987.

Ridgway, K. and **Tarbuck**, K.J., "Particulate mixture bulk densities," Chemical and Process Engineering, Vol. 49, No. 2, p.103, 1968.

Rutz, H.G. and **Hanejko**, F.G., "High Density Processing of High Performance Ferrous Materials", International Journal of Powder Metallurgy, Vol. 31, No. 1, pp. 9-17, 1995.

Shapiro, I., "Compaction of Powders IX. Sized Magnesium Spheres," Advances in Powder Metallurgy & Particulate Materials - 1992, Compiled by J.M. Capus and R.M. German, Metal Powder Industries Federation, New Jersey, Vol. 2, pp. 147-161, 1992.

Shapiro, I., "Compaction of Powders X. Development of a General Compaction Equation," Advances in Powder Metallurgy & Particulate Materials - 1993, Compiled by A. and A. Swanson, Metal Powder Industries Federation, New Jersey, Vol. 3, pp. 229-243, 1993.

Shapiro, I., "Compaction of Powders XI. Application of the General Equation to Both Metal Powders and Ceramic Powders", Advances in Powder Metallurgy & Particulate Materials - 1994, Compiled by C. Lall and A.J. Neupaver, Metal Powder Industries Federation, New Jersey, Vol. 3, 1994, pp. 41-56.

Stauffer, D., 'Introduction to Percolation Theory', Taylor and Francis, London, 1985.

Suzuki, M., **Makino,** K., **Yamada,** M. And **Iinoya,** K., "A Study on the Coordination Number in a System of Random Packed, Uniform-sized spherecal Particles," International Chemical Engineering, Vol. 21, pp. 482-488, 1981.

Suzuki, M. and **Oshima,**T., "Estimation of the Co-ordination Number in a Mullti-Component Mixture of Spheres," Powder Technology, Vol. 35, pp. 159-166, 1983.

Suzuki, M. and **Oshima,** T., "Coordination Number of a Multiple Component Randomly Packed Bed of Spheres with Size Distribution," Powder Technology, Vol. 44, pp. 213-218, 1985.

Ting, M.J. and **Lin,** R.Y., "Effect of Particle-Size Distribution on Sintering", Journal of Materials Science, Vol. 29, pp. 1867-1872, 1994.

Zallen, R., "The Physics of Amorphous Solids," Jonn Wiley & Sons, Chapter Four, 1983.

Zheng, J., **Carlson,** W. B. and **Reed,** J.S. , "Dependence of Compaction Efficiency in Dry Pressing on the Particle Size Distribution," Journal of American Ceramic Society, Vol. 78, No. 9, pp. 2527-2533, 1995.

Zheng, J. and **Reed,** J.S., " Particle and Granule Parameters Affecting Compaction Effeciency in Dry Pressing," Journal of American Ceramic Society, Vol. 71, No. 11, pp. C456-C458, 1988.

Zok, F., **Lange,** F.F. and **Porter,** J.R., " Packing Density of Composite Powder Mixtures," Journal of American Ceramic Society, Vol. 74, No. 8, pp. 1880-1885, 1991.

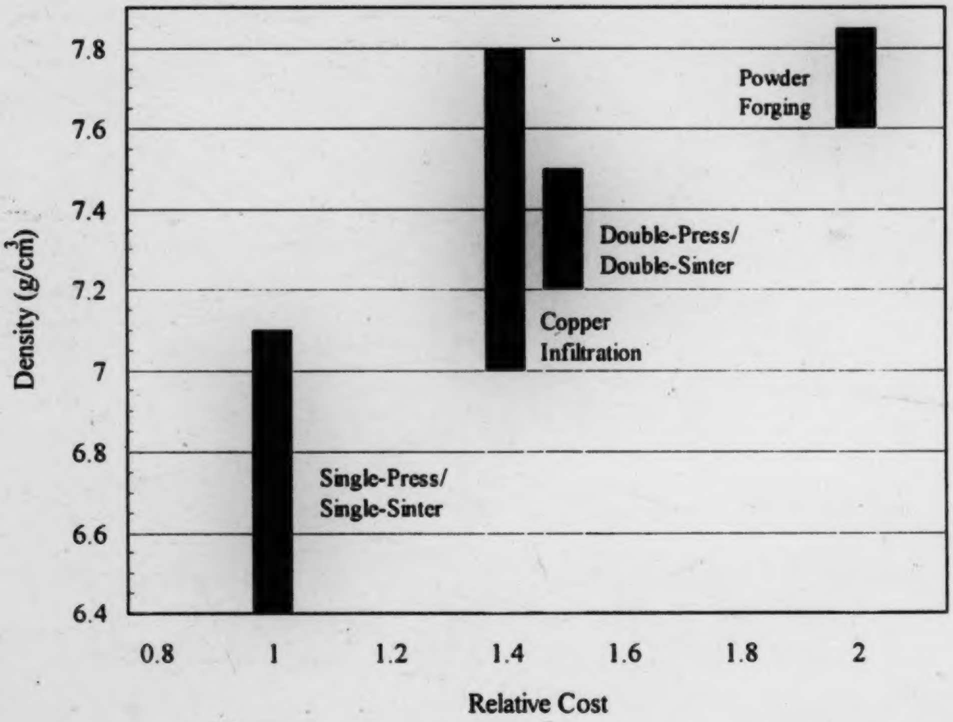

Figure 3-1. The relative cost and density ranges for various P/M processes.

[Rutz and Hanejke, 1995]

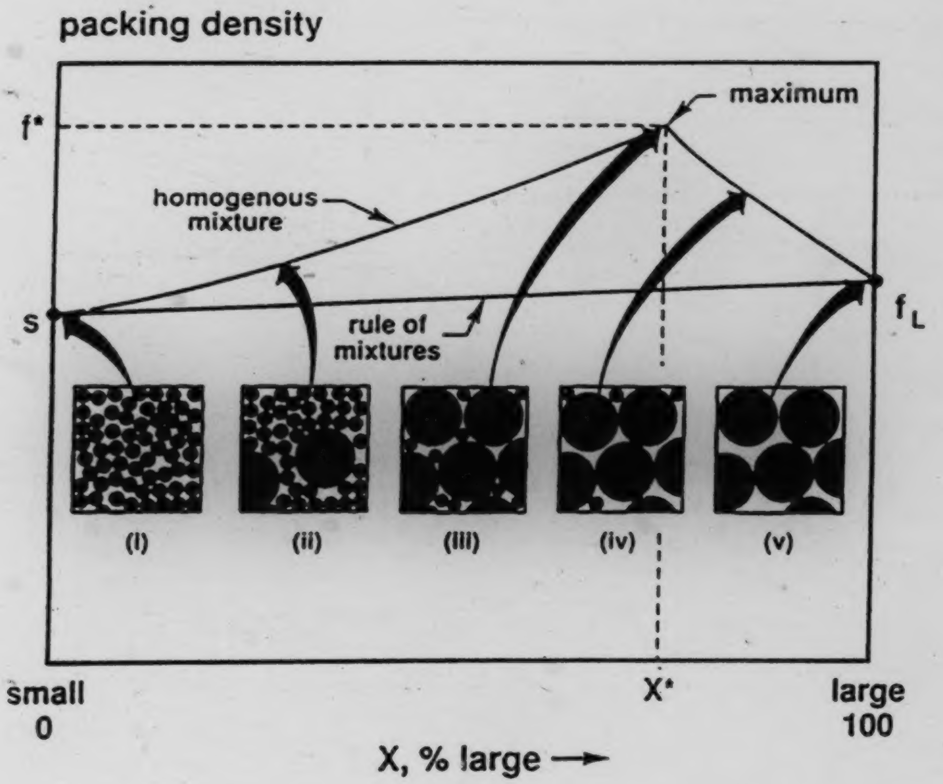

packing density
maximum
f*
homogenous mixture
S
rule of mixtures
f L
(i)
(ii)
(iii)
(iv)
(v)
small
0
X*
large
100
X, % large

Figure 3-2. Schematic illustration of the packing density variation with composition for a bimodal powder distribution. [German, 1992]

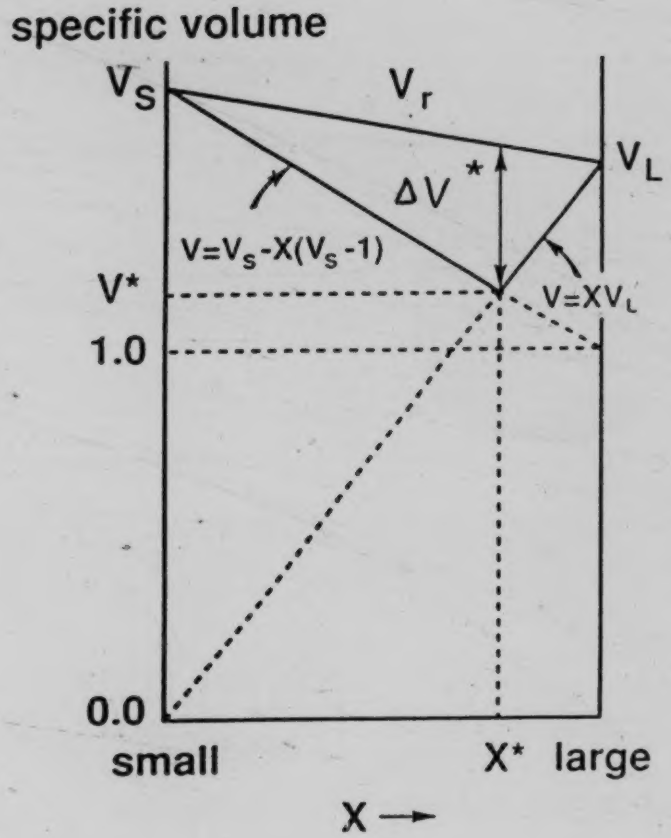
specific volume
V_S
V_r
V_L
ΔV^*
$V=V_S-X(V_S-1)$
$V=XV_L$
V*
1.0
0.0
small
X*
large
X →

Figure 3-3. The specific volume versus composition for bimodal powder distributions with perfect homogeneity and infinitely particle size ratio. [German and Bulger, 1992]

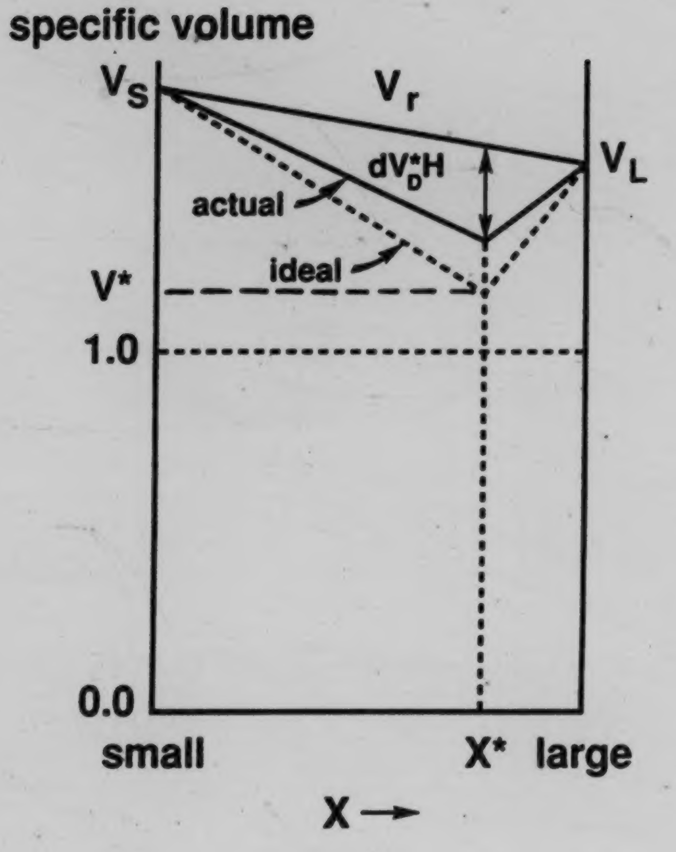
specific volume
V_S
V_r
V_L
dV*_D H
actual
ideal
V*
1.0
0.0
small
X*
large
X →

Figure 3-4. The specific volume versus composition for bimodal powder distributions with less than ideal homogeneity and a finite particle size ratio. [German and Bulger, 1992]

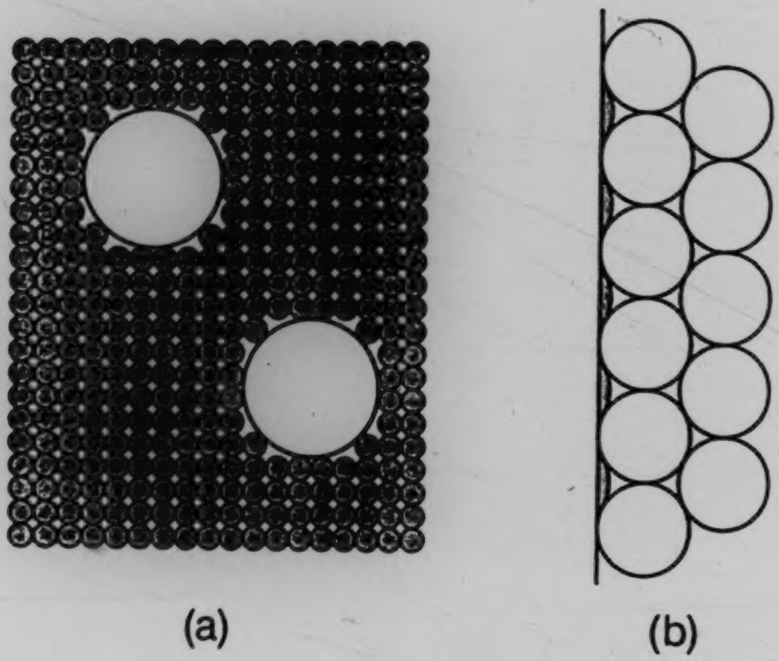

Figure 3-5. Schematic diagram showing the disruption in powder packing around isolated coarse particles. (b) Idealisation of the powder packing at the coarse particle surface. The shaded spherical caps represent the reduction in packing density due to the presence of the coarse particle. [Zok, et al., 1991]

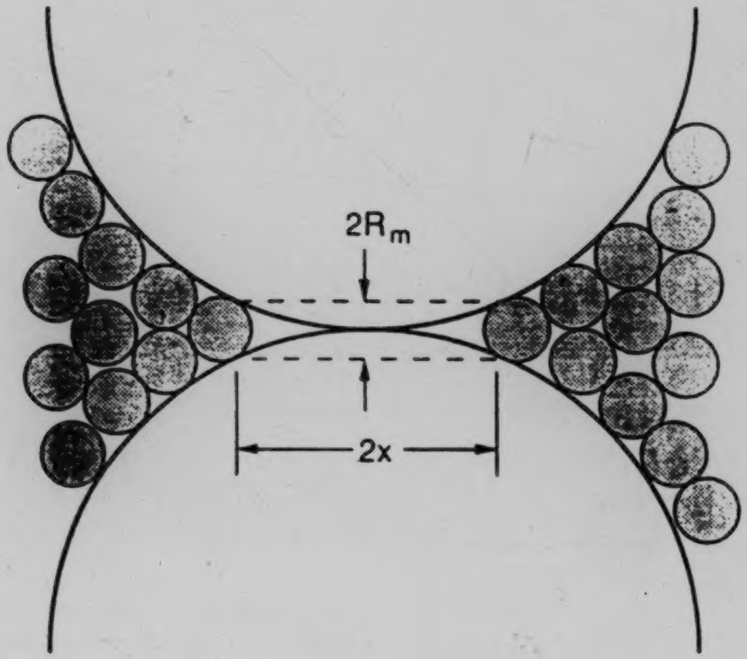

Figure 3-6. Schematic diagram showing the disruption in particle packing at a coarse-coarse particle contact point. Note the presence of the "excluded volume" into which fine particles cannot be packed. [Zok, *et al.*, 1991]

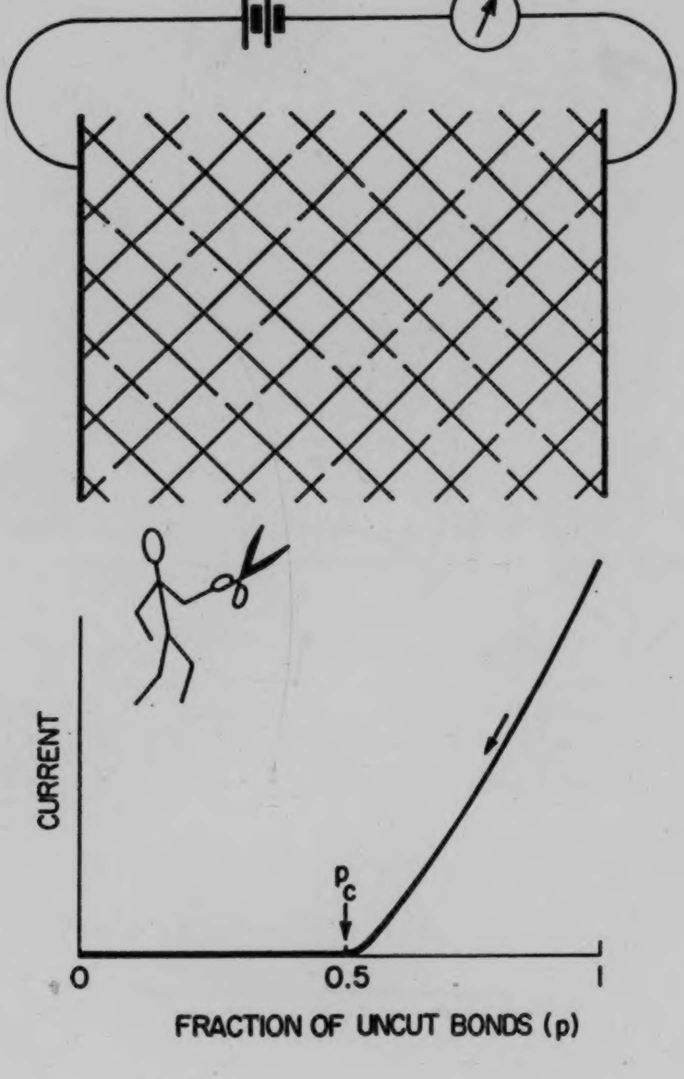
CURRENT
p_c
0
0.5
1
FRACTION OF UNCUT BONDS (p)

Figure 3-7. The randomly cut network as an example of percolation

[Zallen, 1985]

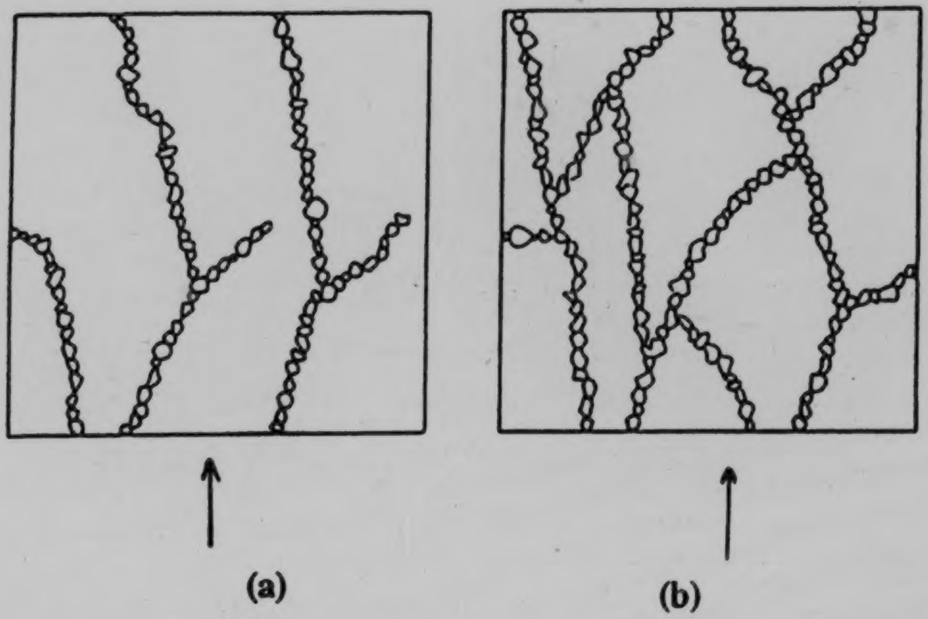

Figure 3-8. Simplified illustrations of clusters of particles held together by bonds formed through application of uniaxial pressure on powders in a rigid die. The arrow indicates the direction of force application. (a), Column of bonded particles oriented in the direction of force application. The columns are separated from each other by several particles. Each column is a finite cluster; (b), a percolating (infinite) cluster of bonded particles just above the percolation threshold of the solid particles D_{CS} traversing the system in all directions. [Holman, 1991]

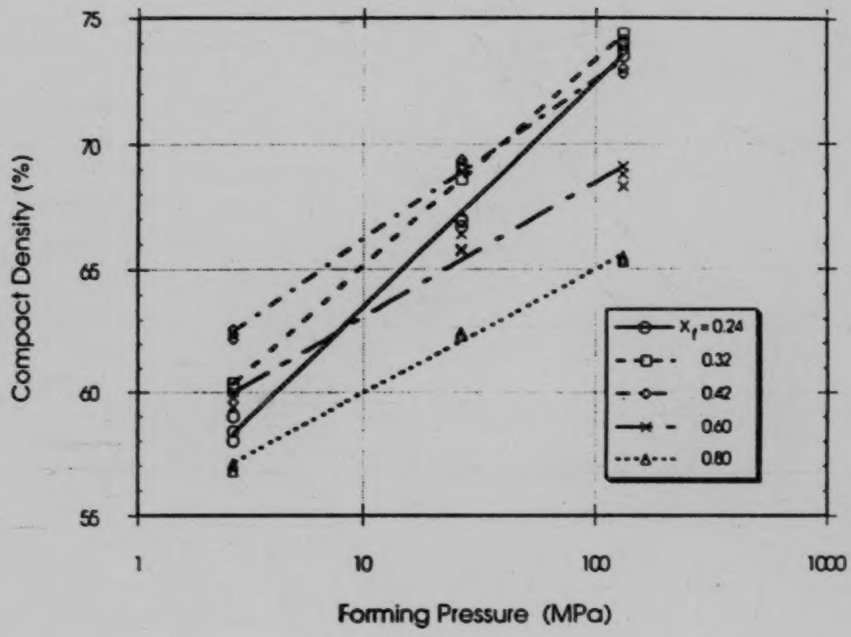

Figure 3-9. Compact density versus log (pressure) of blends of the coarse and fine alumnus, X_f is the volume fraction of the fines.[Zheng, *et al.*,1995]

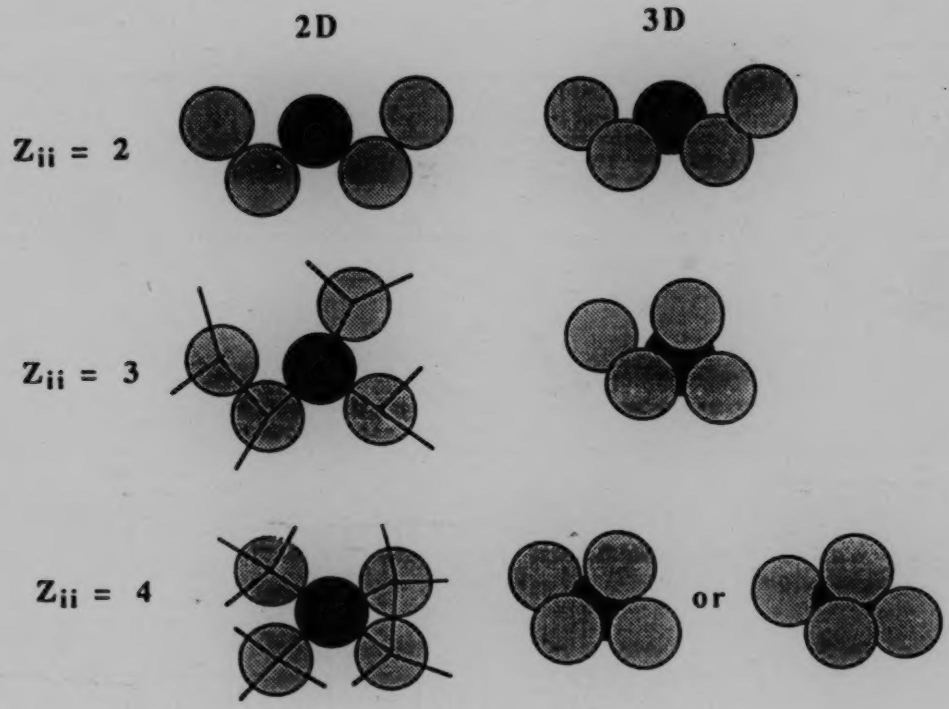
2D
3D
$Z_{ii} = 2$
$Z_{ii} = 3$
$Z_{ii} = 4$
or

Figure 3-10. Correlation between coordination and pressure transmission in a percolating cluster. Transmission paths are figured with line segments. [Bouvard and Lange, 1991]

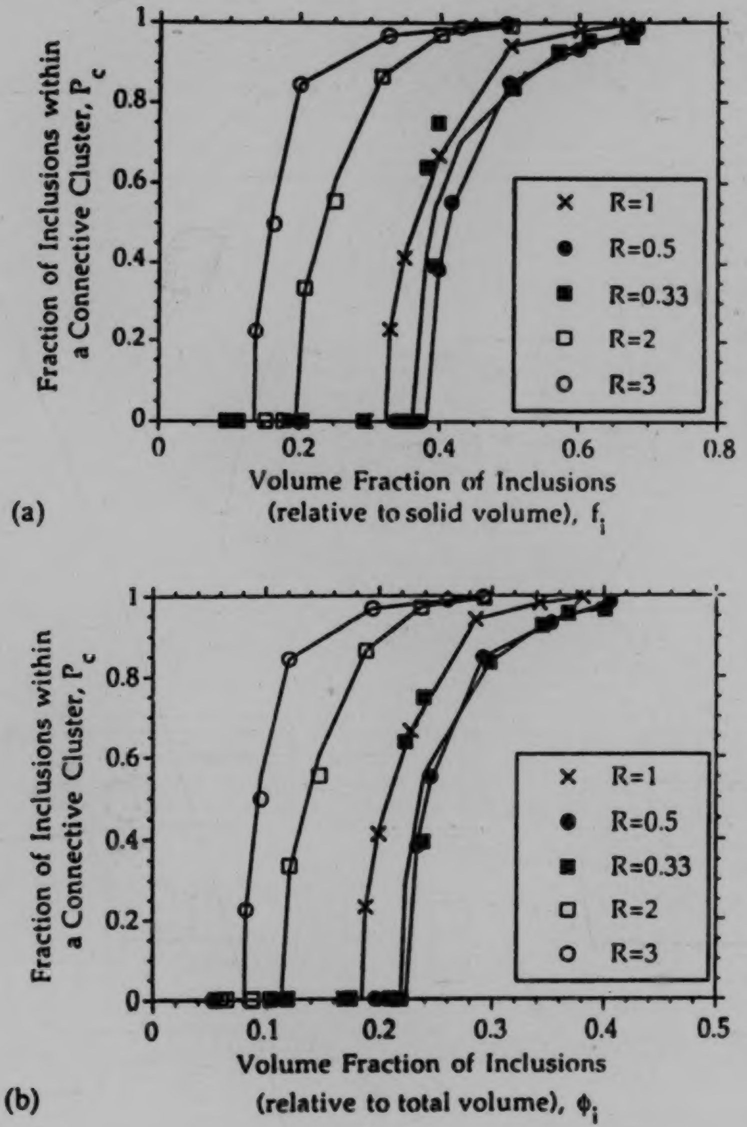

Figure 3-11. Fraction of inclusions in a percolating cluster vs volume fraction of inclusions relative to solid volume (a) or relative to total volume (b), where R is the size ratio. [Bouvard and Lange, 1991]

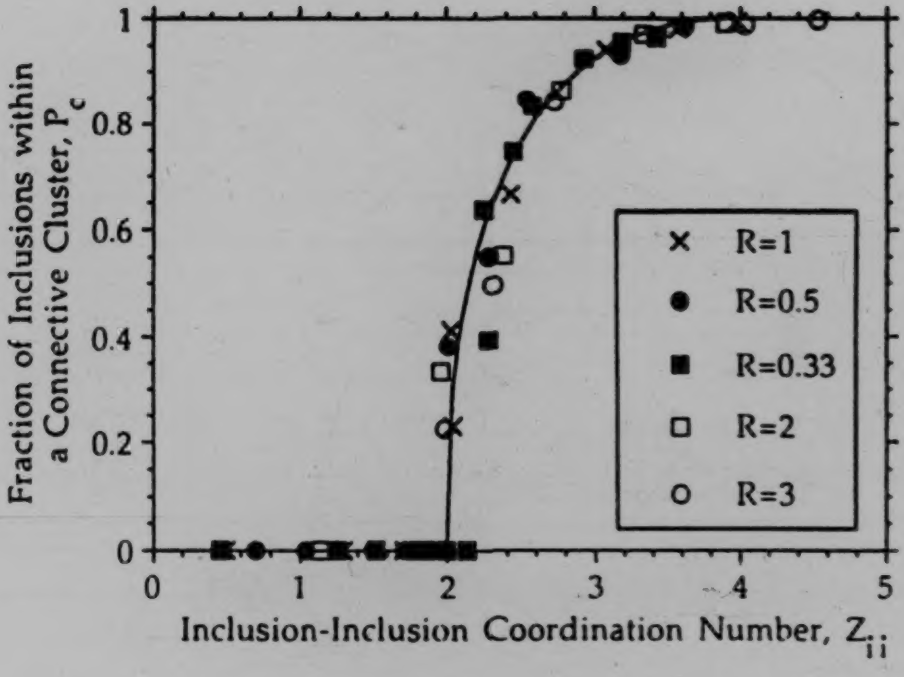

Figure 3-12. Correlation between the percolation parameter and the coordination number for inclusions touching one another. [Bouvard and Lange,1991]

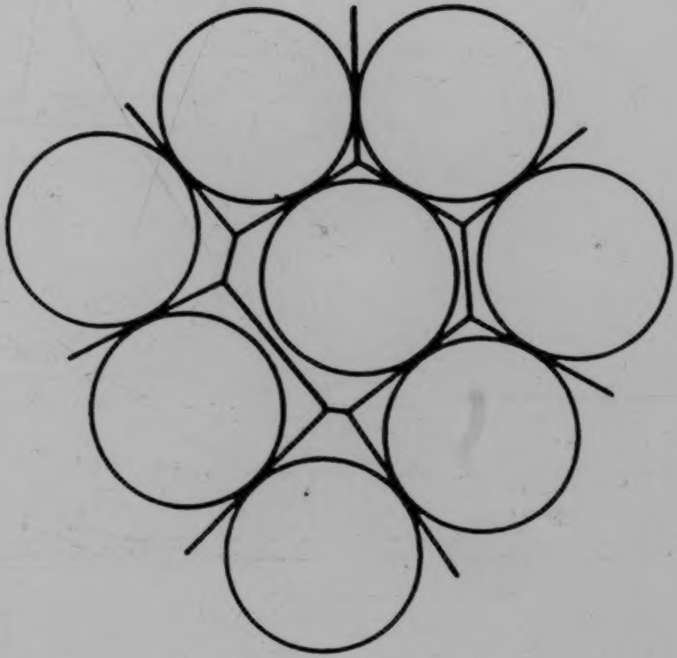

Figure 3-13. Two-dimensional schematic of the division of the powder bed into Voronoi cells. The non-contacting neighbours sharing a cell wall will form contacts as densification proceeds. [Arzt, 1982]

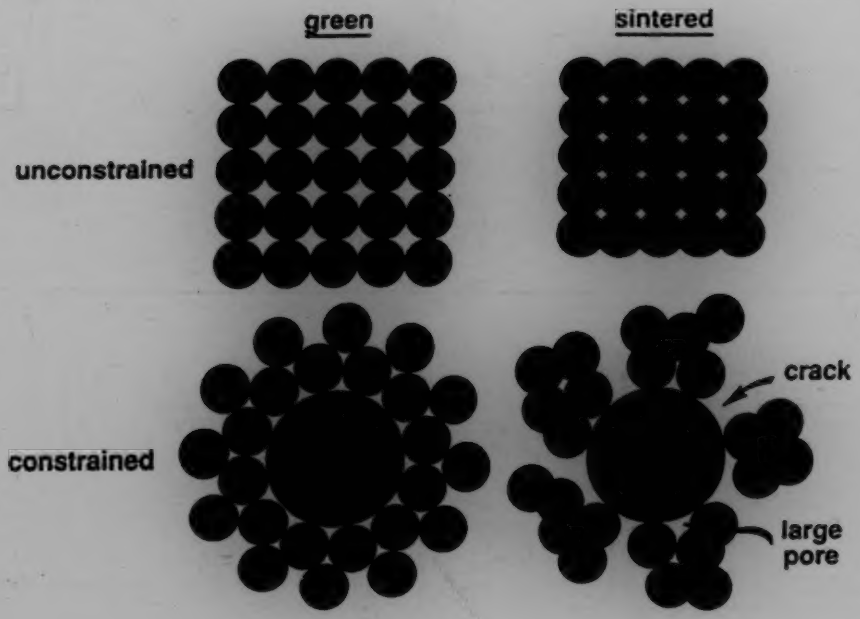
green
sintered
unconstrained
constrained
crack
large pore

Figure 3-14. Sketches of the densification behaviour. [German, 1992a]

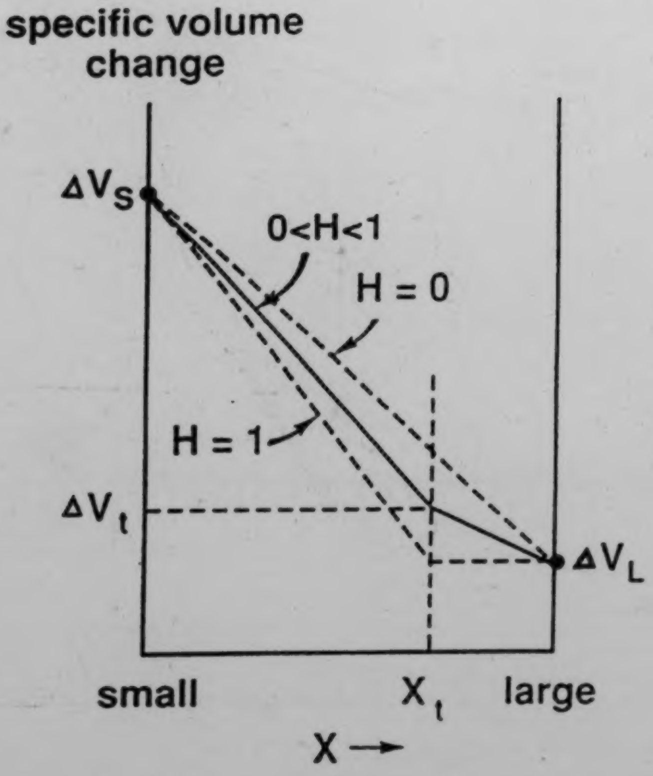

Figure 3-15. The change in specific volume during sintering as a function of the bimodal powder composition. [German, 1992a]

CHAPTER 4.

Improving P/M Parts By Bimodal Powder Distributions -- Experimental Test*

The purpose of this part of the work was to try to achieve comparable properties to wrought materials using standard P/M techniques (*i.e.* cold die pressing & sintering as opposed to HIP or powder forging) and to find the optimal coarse-fine powder composition to maximize green density and final density. Two important results were achieved in this experimental test. One was that the fine-coarse blend powders enhanced the green densities. Another was that very high final densities was achieved. The best results were obtained when the 17-4PH fine-coarse blend powders were compacted under a pressure of 700 MPa. The standard procedure conditions were:

---

*A version of this chapter has been published as "Improving P/M Parts Made with Conventional Processing by Bimodal Powder Mixtures," X.L. Chen, R.L. Eadie, D.S. Ghosh, and G. Roemer, in Advances in Powder Metallurgy & Particulate Materials - 1996, Compiled by T.M. Cadle and K.S. Narasimhan, Metal Powder Industries Federation, Princeton, New Jersey,Vol.1, pp. 3-3 -- 3-26, 1996.

Materials:	75% 17-4PH coarse powders + 25% 17-4PH fine powders (by mass)
Compaction:	die press at 700 MPa (single acting press, lubricant was lithium stearate)
Sintering:	heating rate at 10 K/min, room temperature --> 800°C hold for 1 hour --> 1300°C hold for 2 hours furnace atmosphere was Ar + 10%H_2
Heat treatment:	double ageing at 620°C for total of 8 hours (for precipitation hardening)

The properties of the 17-4PH samples treated following the above procedures were :

Green Density:	6350 ± 10 kg/m^3
Linear Shrinkage during sintering:	5.50 ± 0.01%
Hardness (HRC):	29 - 35 (before heat treatment), 29 ± 1 (after heat treatment)
Final Relative Density:	97.7 ± 0.1%
UTS (MPa):	886 - 900
YS (MPa):	738 - 755
Elongation (gauge length is 50mm) :	6.3 % - 8.2 %

All the test data shown in this Chapter are the average value taken from more than three points except the data for pure fine powder and 25% coarse + 75% fine powder which are based on two points.

4.1. Testing Materials

4.1.1. Chemical Composition

Two sizes of 17-4PH stainless steel powders (coarse and fine) were chosen for the experimental investigation. They have the same chemical composition which is shown in Table 4-1.

4.1.2. Size Distribution

The coarse and the fine powder size distribution were investigated using screen analysis and centrifugal sedimentation analysis, respectively. The results were close to the manufacturer's reports. The powder size distributions for coarse and fine powders are shown in Figure 4-1 and Figure 4-2 (Figure 4-1 : 100% coarse; Figure 4-2 : 100% fine). The mean particle sizes were 64.4 μm for coarse powders and 12.8 μm for fine powders based on mass. Based on population, the mean particle size were 39.5 μm for coarse powders and 7.3 μm for fine powders. The coarse/fine powder size ratio is around 5 : 1 (based on mass).

Analyzing the pure coarse and pure fine powders, it was found that they were approximately log-normal distributions. The log-normal distribution is described in terms of the mean particle size D and the geometric standard deviation σ as follows:

$$P(x) = \frac{1}{(2\pi)^{1/2}\sigma} \exp\left[- \frac{(x - \bar{x})^2}{2\sigma^2} \right] \tag{4-1}$$

where P(x) is the probability of finding a particle with size x = ln(D) where D is the particle diameter in μm. The mean particle size is given as $\bar{x} = \ln(\bar{D})$. The distribution spread parameter, σ, is defined as:

$$\sigma = \ln(D_{84} / D_{50}) \tag{4-2}$$

where D is the particle diameter and the subscripts indicate the percentage points in the cumulative particle size distribution (on the cumulative particle size distribution, 84 mass % corresponds to one standard deviation from the mean at 50 mass %). Thus, σ is the measure of the distribution width expressed in terms of the logarithm of the size at one standard deviation divided by the size at the mean. This is the logarithm of the size ratio giving one geometric standard deviation. Only two parameters are needed to describe a log-normal distribution, the mean size and the deviation.

The probability functions for coarse powder is :

$$P(x) = \frac{1}{(2\pi)^{1/2} \times 0.44} \exp\left[-\frac{(x - 4.165)^2}{2 \times (0.44)^2} \right] \tag{4-3}$$

and the probability functions for fine powder is:

$$P(x) = \frac{1}{(2\pi)^{1/2} \times 0.521} \exp\left[-\frac{(x - 2.545)^2}{2 \times (0.521)^2} \right] \tag{4-4}$$

Based on the coarse and fine powder distribution functions, the size distribution of the bimodal systems for different coarse-fine mass fractions were calculated and several examples are shown as Figure 4-3: 90% coarse + 10% fine; Figure 4-4 : 75% coarse + 25% fine; Figure 4-5 : 60% coarse + 40% fine; Figure 4-6 : 45% coarse + 55% fine). The majority component in the distribution changes from coarse to fine powder from Figure 4-3 to Figure 4-6.

4.1.3. Particle Shape

The coarse powder and the fine powder were produced by water atomisation and gas atomisation respectively. Figure 4-7 shows micrographs of the coarse and the fine powders. The coarse powder's shape is somewhat irregular but is mostly equiaxed. The shape of the fine powders is spherical. The shape of the coarse particles will be modelled using equivalent sized spherical powder -- the closest approximation which is tractable. This approximation will have errors – especially prior to compaction. After compaction and sintering, the expected difference between the actual powder and the nearest size spherical approximation would be small.

4.1.4. Particle Cross-Section and Grain Structure

Powders were mounted and polished. Both unetched and etched cross sections were examined. Figure 4-8 and Figure 4-9 show the cross-section and grain structure of the powders. It is observed that there are no internal pores in the fine powders and there are very few internal pores in the coarse powders. The grain size (around 2-3μm) is the same in both fine and coarse powders. The reason may be that coarse powders were made by water-atomisation and fine powders were made by gas-atomisation. The grain size tends to be small in the large particles because of the higher cooling rate even though the diameter is larger.

4.1.5. Flow Rate, Apparent Density and Tap Density

Flow rates of powders were measured according to standard MPIF 03. Apparent density were measured according to standard MPIFSP 04 (free-flowing bimodal powder distributions) or standard MPIF 28 (non-free-flowing bimodal powder distributions). Tap densities were measured according to MPIF 46. [Metal Powder Industries Federation, 1991]

The flow rates for the different distributions are listed in Table 4-2. In this experimental test, the pure coarse powder was studied first then different amounts of fine powder were added into pure coarse powder. Apparent and tap density versus coarse-fine composition is shown in Figure 4-10. The experimental errors are ±0.02g/cm^3 for apparent density and ±0.014 g/cm^3 for tap density. The mass per cent of fine powder will be used for the x axis in this and the following chapters. It is observed that the highest value of apparent and tap density is at 40% fine. The peak is not sharp. From 30% to 55% fine, the apparent and tap density only changed a little. Apparent density is related to loose random packing and tap density expresses the close random packing. They also have a direct correlation to the coordination number.

4.2. Testing Procedure (Powder Compacts)

The preparation procedure followed that for conventional P/M processes. Different compositions of coarse and fine powders were weighed and then mixed by ball milling for 2 hrs. The lubricant - lithium stearate (0.6% by mass) was added to the powders before milling. Plastic bottles with a radius of 2.5 cm and 3.5 mm radius iron balls were used in mixing. The mixing time was 1 hour. After ball mixing, the size distribution of the coarse powder was measured by sieving and it had remained the same. Each sample was weighed out and compacted with a single acting die press machine. Samples were pressed at 700 MPa. The powders were pressed into tensile test samples corresponding to MPIF Standard 10. After pressing, the green densities of the samples were measured according to MPIF Standard 42 [Metal Powder Industries Federation, 1991]. Then, the samples were sintered under the same conditions at 1300 °C with one exception which was sintered at 1250 °C. The following standard procedure was used for sintering: The heating rate was kept at 10 K/min; the samples were heated to 800 °C and were held at that temperature for 1 hour to burn off the binder; then the samples were heated to 1300 °C and held 2 hours for sintering. The furnace atmosphere was Ar + 10%H_2. After sintering, some samples were tested as-sintered, while, others were given heat-treatments according to NACE Standard TM0175-90. Finally, the linear shrinkages, final densities, hardness, UTS, YS, and elongation were measured. For some of the samples, the porosity was measured.

4.3. Compaction of Bimodal Powder Distributions

4.3.1. Green Compact's Characteristics

The green compacts were easily broken by hand. Fresh fracture surfaces of the green compacts for different distributions were examined using the SEM. The bonding in pressed samples and mixing of coarse and fine particles can be directly observed in Figure 4-11 (360X). Even though the powder particles were pressed, the individual particles can be clearly observed. There were different amounts of deformation for the particles. Most particles had flat polygonal shapes.

In Fig. 4-11a and 4-11e (100% coarse and 100% fine powders), there are a large number of bridges between particles. The networks are pure coarse and pure fine particle networks respectively. In Fig. 4-11b (75% coarse powders), there is a coarse particle network and the fine particles fit in the spaces between the coarse particle sites. It is apparent that some areas have concave surfaces where large particles have been pulled out during fracture. In these areas, the fine particles seem to be clustered together. In Fig. 4-11d (25% coarse powders), coarse particles mix in the fine particle matrix. In Fig. 4-11c (50% coarse powders), a fine particle network exists but the coarse particle network just disappears. Note that more local plastic deformation (flat polygonal surfaces) is observed in Fig. 4-11b (75% coarse +25% fine powders) which corresponds to the highest green density.

4.3.2. Green Density

The relationship between coarse-fine powder composition and green density is shown in Figure 4-12. The experimental error is ± 0.01g/cm^3 (0.1%). As shown in Figure 4-12, the green density has a maxima at about 20% fine composition.

Comparing German's results [German and Bulger, 1992] (Figure 3-4) and the current experimental result, it is observed that they are quite similar (maximum density and minimum specific volume have the same meaning). The coarse to fine size ratio was around 10:1 in German's study. Coarse to fine size ratio of 5:1 was used in these tests. Considering the interstitial site size, it is believed that there is only a small difference expected when the coarse/fine radius ratio changes from 10:1 to 5:1. These experimental results showed that the distributions had higher densities, but the peak was not sharp (Fig. 4-12). One of the reasons may be that the size ratio is not large enough. Another reason may be that both coarse and fine powders have size distributions. It's worth mentioning that German studied the packing density in a powder injection molding system. In this system binder which should have flowability was used to improve the homogeneity of the distributions and prevent fine powder aggregation. In the kind of system which is being studied, the homogeneity of distributions are achieved by applying ball milling and then external pressure which caused powder rearrangement and plastic deformation.

4.4. Sintering of Bimodal Powder Distributions

4.4.1. Sintered Density for Bimodal Powder Distributions

The samples were sintered at 1300 °C and the sintering test results are shown in Figure 4-13 (final density versus wt % fine powder) and Figure 4-14 (specific volume change versus wt % fine powder). The experimental errors are around ±0.1%. The highest final density (97.7% relative density) was achieved with approximately 30% fine powder mass fraction (Figure 4-13). In Figure 4-14, specific volume change of bimodal distributions stayed approximately constant (it agrees with German's prediction [German, 1992]) when the fine mass fraction changes from 0% to 30%. On the other hand, at mass fractions rich in fine particles, the specific volume change decreases as coarse particles are added, since the regions occupied by coarse particles are already dense. The shrinkage during sintering increases with an increasing amount of fine powder. This corresponds to higher powder surface areas - hence higher driving force for the sintering process.

It is found that there are some conflicts between these experimental results and German's model [German and Bulger,1992]. The model indicates that the highest final densities are obtained by using fine powder. The highest final densities were obtained by using mixed coarse-fine powders. Even though the shrinkage of fine powder-rich distribution is larger than that of coarse-rich powder distribution, their final densities are very similar. The higher green density compensates for lower shrinkage. With respect to final density, any coarse-fine composition between 10% and 55% fine composition could be chosen to satisfy the need.

But from the view of practise and economy, mixed powder (about 30% fine composition) is preferred. When the fine composition is above 35%, there are often laminations in the samples and the pressed samples are easily broken (lower green strength). If the coarse powder composition is lower, then a binder is needed. The fine powders are more expensive and harder to handle (they tend to oxidise). Also, the shrinkage during sintering is higher which reduces dimensional control when the amount of fine powder is higher.

4.4.2. Grain Structure of the Sintered Samples

Pore and grain size, shape and distribution are important factors in sintering, especially in the later sintering stage, to control final density. The SEM and optical microscope were used to observe them. The sintered samples were first cut with a rotary diamond or silicon carbide saw then mounted and polished. The etched samples were prepared for examination of grain structure and unetched samples were prepared for examination of pore structure. It is observed that the grain sizes are the same (around 30μm) but pore sizes are different in different distributions (Figure 4-15 and 4-16). Sintering conditions control the grain size. Pore size is influenced by particle size.

Figure 4-16 shows the pore structures of sintered samples for different coarse-fine mass fractions. In Figure 4-16, all the samples contain 0.56 mass % lubricant and were sintered at the same condition (1300 °C for 2 hours). For the pore size distribution, there is an obvious difference between sintered samples of pure coarse powders and those in the rest of the samples. For the coarse powders, the pore sizes are highly variable, the pore distribution is not uniform and the average pore size is larger in the sintered 100% coarse powder. For more than 25% by mass fine powders, the pore structures are similar (Figures 4-16b to 4-16e). The pore size distribution is more uniform. One of the interesting phenomena of sintering bimodal distributions is that the pore structure difference between bimodal distributions and 100% fine powders is small. This is also one of the important factors which produce very high final density with only a small amount of fine powder (25%). The porosity measured by SEM image analysis were shown in Table 4-3. The results agree with the results measured by the MPIF standard 42 method. The 75%-25% sample has the highest final density. Since SEM image analysis uses an area about 500 μm^2 (very small) to calculate porosity and the pore distribution usually is not uniform, the results are only approximate.

4.4.3. Influence of Temperature

Since sintering is a thermally-activated process, the temperature is a more effective factor than any other variable. The results from sintering at 1250 °C are shown in Figure 4-17. The experimental error is ± 0.01 g/cm^3. Compared with Figure 4-13 (sintering at 1300 °C), it is clear that final densities are lower for the entire range of samples sintered at lower temperature. When the density difference caused by different powder distributions is less than 0.1 g/cm^3, the difference in density caused by temperature difference (only 50 °C) reached 0.2 g/cm^3. The lower temperature does not simply favour the sintering for coarse particle-rich distributions. Firstly, there is no shift for the maximum density composition when sintering temperature decreases. Secondly, with a decrease of temperature, the difference between the coarse-rich end and maximum value changes from 0.06 g/cm^3 to 0.09 g/cm^3, while the difference between the fine-rich end and maximum value changes from

0.06 g/cm^3 to 0.04 g/cm^3.

4.5. Mechanical Properties

Both high green density and high final density were achieved by using bimodal powder distributions. The average results (75% coarse + 25% fine powders) of the properties for 17-4PH samples treated according to the above procedures (pressed at 700 MPa, sintered at 1300 °C) and the data of 17-4PH wrought products (both samples are heat-treated at same condition - H1150) are given below:

	P/M sample (this result)	Wrought products
UTS	131 ksi (900 MPa)	135 ksi (930 MPa)
YS	106 ksi (730 MPa)	105 ksi (725 MPa)
Hardness	30 HRC	28-36HRC
Elongation	7.4%	16%

The mechanical properties of high density bimodal powder metallurgy products are close to those of wrought products. The lower elongation value is expected because there is 2% porosity in the P/M compacts.

Tensile tests and hardness tests were done for different coarse-fine composition powder distributions. The UTS and hardness data are shown in Tables 4-4. The mechanical properties of the mixed powder system are very good, even for the samples which were sintered at 1250^{0}C. For most samples, the relation between the final density and mechanical properties obeys the common rule -- the higher the density, the higher the mechanical properties, One exception is that the UTS and hardness reach the highest value when the coarse-fine composition are around 60%-40%. This phenomenon may be explained by Figure 4-16. Although the 60%-40% samples are not the most dense, it has the smallest pore size , round shape and most uniform pore distribution. At a given porosity, smooth, small and uniformly distributed pores give the greatest strength since the effective solid fraction volume is largest.

Very high sintered densities (97.7% relative density) and mechanical properties (comparable to wrought products) were achieved by using the conventional P/M processes of single compaction and single sintering in bimodal distributions of precipitation hardening stainless steel powders. Both coarse and fine powders had log-normal size distributions. The medians of the two sizes were in the ratio of about 5:1. A 2% increase of final density is achieved by adding only 25% fine powders and the final density of the bimodal powders reached the same value as 100% fine powders. This offers a more effective way to get high performance P/M products. Using bimodal powders has practical significance in reducing cost and achieving better dimensional control (lower shrinkage) with a high final density. Among the influences, it is concluded that sintering temperature is the most powerful influence, the next most important is the coarse-fine composition.

4.6. References

German, R.M., "Prediction of Sintered Density for Bimodal Powder Mixtures", Metallurgical Transactions A, Vol. 23A, No. 5, pp. 1455-1465, 1992.

German, R. M. and **Bulger**, M., " A Model for Densification by Sintering of Bimodal

Particle Size Distributions," International Journal of Powder Metallurgy, Vol.28, No. 3, pp.301-311, 1992.

Metal Powder Industries Federation, " Standard Test Methods for Metal Powders and Powder Metallurgy Products," 1991.

Table 4-1. Compositions of the 17-4 PH Powders

Cr%	Ni %	Mo %	Mn %	Graphite % *	Si %	S %	Cu %	C %	Iron
16.3	4.11	0.01	0.17	0	0.46	0.01	3.86	0.026	rest

* Graphite % -- Added to Powders

Table 4-2. Flow rates of bimodal powder distributions

Coarse-Fine composition (%--%)	Flow Rate (S/50g)
100--0	32
90--10	41
85--15	46
80--20	no flow
75--25	no flow
70--30	no flow
65--35	no flow
60--40	no flow
55--45	no flow
50--50	no flow
45--55	no flow
0--100	no flow
0--100 (+binder)	no flow

Table 4-3. Porosities for different coarse-fine composition
17-4 PH coarse-fine powder distributions

Coarse-fine composition (% -- %)	Porosity % (SEM image analysis)	Porosity % (MPIF standard 42)
90 -- 10	5.03	3.58
75 -- 25	2.8	2.3
60 -- 40	2.87	2.6
45 -- 55	3.22	3.7

Table 4-4. The coarse-fine composition vs. UTS and hardness

Coarse-fine composition %-%	Hardness* HRC	UTS* MPa	Hardness** HRC	UTS** MPa
90% - 10%	29	843.1	30.5	888.9
85% - 15%	29.5	863.3	31	
80% - 20%	30	865.6	32	905.1
75% - 25%	32	893.4	33	907.2
70% - 30%	32.5	896.3	32.5	917.8
65% - 35%	31.5	889.6	32	930.2
60% - 40%	31.75	912.3	33.5	922.2
55% - 45%	31.75	904.4	33	934.9
50% - 50%	32	931.3***	33.5	915.2
45% - 55%	30.5	913.1	33.3	929.5

* The samples were sintered at 1250 ^{0}C. Their final densities are about 95% relative density.

** The samples were sintered at 1300 ^{0}C. Their final densities are about 98% relative density.

*** This data is seem not reasonable since it is higher than the UTS of the same coarse - fine composition sample sintered at higher temperature and gave a much higher final density.

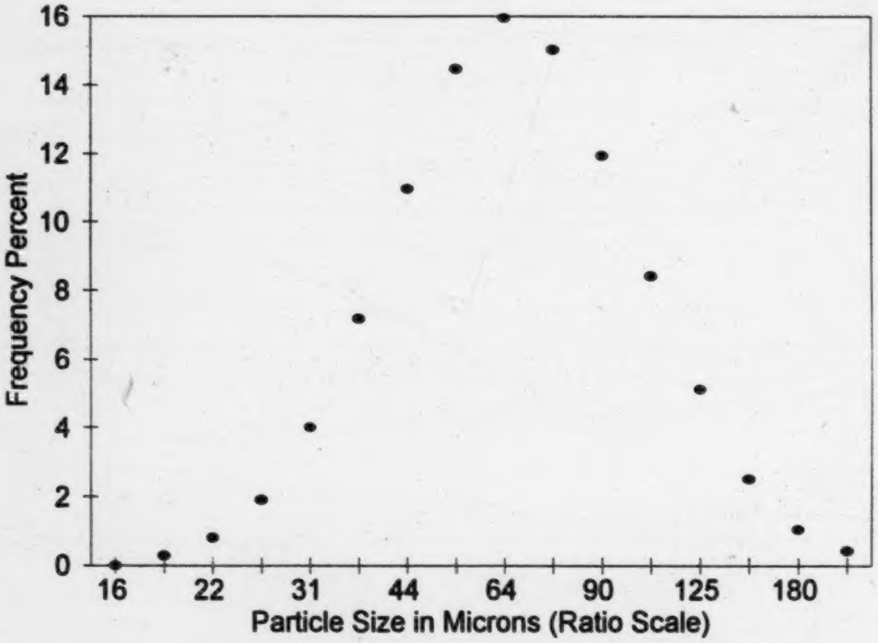

Figure 4-1. Size distribution of 100% coarse powder

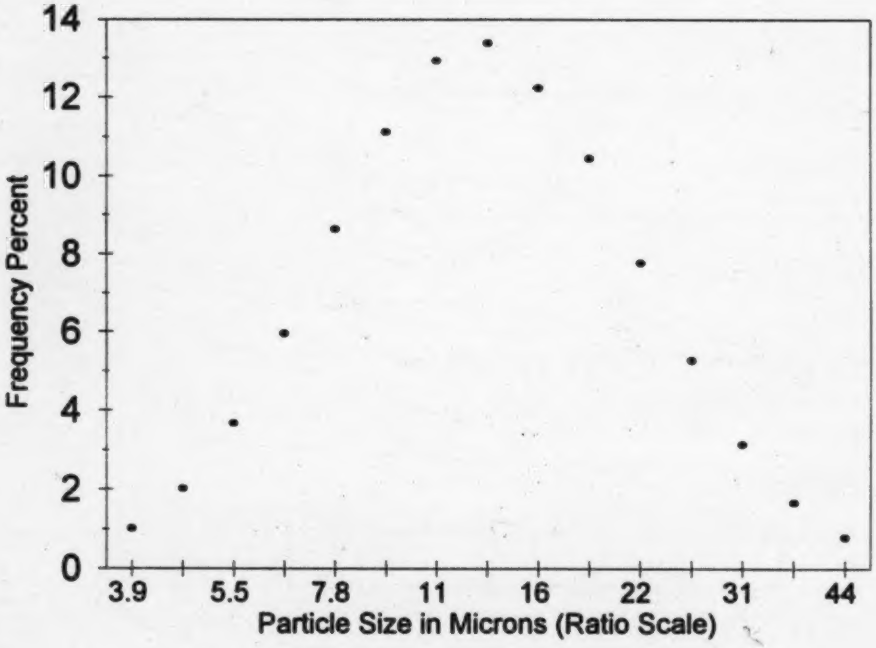

Figure 4-2. Size distribution of 100% fine powder

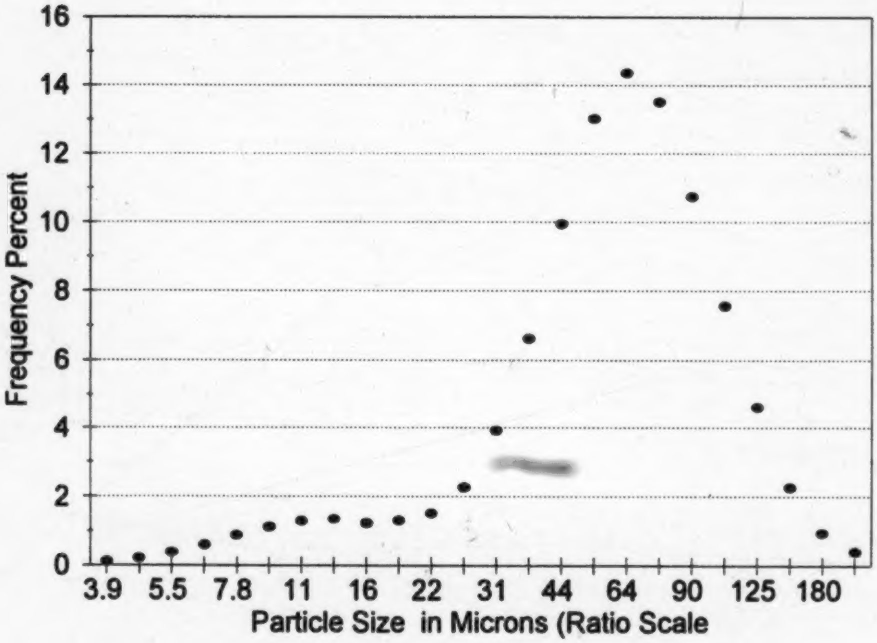

Figure 4-3. Size distribution of 90% coarse powder + 10% fine powder

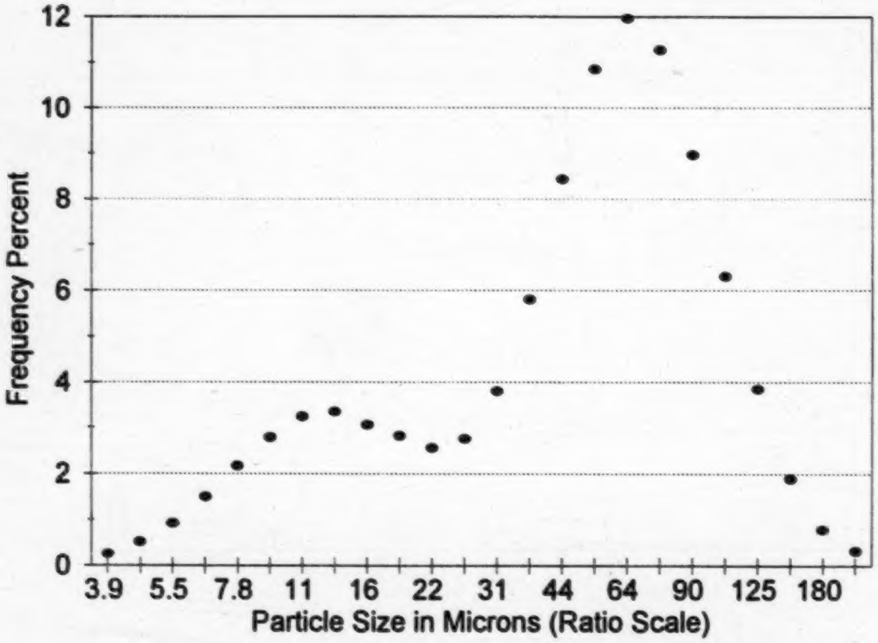

Figure 4-4. Size distribution of 75% coarse powder + 25% fine powder

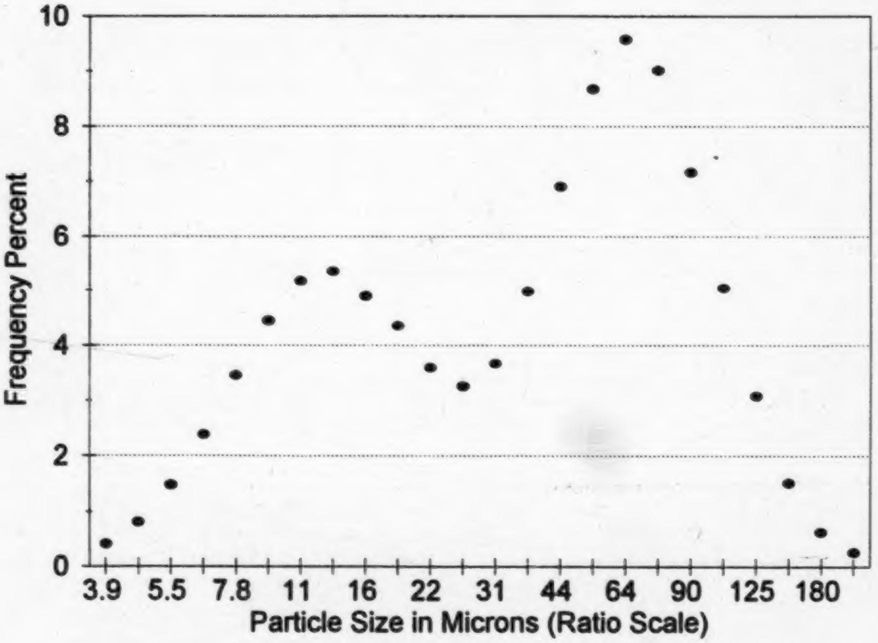

Figure 4-5. Size distribution of 60% coarse powder + 40% fine powder

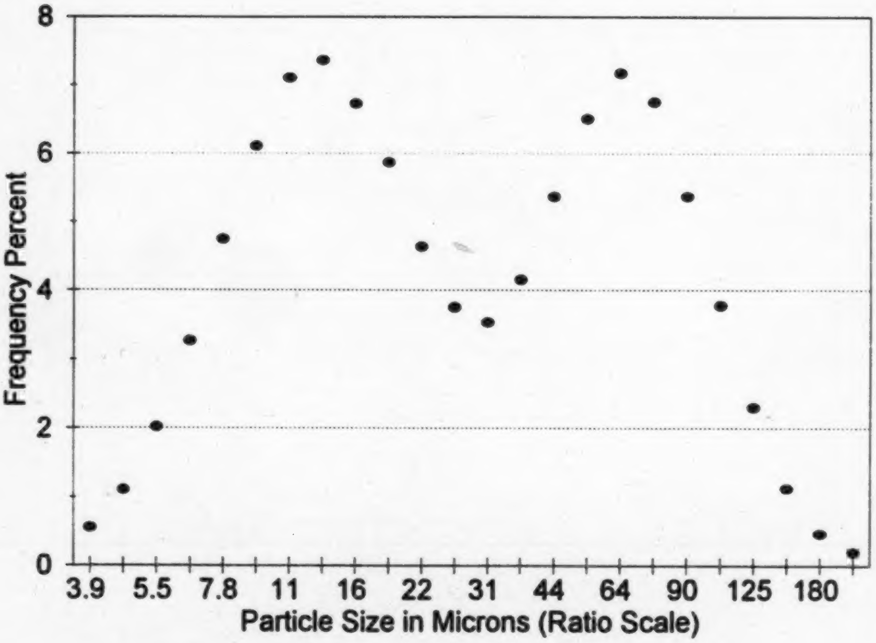

Figure 4-6. Size distribution of 45% coarse powder + 55% fine powder

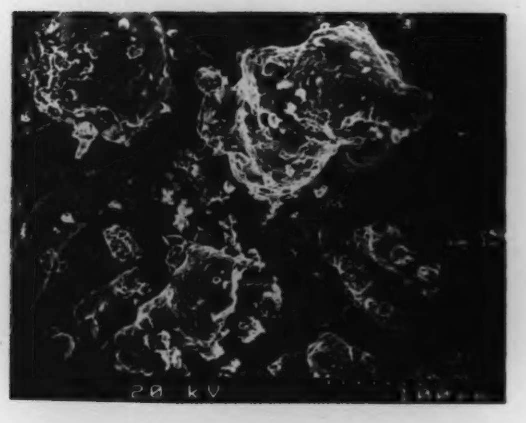

4-7 (a)

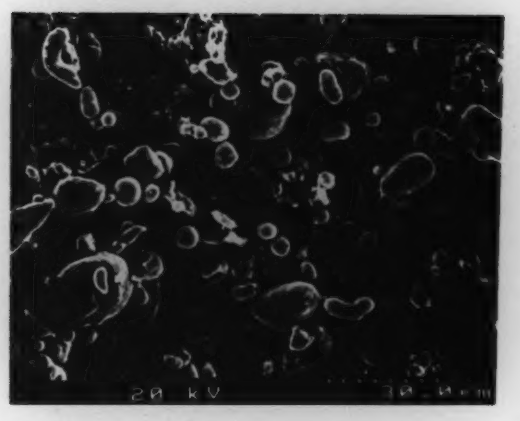

4-7 (b)

Figure 4-7. SEM micrograph of coarse 4-7 (a) and fine 4-7 (b) powders

4-8 (a)

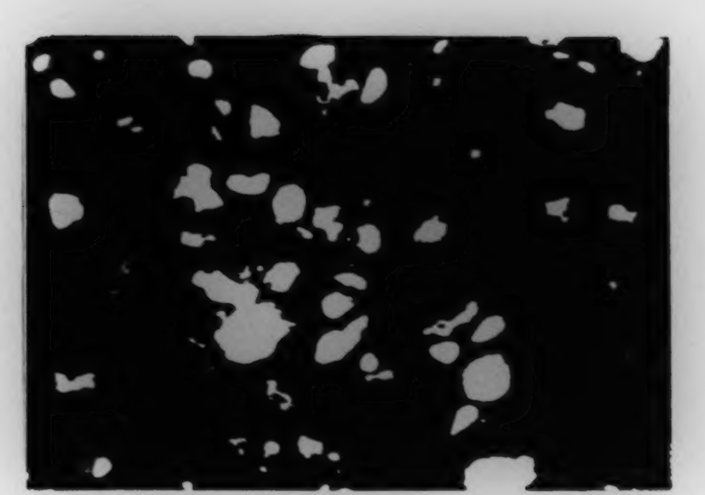

4-8 (b)

Figure 4-8. Optical micrograph of cross-section of the powders

4-8 (a) : coarse powders; 4-8 (b): fine powders.

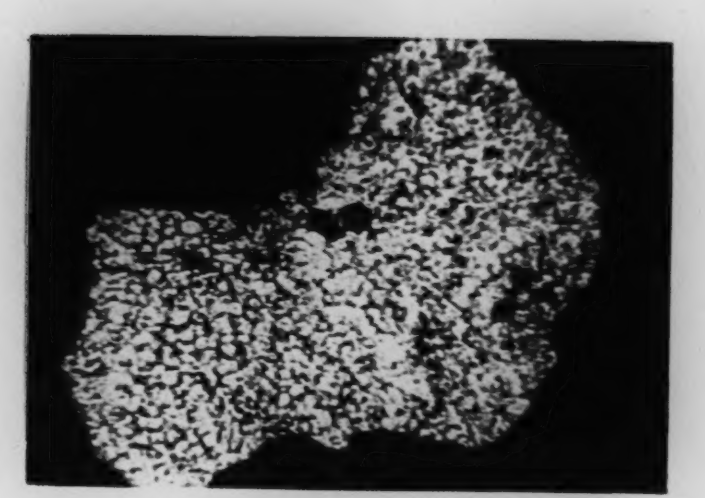

4-9 (a)

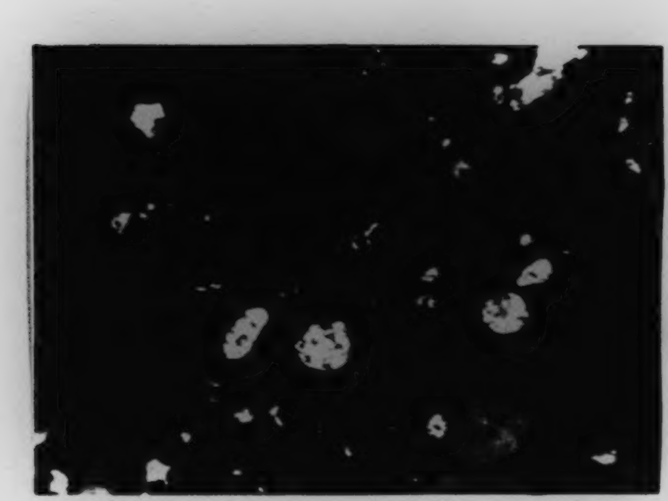

4-9 (b)

Figure 4-9. Optical micrograph of etched cross-section of the powders.
4-9 (a) : coarse powders; 4-9 (b): fine powders.

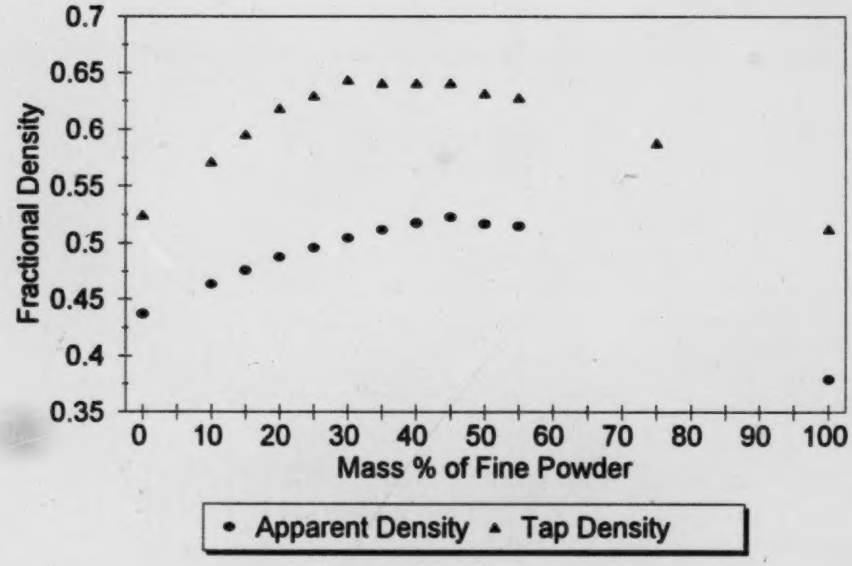

Figure 4-10. Densities versus mass fraction for bimodal powder distributions

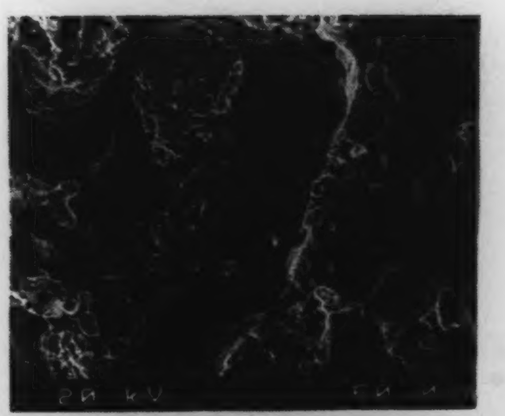

a: 100% coarse powders

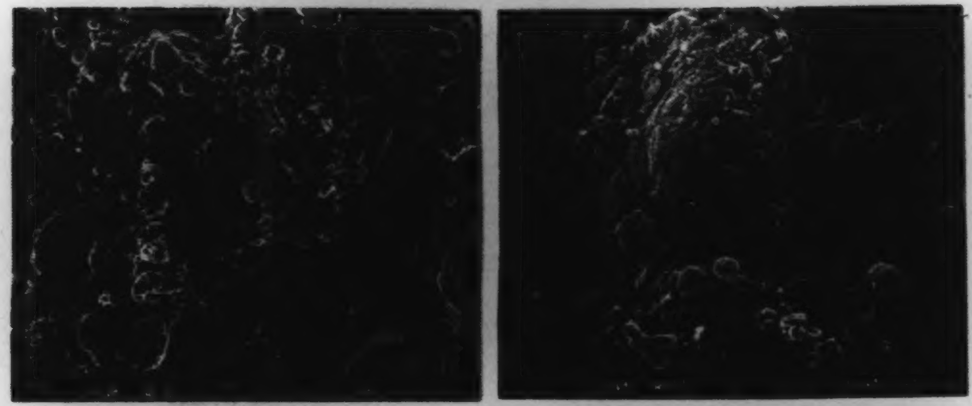

b: 75% coarse+25% fine

c: 50% coarse+50% fine

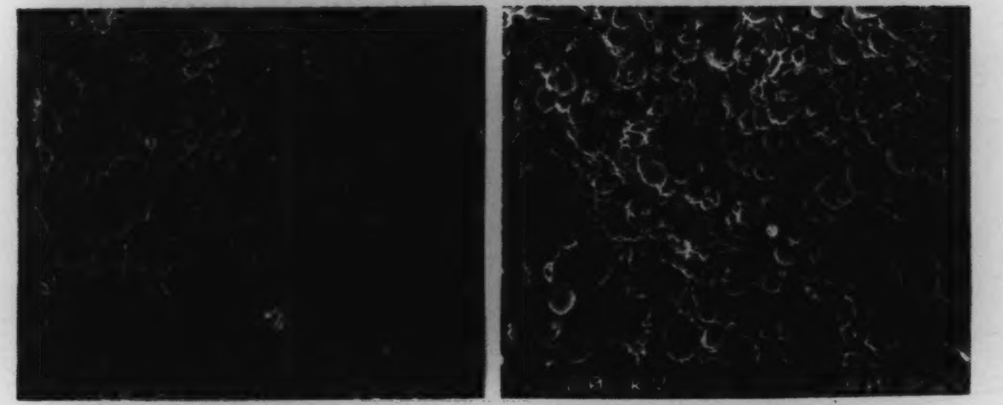

d: 25% coarse+75% fine

e: 100% fine powders

Figure 4-11. Fracture surface of green compacts for different coarse-fine mass fractions.

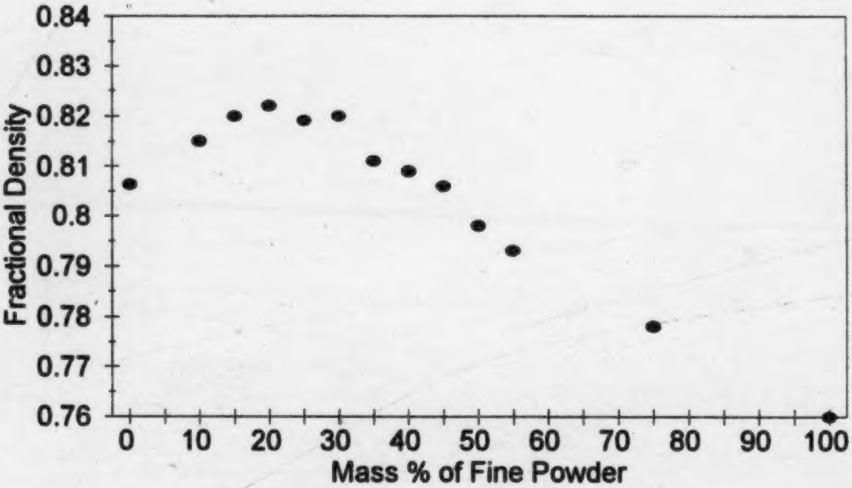

Figure 4-12. Green densities versus mass % of fine powder

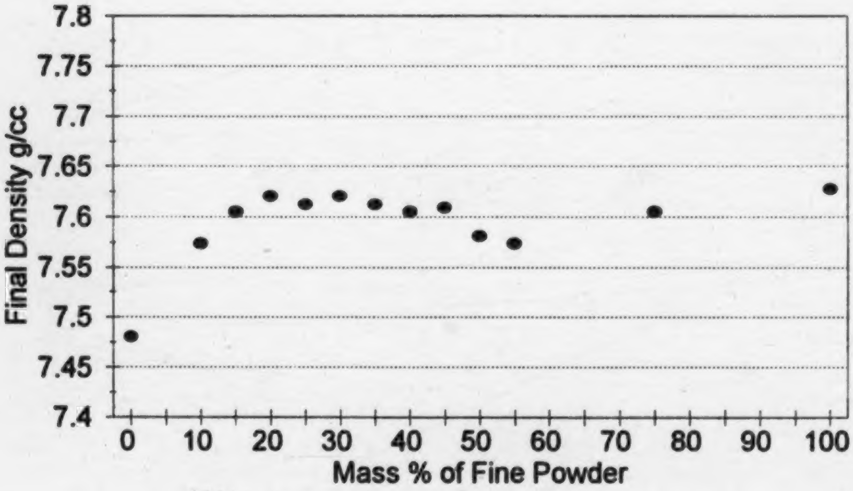

Figure 4-13. Final densities versus mass % of fine powder

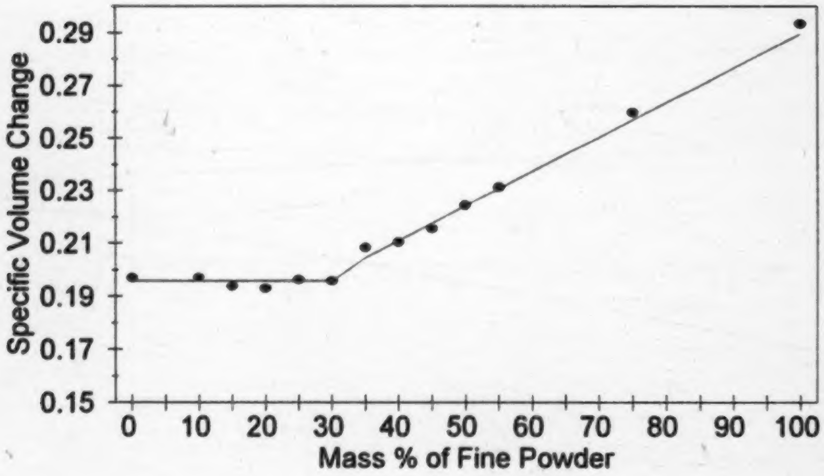

Figure 4-14. Specific volume change versus mass % of fine powder during sintering

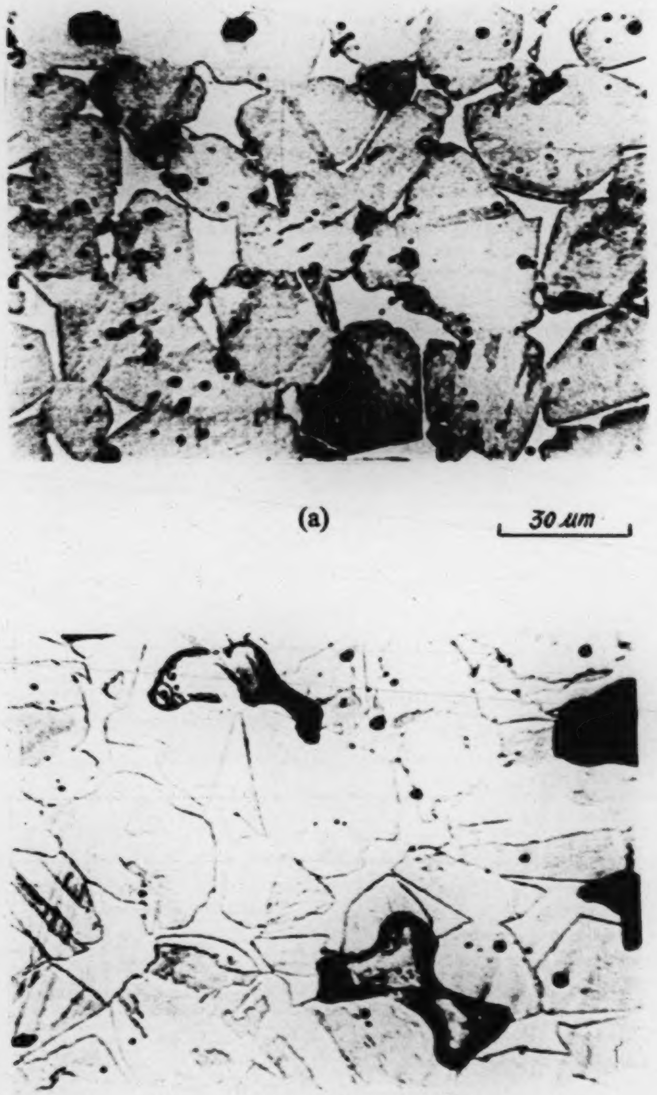

(a)

(b)

Figure 4-15. Grain Structures for Sintered Samples (1300 °C 2 hrs) 720X

(a) : 75% coarse - 25% fine ; (b): pure coarse powders

a: 100% coarse powders

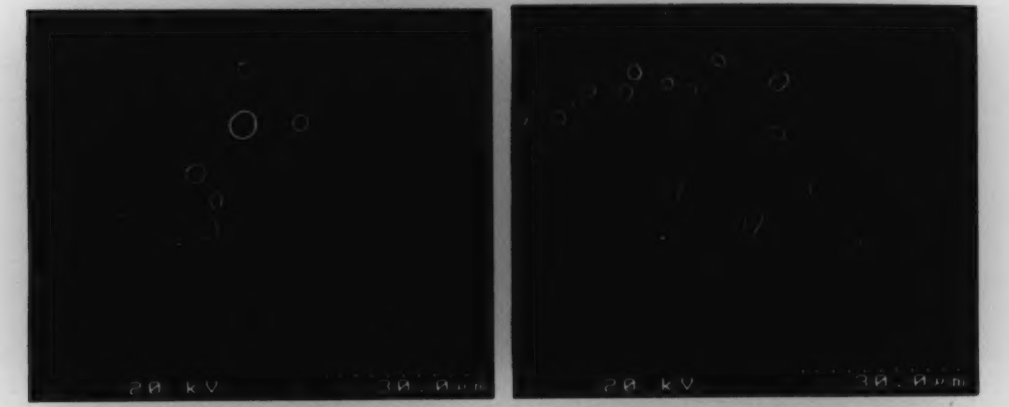

b: 75% coarse+25% fine

c: 50% coarse+50% fine

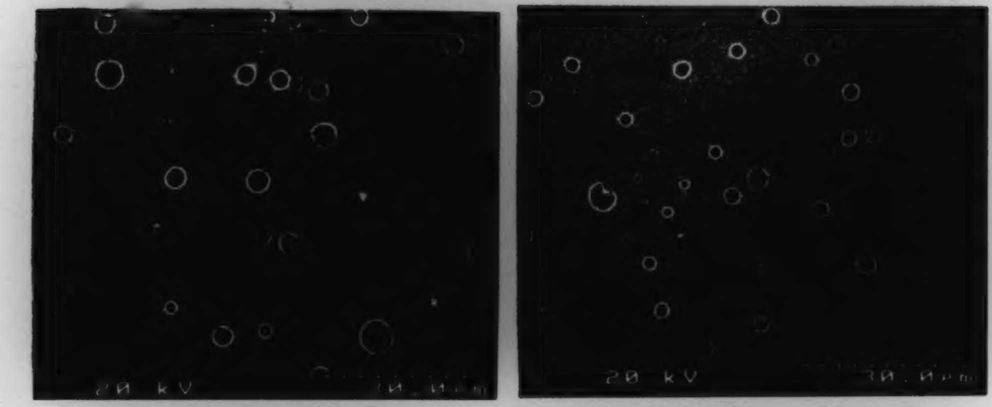

d: 25% coarse+75% fine

e: 100% fine powders

Figure 4-16. Pore structures of sintered samples for different coarse-fine mass fractions.

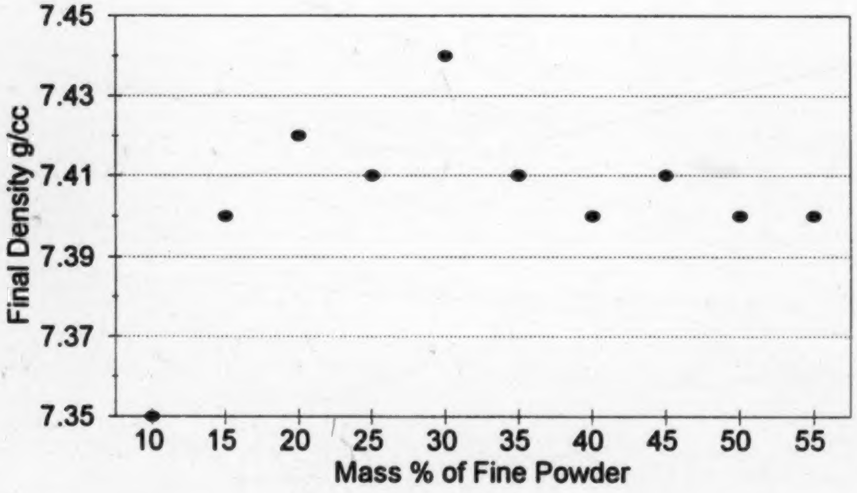

Figure 4-17. Final densities versus mass % of fine powder

(Sintered at 1250 °C for 2 hours)

CHAPTER 5.

Packing Models In Random Close Packed Bimodal Powder Distributions

As introduced in Chapter Three, the advantages of bimodal systems were first proposed by Furnas [Furnas, 1931] and subsequently applied to ceramics and refractoriness. More recently these ideas have found application in powder metallurgy as well [German, 1992a; German, 1992b]. The objective of the work presented in this chapter was to develop a better understanding of the structure in bimodal packing.

In order to set up the model, the fundamental factors which influence the packing behaviour and some ideas about networks which are embodied in the percolation concept were considered. The coordination number of the particles was used as a fundamental parameter to evaluate the different structures and compare them to experiment. The powder system which was studied experimentally (see Chapter Four) was a bimodal system with a coarse/fine powder size ratio of around 5 : 1. Both coarse and fine powders had approximately log-normal distributions. A percolation model based on the saturated structure proposed by German [German, 1992b] was developed and calculated results for co-ordination number based on this model were compared with Suzuki and Oshima's model [Suzuki and Oshima, 1983] for coordination number based on random structures. These models disagree with one another and the experimental results lie somewhere in between. Modifications to the saturated model are proposed to bring the theory and experiment into agreement. It is concluded that the structures that arise in bimodal distributions are best described by this new model.

5.1. Background For Packing Models

5.1.1. Packing Behaviour in Bimodal Powder Distributions

What sort of increase to the tap density can be achieved by mixing size fractions of powders? Considerable theoretical and experimental work has been done in this area. One of the early mathematical treatments of this was by Furnas [Furnas, 1931]. German has recently summarised this literature [German, 1992b]. As noted in Chapter Three, German defines what he calls a saturated structure in which all the interstitial spaces in a packing of larger particles are occupied to the maximum extent possible by smaller size particles. The density increases achieved in this saturated structure depend on the ratio of the two particle sizes, the initial density of the large particle packing and the degree of homogeneity obtained in the bimodal packing. The more difficult concept is the question of inhomogeneity - whether the two particle sizes have been mixed together to achieve uniformity to the maximum extent possible. German [German, 1992b] treats this following Onoda and Messing [Onoda and

Messing, 1978] with the introduction of a parameter "the distribution homogeneity index which can vary from 0 to 1, with 1 representing "perfect" mixing. According to the theory of saturated structures it is predicted that for random dense packing and very large ratios of large to small particle radii a theoretical density of 87% can be achieved. In practice this is not observed. The density increases with the ratio of large to small particle radii with experimental results [McGeary, 1961] showing an increase from 64% theoretical density at a ratio of 1 (random close packing of equal spheres) to about 80% theoretical density at a ratio of 8, with rather smaller asymptotic increases in density for higher size ratios to a maximum of about 84% which is essentially achieved at a size ratio of 15. These results are shown graphically in Figure 5-1.

5.1.2. Networks and Percolation

An additional factor which has proven to be significant to the behaviour of packings of two components is the question of whether the components are interconnected with one another or not. If the particles are interconnected they form a network. When a network is formed then the component is said to percolate the structure [Stauffer, 1985]. Holman [Holman and Leuenberger, 1990; Holman, 1991] has shown that a range of properties of two component distributions such as tap densities, compaction behaviour and hardness show different behaviour in the regions where the different components percolate the structure. One of his graphs of tap density versus composition is shown in Figure 5-2. The [V/V] indicates the solid volume fraction of AVI in AVI/LACT bimodal powder distributions. The percolation threshold for two mono- particle size was at volumes of 31% and 66 %.

Details of this experimental study were given in Chapter Four, but the percolation result will be reported here. In this experimental study of stainless steel powders the different components have the same composition, but different sizes. The tap density for the two component distributions is shown in Figure 5-3. The packings show percolation thresholds at around 30% by volume of the finer particle. This indicates that in the tapped packing there were just particle networks of coarse particles at compositions from 0% to around 30% of fine particles by volume or mass.

5.1.3. Suzuki and Oshima's Model for Coordination Number

As mentioned in Chapter Three, this coordination number model has proven useful for considering bimodal packing. It considers a two component distribution comprising coarse and fine particles. Since this model has already been introduced in Chapter Three, only the equations according to Suzuki and Oshima's model are listed [Suzuki and Oshima, 1983]:

$$N_{1\text{-}2} = \frac{2\alpha\left(\frac{D_c}{D_f}+1\right)}{1+\frac{D_c}{D_f}-\left[\frac{D_c}{D_f}\left(\frac{D_c}{D_f}+2\right)\right]^{1/2}} \qquad \text{(5-1)}$$

$$N_c = S_a N_{1\text{-}2} + (1-S_a)N_{1\text{-}1} \qquad \text{(5-2)}$$

$$S_a = \frac{S_p}{S_p+\left(\frac{D_c}{D_f}\right)^2 (1-S_p)} \qquad \text{(5-3)}$$

$$N_f = S_a N_{2-2} + (1-S_a) N_{2-1} \tag{5-4}$$

$$N_{2-1} = \frac{2\alpha(\frac{D_f}{D_c} + 1)}{1 + \frac{D_f}{D_c} - [\frac{D_f}{D_c}(\frac{D_f}{D_c} + 2)]^{1/2}} \tag{5-5}$$

$$N = \Sigma S_{(j)} N_j \tag{5-6}$$

The constant α is 0.402 based on $\alpha = 0.067N$, where N is 6 the coordination number for particles in packing of normally distributed dense (tapped) packing including random dense packing. A sample calculation for 75% coarse +25% fine powder is shown in Appendix Five.

5.1.4. The Experimental Packing and Calculated Coordination Numbers

The powder system which was studied experimentally was a bimodal system. Both coarse and fine powders had approximately log-normal distributions which are shown in Figure 4-1 and Figure 4-2. The distributions of coordination number N in the coarse and the fine powder in pure form at their uncompacted densities based on the model of Ouchiyama and Tanaka [Ouchiyama and Tanaka, 1980] are shown in Figure 5-4 and Figure 5-5.

The coordination numbers for the bimodal distributions were calculated using Equations (5-1) to (5-6). The calculated results are shown as follows: N_{ff} in Figure 5-6, N_{cc} in Figure 5-7a, N_{cf} in Figure 5-8, N_{fc} in Figure 5-9 and total coordination number, N, in Figure 5-10a.

These co-ordination numbers are required to understand the percolation thresholds in the compacts.

5.1.5. Contacts, Saturated Structures and Percolation Thresholds.

According to Bouvard and Lange [Bouvard and Lange, 1991], a coordination number of 4 or more characterises the complete connectivity of all the particles and a coordination number of 2 corresponds to the onset of percolation (threshold). According to German's concept of a saturated structure, small particles going into the interstitial spaces between the coarse powder and not influencing the coarse packing can be visualised. So, the percolation threshold would have direct relation to the saturated structure in this case and would occur when the pores were full.

In fact according to the ideal saturated structure, the coarse pores can be filled with fine particles to the extent of the tap density of the fine powder before the coarse powder is affected. There are different shapes of three-dimensional voids in a coarse particle network, such as: tetrahedron, octahedron, cube, etc. The void of the tetrahedron is the smallest one among them. If the coarse / fine particle size ratio is approximately larger than 4.5:1, the fine particles can fill in the tetrahedron voids as well as other three-dimensional types of voids. In Figure 5-11, schematic figures are drawn to indicate that the fine particles which are in the void of the coarse particles do not influence the packing and the coarse-coarse contact numbers of the coarse particles. The pure coarse particle packing is shown in Figure 5-11a. In Figure 5-11b, one fine particle is in the void of the coarse particle while there are three fine particles in the void of the coarse particles in Figure 5-11c. The packing of the coarse particles are the same in Figure 5-11a, 11b and 11c. So the coarse particle packing does not change with addition of fine particles to the coarse particles as long as the fine particles are in the voids of the coarse particles.

Based on Figure 5-7a, the coarse infinite network starts to lose complete connectivity at around 10% fine particles (CN $\leq$ 4) and is completely disconnected at 30% fine particles (CN $\leq$ 2). The observed percolation threshold from Fig 5-3 is 30% fine powder. There would appear to be a substantial disagreement between the coordination number calculated from computer generated random packing (Suzuki and Oshima's model) and the experiments.

How can this be explained? Because the coarse/fine particle size ratio is larger than 5 in this bimodal systems, the particle number fraction of the fine particle in the powder distributions (S_p) increased rapidly as the mass of the fine particle increased. So, the surface area fraction of the fine particles (S_a) in Equation (5-2) increases and the calculated coarse-coarse contact number decreases quickly with increase of the mass of the fine particles. But the fact that the fine particles which are in the voids of the coarse particles do not decrease the coarse-coarse contact numbers is not considered in Equation (5-3), so in Figure 5-7a, the coarse-coarse contact numbers calculated by using Equation (5-3) are smaller than the actual case. Considering the fact that fine particles which are in the voids of the coarse particles do not influence the coarse-coarse contacts, it is necessary to modify the factor $(1-S_a)N_{1-1}$ in Equation (5-3) by using S_a' to replace S_a :

$$N_{c-c} = (1-S_a')N_{1-1} \qquad (5\text{-}7)$$

where S_s' represents the surface area fraction for the fine particle in the powder distribution which influences the coarse-coarse contact. This S_s' is explained and calculated for a new proposed model in the next section.

5.2. New Models for Bimodal Particle Packing

5.2.1. Saturated Model

5.2.1.1. Saturation point

German defined the saturation point ($X = X^*$) as the point at which all the coarse particles were in point contact with one another and all of the interstitial voids were filled to be extent possible with fine particles [German, 1992b]. This is an idealised concept which maximises density. If f_c and f_s were the relative tap density of 100% coarse powder and 100% fine powder, ρ_c and ρ_f were the theoretical densities of the coarse powder and the fine powder (general case where the fine and coarse powders may be different alloys), the amount of void space of coarse powder would be equal to ($1 - f_c$) and the saturation point X^* would be given as follows [German, 1989]:

$$X^* = f_c \rho_c / [f_c \rho_c + (1 - f_c) f_s \rho_f] \qquad (5\text{-}8)$$

In this study, f_c was 0.525, f_s was 0.513 and ρ_c was equal to ρ_f. So the density factors cancelled. The saturation point X^* calculated from Equation (5-8) was about 70% coarse powder. As mentioned in Chapter Four, X was used for mass % of fine powder. In this study system, the saturation point is $X^* = 30\%$ fine powder.

5.2.1.2. Percolation of Microstructure (idealised or simplified concepts)

5.2.1.2.1. In the region $0\% < X < X_f$

As calculated above, the saturation point was $X^* = 30\%$. At this point, the fine particles were all in the interstices of the coarse particle network [German, 1989]. When the mass fraction of fine powder (X) increased above 30%, the coarse particle network would be dilated by adding more fine particles into the coarse powders. In the region $0\% < X < 30\%$, finite clusters of the fine particles were dispersed in the infinite network of the coarse particles. So, the threshold X_f was the same point as the saturation point ($X_f = X^* = 30\%$). Because the fine particles which were in the voids of the coarse powders would not influence the network of the coarse particles, the coarse-coarse contact numbers would remain the same as the coordination number of the pure coarse powder. The above consideration of the microstructure was an idealised concept -- assuming that all the fine powders were in the interstices of the coarse powder network. It is unrealistic from an entropy point of view.

5.2.1.2.2. In the region $X_f < X < X_c$

In the region $X_f < X < X_c$, infinite networks of both coarse and fine particles would coexist. At the point $X = 30\%$, the relative mass (the mass of the fine particles (M_f) / the mass of the coarse particles (M_c)) of the fine powder was 0.4286 and the fine particles were all in the interstices of the coarse particle network. When the relative mass of the fine powder is more than 0.4286, the coarse particle network would be dilated and the coarse-coarse contact numbers could not remain the same as the coordination number of the pure coarse powder. Because the infinite coarse network still existed in region of $X_f < X < X_c$, some of the fine powders which filled in the space between the coarse powders would not influence the coarse-coarse contact number. But the rest of the fine powders would dilate the coarse powder network and influence the coarse-coarse contact number.

5.2.1.2.3. In the region 0% < $X < X_c$

At the point $X = X_c$, the infinite network of the coarse particles would just disappear if the value of X increased and only the pure infinite network of the fine particles would remain in the powder distribution. In the region 0% < $X < X_c$, finite clusters of coarse particles would be dispersed in an infinite network of fine particles.

5.2.1.3. Calculation

For calculation purposes, the total mass of the powders was assumed as 1 g. This could be thought of as a calculation cell. The calculation of the coarse-coarse contact number ($N_{c\text{-}c}$) was based on considerations of packing microstructure.

5.2.1.3.1. In the region 0% < X < 30%

With the addition of fine powders into the coarse powders, the total mass of the powder in the calculation cell was constant at 1g but the mass of the coarse powder changed from 1g to 0.7g. Because the fine powders were all in the voids of the coarse powders and did not influence the coarse particle network, the coarse-coarse contact number remained constant at 6, the average coordination number of the pure coarse powder.

5.2.1.3.2. In the region 30% < X < 45%

In this region, the fine particles were divided into two parts: the fine particles which did not influence the coarse-coarse contact (part 1) and the fine particles which influenced the coarse-coarse contact (part 2). The stable stage for any system is when the total potential energy of the system reached the lowest point. In the powder distributions, if the infinite coarse network existed, the fine particles tend to fill all the voids of coarse powders without dilating the coarse network in order to lower the total potential energy of the system relative to gravitation forces. The relative mass of the fine powders in part 1 (the mass of the fine particle in part 1 ($M_{f\text{-}1}$) / the mass of the coarse particle (M_c)) was 0.4286 and all of the interstitial voids were filled with fine particles at X=30%. Assuming that the void volume (which could be filled without affecting the coarse network) per unit mass of the coarse powder was constant, the relative mass of the fine powders in part 1 ($M_{f\text{-}1}/M_c$) remained the same as 0.4286 because the infinite coarse network still existed in the region of $X_f < X < X_c$. The fine powder mass in part 1 ($M_{f\text{-}1}$) and in part 2 ($M_{f\text{-}2}$) could be calculated from the following mass relationship:

$$M_{f\text{-}1} = M_c\,(30/70) \tag{5-9}$$

$$M_{f\text{-}2} = 1 - M_c - M_{f\text{-}1} \tag{5-10}$$

The S_a' and $N_{c\text{-}c}$ (coarse-coarse contact number) could be calculated by Equations (5-2), (5-7), (5-9) and (5-10).

The calculated $N_{c\text{-}c}$ was about 2 at the point X = 45%. If the coarse-coarse contact number was below 2, the infinite coarse powder network could not exist [Bouvard and Lange, 1991]. So, the value of X_f was chosen as 45%.

5.2.1.3.3. In the region 45% < X < 100%

There was no infinite coarse powder network in this region. The calculation of the coordination numbers was based on Suzuki and Oshima's model.

The results of the coarse-coarse contact numbers (N_{c-c}) were shown in Figure 5-7b. The average coordination numbers N were also calculated and shown in Figure 5-10b. Compared with Suzuki and Oshima's model (Figure 5-10a), the values of N were very similar. The values of N_{c-c} were obviously different because of the microstructure factor from the fine particles which were in the voids of the coarse particles. The fact that those fine particles did not influence the packing and the coarse-coarse contact numbers was considered in the saturated model.

But the saturated model presented a problem since at the point X=30%, the experimental results and calculated values for tap density were different. If all the fine particles were in the interstices of coarse particles without influencing the coarse network, the relative tap density of the powder distribution would be 0.753 according to the saturated model. The experimental relative tap density however was 0.644. In Figure 5-12, the volume of powder distributions obtained from the experimental test and the volume of powder distributions calculated from saturated model are shown. The lower value in the experimental relative tap density indicated that the coarse powder network was dilated. The coarse-coarse contact numbers in the region of 0% < X < 30% must be decreasing instead of remaining constant with the addition of the fine powders. As suggested by entropy considerations, the saturated model needed to be modified since there were differences between the experimental results and calculated values.

5.2.2. Modified Saturated Model – The Perturbation of the Ideal Saturation Concept

5.2.2.1. The perturbation of the saturated microstructure

The difference in relative tap density (or volume of the powder distributions) between the experimental results and the saturated model was caused by the perturbation (dilation) of the coarse network. There are several reasons, such as friction, geometric limitation, irregular shape of powders, which cause the perturbation of the coarse network. In the saturated structure, 0.4286 relative mass of fine particle (mass of the fine particles/mass of the coarse particles) could be added to coarse powders without dilating the coarse network. In the non-ideal structure, the fine powders dilated the coarse powder network and influenced the coarse-coarse contact number even though the relative mass of the fine powder was less than 0.4286. The coarse-coarse contact number would then decrease with the addition of fine powders in this region. In the region $30\% < X < 45\%$, the infinite coarse network still existed. With the addition of fine powders, the coarse network was continuously dilated or perturbed. The differences between these two regions were as follows. In the region $0 < X < 30\%$, there was only an infinite coarse particle network and most of the fine particle did not dilate the coarse particle network and did not influence the coarse-coarse contact number. In the region of $30\% < X < 45\%$, there was both an infinite coarse particle and an infinite fine particle network in the powder distribution and the per cent of fine particles which belonged to part 2 (fine particle in part 2 (M_{f-2}) / total fine particle mass(M_f)) was increasing with the addition of fine particles.

5.2.2.2. Relationship Between the Coordination Number and the Fractional Density

In order to calculate the mass per cent of fine particles which influence the coarse-coarse contact, the relationship between the coordination number and the fractional density must be hold.

5.2.2.2.1. Monosize Spherical Powders

There were several models which linked the coordination number and the fractional density in random packed monosize powders [German, 1989; Mason, 1968; Iwata and Homma, 1974; Wisdom, 1966; Visscher and Bolsterli, 1972; Jernot, *et al.*, 1981]. These models do not agree exactly with each other, although they show similar trends [German, 1989]. Substituting the experimental results of relative tap density of the pure coarse (0.525) and the coordination number of the pure coarse (6) into the different models, these data fitted Smith's model very well. According to Smith *et al.*, the coordination number increased with the fractional density according to ([German, 1989; Aim and Goff , 1968; Smith *et al.*, 1929]):

$$N = 26.5 - 10.7/F \tag{5-11}$$

where N was the average coordination number and F was the fractional density. In using this kind of model, the coarse powder was considered as if it existed by itself in a range of different densities. For high densities, this is like compaction and for low densities, it is like powders in a fluidised bed.

5.2.2.2.2. Bimodal Powder Distributions

Bimodal powder distributions could be considered as an assembly of the coarse and the fine micro regions which were homogeneously mixed [Nikolenko and Kovalchenko, 1985]. If Equation (5-11) was extended, then the tap density of the coarse particle micro regions could be calculated from the following equation:

$$N_{c\text{-}c} = 26.5 - 10.7/F_c \tag{5-12}$$

where F_c was the fractional density of the coarse powder and $N_{c\text{-}c}$ was the average coarse-

coarse contact number (100% coarse powders, $N_{c\text{-}c} = N$).

As mentioned above, for system of particles with a continuous distribution, typically, the mean coordination number for the distribution is near six [German, 1989]. Substituting the fractional density of the pure coarse powder 0.52 (experimental data) into Equation (5-11), the same coordination number of 6 was achieved. So, there was some justification for using Equation (5-11) and the extended Equation (5-12) to calculate the coordination numbers in random packed powder distributions in which fractional densities were around 0.52.

$M_{f\text{-}in}$ at low values of X can be determined as follows. At the point X=10%, the fractional density of coarse powder was 0.515. Because this value is close to the tap density of pure coarse powders, Equation (5-12) could be used to calculate the coarse-coarse contact at this point. $N_{c\text{-}c}$ was calculated to be 5.72. The S_a' (the surface area fraction for the fine particle which influenced the coarse-coarse contact) could be calculated from : $5.72 = (1-S_a')*6$. Rearranging Equation (5-3), the particle number fraction of the fine particle (S_p') which influenced the coarse-coarse contact could be calculated by Equation (5-13):

$$S_p' = [S_a'(D_c / D_f)^2] / [S_a'(D_c / D_f)^2 + 1 - S_a'] \qquad (5\text{-}13)$$

The amount of the fine powder ($M_{f\text{-}2}$) which dilated the coarse powder network and influenced the coarse-coarse contact could be calculated at 10% fine + 90% coarse powder distribution from Equation (5-14):

$$S_p' = (M_{f\text{-}2} / D_f^3) / [(M_c / D_c^3) + (M_{f\text{-}2} / D_f^3)] \qquad (5\text{-}14)$$

So, at 90% coarse + 10% fine powder distribution, the $M_{f\text{-}2}$ was 0.00814 g and $M_{f\text{-}1}$ was (0.1-0.00814)g.

5.2.2.3. Calculation of Coordination Number

5.2.2.3.1. In the region 0% < X < 30%

By the definition of $M_{f\text{-}2}$, the extent of the perturbation of the coarse network was related to the value of $M_{f\text{-}2}$. It was reasonable to assume that the difference between the calculated volume of powder distributions from the saturated model and the volume of powder distributions from experimental test (V) would be proportional to $M_{f\text{-}2}$. As calculated above, the $M_{f\text{-}2}$ was 0.00814 g and the V was 0.004433 cm^3 at 90% coarse + 10% fine powder distribution. According to the data of V from Figure 5-12 and proportional relationship between $M_{f\text{-}2}$ and V, $M_{f\text{-}2}$ were calculated and shown in Figure 5-13. $M_{f\text{-}1}$ and M_f are also shown in Figure 5-13. Based on the value of $M_{f\text{-}2}$, the S_p' ,S_a', and $N_{c\text{-}c}$ could be calculated from Equations (5-7) , (5-13) and (5-14).

5.2.2.3.2. In the region 30% < X < 45%

According to the results shown in Figure 5-7b, the infinite coarse network disappeared rapidly after the mass fraction of fine powders was more than 30%. The infinite coarse powder network totally disappeared at X = 45% (corresponding to $N_{c\text{-}c} = 2$). In the saturated model, $M_{f\text{-}2}$ was calculated from Equations (5-9) and (5-10). It was reasonable to assume that the difference between the calculated volume of powder distributions from the saturated model and the volume of powder distributions from experimental test (V) was proportional to $M_{f\text{-}2}$ which was defined as difference between the value of $M_{f\text{-}2}$ in an ideal saturated structure and the value of $M_{f\text{-}2}$ in the non-ideal structure (in modified model). $M_{f\text{-}2}$ in the modified model ,as well as $M_{f\text{-}1}$ and M_f , were calculated and shown in Figure 5-13. Based on the modified value of $M_{f\text{-}2}$, the S_p' ,S_a', and $N_{c\text{-}c}$ could be calculated from

Equations (5-7),(5-13) and (5-14).

5.2.2.3.3. In the region X > 45%

In the region $X > 45\%$, there was no infinite coarse powder network and the coarse-coarse contact number was very low (< 2). The calculation of Suzuki and Oshima's model gave an estimate of the contact numbers which were not too different from an extrapolation of the calculation based on this perturbed models.

The calculated results are shown in the Figure 5-7c (N_{c-c}) and Figure 5-10c (N).

5.3. Discussion

From Figure 5-7d, it was observed that Suzuki and Oshima's model underestimated the coarse-coarse contact number N_{c-c}. From the calculation based on the saturated model, the coarse infinite network started to lose complete connectivity at around $X = 35\%$ and disappeared at $X = 45\%$. It was assumed in the saturated model that all the fine powder are in the voids of the coarse powder if there is enough void space. It is correct from the gravitational force point of the view. The gravitational force drives the fine powder to the voids of the coarse powders. The free energy of distribution get lower when the fine powders fill in the voids. But from the kinetic point of the view, the fine powder moving into the voids of the coarse powders need to overcome the energy barrier and also there are geometric limitations. Since the ideal saturated microstructure was used in this model, the coarse-coarse contact numbers were overestimated. The packing structure can not be perfect so the saturated model was modified. According to the modified saturated model, the coarse infinite network would start to lose complete connectivity at around X = 30%. The percolation point would be at X= 10% based on Suzuki and Oshima's model. From these test results (Figure 5-3), it is found that the percolation point is in fact around X=30%. So, the results of the modified saturated model were more reasonable than Suzuki and Oshima's model in the case of high powder size ratio ($D_c/D_f > 3$).

From the experimental results it can be concluded that the reality lies between the saturated structure and the random structure - "a modified saturated structure" or "a modified random structure".

These modifications are important because they modify the percolation thresholds and this in turn influences subsequent operations like compaction and sintering. It is helpful to think of the balance between the randomising forces like the mixing that goes on in the ball mill during the processing of the mixed powder and the small potential energy gain that occurs when the volume is minimised in a gravitational field.

5.4. References

Aim, R.B. and **Goff**, P.L., "La Coordinance des Empilements Desordonnes de Spheres. Application aux Melanges Binaires de Spheres,"Powder Technology, Vol.2, pp.1-12, 1968.

Borvard, D. and **Lange**, F.F., "Relation Between Percolation and Particle Coordination in Binary Powder Mixtures," Acta Metall. Mater. , Vol. 39, No. 12, pp. 3083-3090, 1991.

German, R.M., "Particle Packing Characteristics," Metal Powder Industries Federation, Princeton, New Jersey, 1989.

German, R.M., "The Role of Particle Parking Density in Powder Injection Molding", Reviews on Powder Metallurgy and Physical Ceramics, Vol. 5, No. 2, pp. 81-110, 1992a.

German, R.M., "Prediction of Sintered Density for Bimodal Powder Mixtures", Metallurgical Transactions A, Vol. 23A, No. 5, pp. 1455-1465, 1992b.

Furnas, C.C., "Grading Aggregates I - Mathematical Relations for Beds of Broken Solids", Ind. Eng. Chem., Vol. 23, p. 1052, 1931.

Holman, L.E., "The Compaction Behaviour of Particulate Materials. An Elucidation Based on Percolation Theory," Powder Technology, Vol. 66, pp. 265-280, 1991.

Holman, L.E. and **Leuenberger**, H., "The Effect of Varying the Composition of Binary Powder Mixtures and Compacts on Their Properties: A Percolation Phenomenon," Powder Technology, Vol. 60, pp. 249-258, 1990.

Iwata, H. and **Homma**, T., “Distribution of Coordination Numbers in Random Packing of Homogeneous Spheres,” Powder Technology, Vol. 10, pp. 79-83, 1974.

Jernot, J.P., **Coster**, M. and **Chermant**, J.L., “Model of Variation of the Specific Surface Area During Sintering,” Powder Technology, Vol. 30, pp.21-29, 1981.

Mason, G., “Radial Distribution Functions from Small Packing of Spheres,” Nature, Vol. 217, pp. 733-735, 1968.

McGeary, R.K., “Mechanical Packing of Spherical Particles,” Journal of the American Ceramic Society, Vol.34, pp. 513-522, 1961.

Nikolenko, N. and **Kovalchenko**, M.S., “Analysis of the Random Packing of Identical Particles I. General Theory,” soviet Powder Metallurgy and Metal Ceramics, Vol. 24, pp. 818-821, 1985.

Onoda, G.Y. and **Messing**, G.L., “Packing and Sintering Relations for Binary Powders” in "Processing of Crystalline Ceramics" H. Palmour, R.F. Davis and T.M. Hare eds. Plenum Press, New York, N.Y., pp 99-112, 1978.

Ouchiyama, N. and **Tanaka**, T., "Estimation of the Average Number of Contacts Between Randomly Mixed Solid Particles," Industrial and Engineering Chemistry Fundamentals, Vol. 19, pp. 338-340, 1980.

Smith, W.O., **Foote**, P.D. and **Busang**, P.F., "Packing of Homogeneous Spheres," Physical Review, Vol. 34, pp. 1271-1274, 1929.

Stauffer, D., "Introduction to Percolation Theory", Taylor and Francis, London, 1985.

Suzuki , M. and **Oshima** ,T., "Estimation of the Co-ordination Number in a Mullti-Component Mixture of Spheres," Powder Technology, Vol. 35, pp. 159-166, 1983.

Visscher, W.M. and **Bolsterli**, M., "Random Packing of Equal and Unequal Spheres in Two and Three Dimension," Nature, Vol. 239, pp. 504-507, 1972.

Wisdom, B., " Random Sequential Addition of Hard Spheres to a Volume," The Journal of Chemical Physics, Vol. 44, pp. 3888-3894, 1966.

5.5. Appendix

Size(um)	Ln(size)	P(X) (coarse)	wt% (coarse)	P(x) (fine)	wt% (fine)	wt%(75%coarse+25%fine)	wt%/R^3	Sp	Ni	Sp*Ni
3.9	1.360977	1.2343E-09	0	0.0579083	1.01704	0.25425999603022	0.004286	0.125049	2.54	0.317625
4.6	1.529548	1.3423E-08	0	0.1146423	2.0134557	0.50336391769121	0.005171	0.150871	2.85	0.429982
5.5	1.704748	1.3702E-07	0	0.2086561	3.6646125	0.91615312175907	0.005507	0.160649	3.27	0.525321
6.55	1.878924	1.1773E-06	0	0.338311	5.9417329	1.485433225129	0.005286	0.154215	3.8	0.586017
7.8	2.054124	8.7321E-06	0	0.4914375	8.6310834	2.1577708621334	0.004547	0.132653	4.47	0.592961
9.2	2.222695	5.1617E-05	0	0.6325974	11.110266	2.7775665170938	0.003567	0.104063	5.27	0.548414
11	2.397895	0.000279633	0	0.7360673	12.9275	3.2318749055296	0.002428	0.070839	6.41	0.454079
13.4	2.597389	0.001575621	0	0.7621372	13.385364	3.3463410635697	0.001391	0.040574	8.11	0.329059
16	2.772589	0.006060517	0	0.6962944	12.228971	3.0572428393717	0.000746	0.021775	10.18	0.221674
18.5	2.915842	0.016116642	0.28339789	0.5945848	10.442653	2.8232115854484	0.000446	0.013008	12.38	0.161045
22	3.091042	0.046109296	0.810794007	0.442291	7.7679267	2.5500771909845	0.000239	0.006987	15.82	0.110532
26	3.25867	0.108671331	1.910895894	0.2997671	5.2647889	2.7493691434301	0.000156	0.004564	20.28	0.09255
31	3.433987	0.22807779	4.010560176	0.1786544	3.1376959	3.7923441144586	0.000127	0.003714	26.64	0.098936
37	3.60899	0.408047399	7.175177595	0.0951924	1.6718584	5.7993477965689	0.000114	0.00334	35.43	0.118343
44	3.78419	0.623453621	10.96291867	0.0452691	0.7950573	8.4209533347547	9.9E-05	0.002884	47.26	0.136299
53	3.970292	0.822122437	14.45634626	Total	0	10.842259694195	7.3E-05	0.002125	64.99	0.138082
64	4.158883	0.906602387	15.94185664		0	11.956392479209	4.6E-05	0.001331	90.49	0.120409
75	4.317488	0.853842995	15.01412616		0	11.26059462266	2.7E-05	0.000779	120.21	0.093609
90	4.49981	0.678776911	11.93573319		0	8.9517998918308	1.2E-05	0.000358	167.54	0.06002
106	4.663439	0.477309119	8.393087922		0	6.294815941215	5.3E-06	0.000154	226.68	0.034952
125	4.828314	0.291044231	5.117773199		0	3.8383298989058	2E-06	5.7E-05	308.51	0.017688
150	5.010635	0.143015586	2.514811347		0	1.8861085103967	5.6E-07	1.6E-05	435.36	0.007098
180	5.19296	0.059187779	1.040768368		0	0.78057627634265	1.3E-07	3.9E-06	616.37	0.002407

A sample calculation for 75% coarse + 25% fine powder

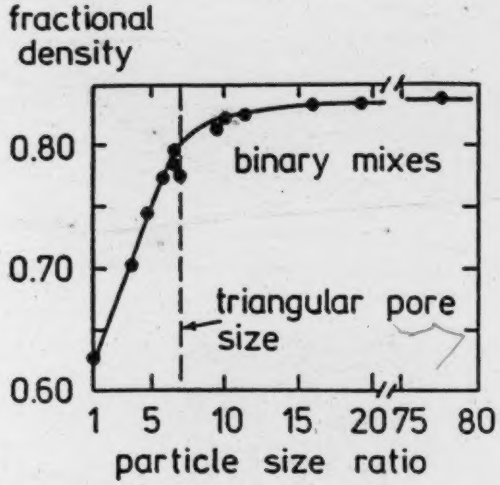

Figure 5-1. Fractional density versus particle size ratio in bimodal powder distributions (the experimental results of McGeary) [McGeary, 1961]

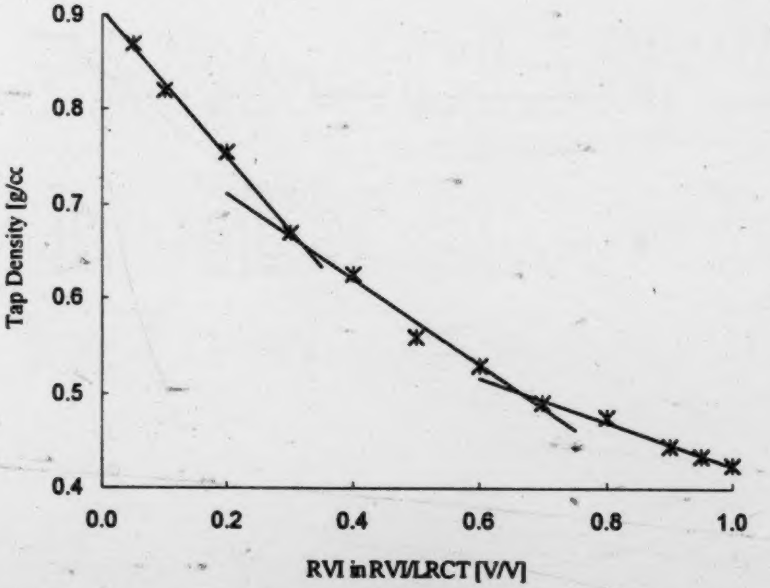

Figure 5-2. Tap densities of different compositions of blends of bimodal powders [Holman, 1991]

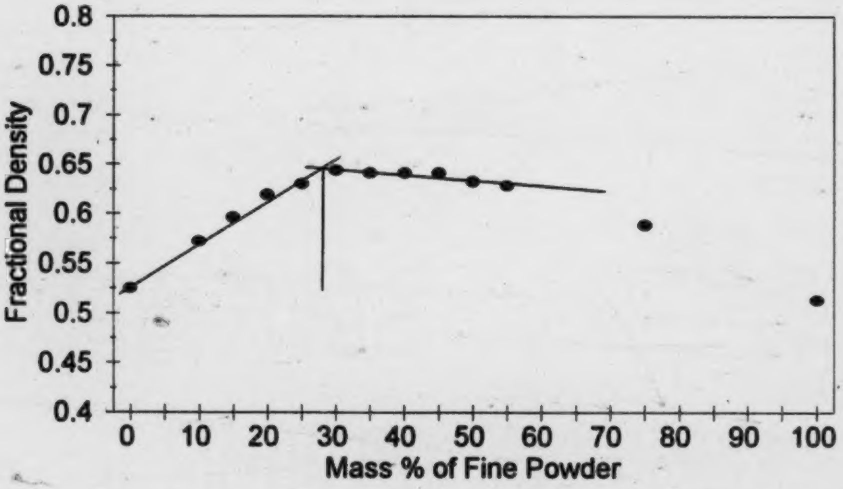

Figure 5-3. Tap densities versus mass % of fine powder

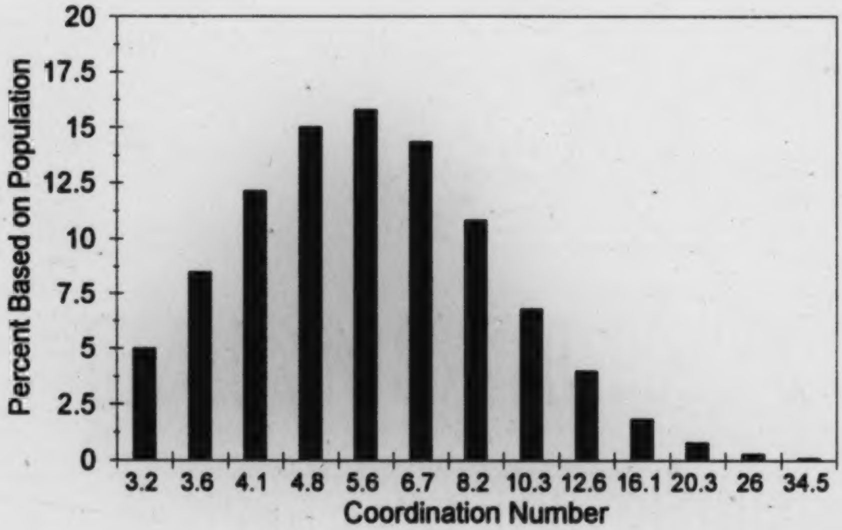

Figure 5-4. Coordination numbers in coarse powder of figure 4-1

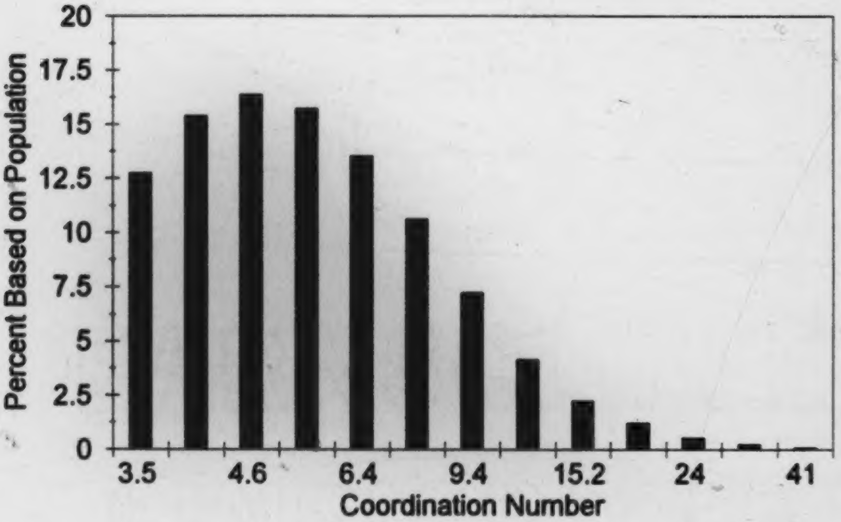

Figure 5-5. Coordination numbers in fine powder of figure 4-2

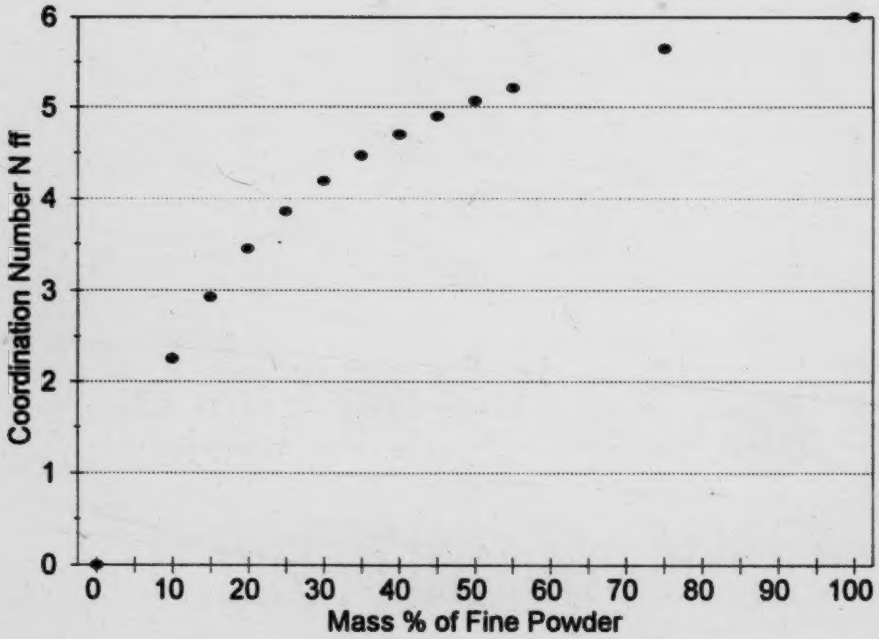

Figure 5-6. N_{ff} versus mass % of fine powder

(Based on Suzuki and Oshima's model)

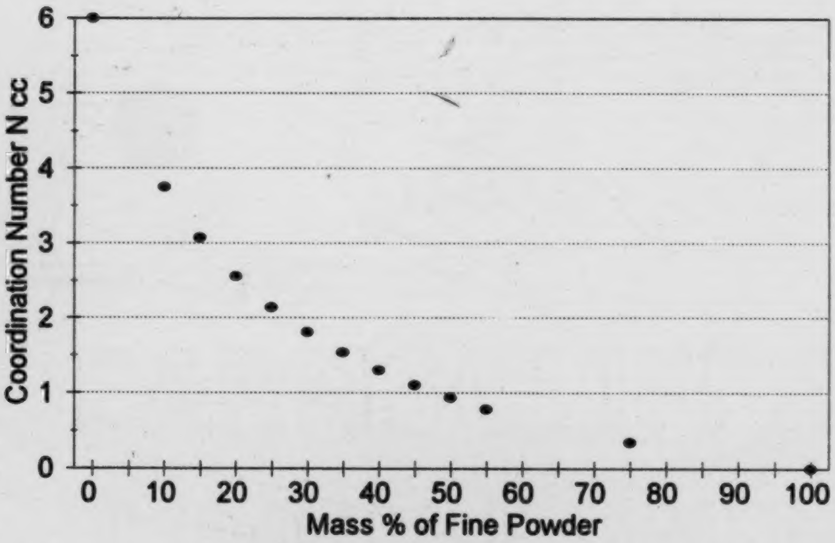

Figure 5-7 (a). N_{cc} versus mass % of fine powder

(Based on Suzuki and Oshima's model)

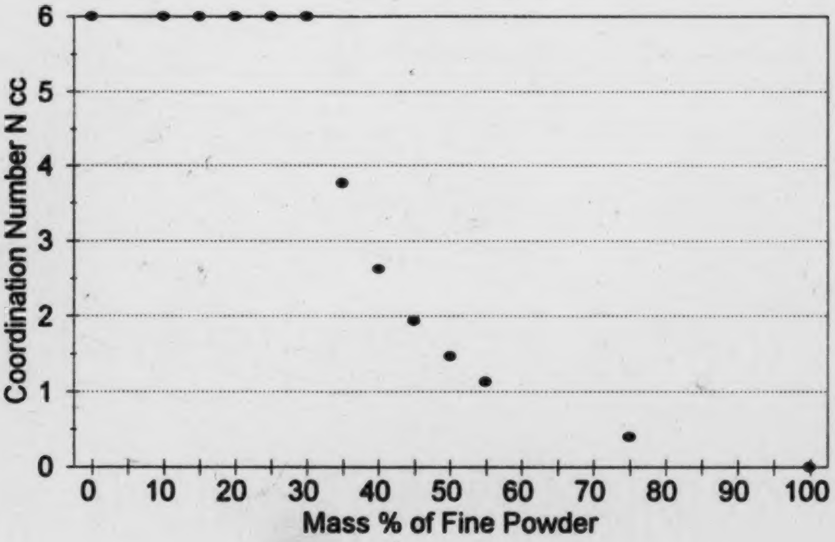

Figure 5-7 (b). N_{cc} versus mass % of fine powder

(Based on Saturated model)

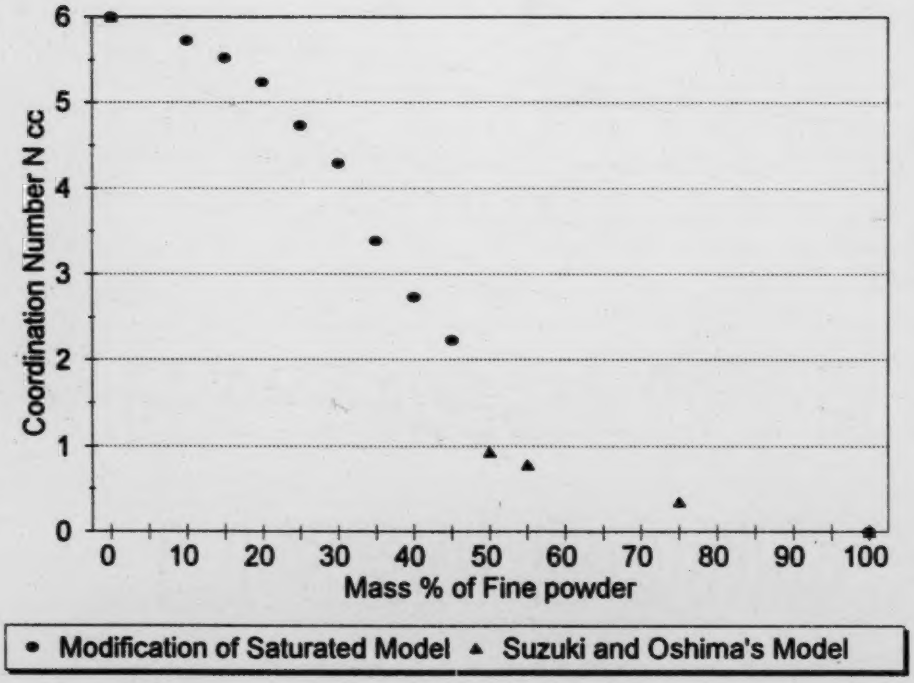

Figure 5-7 (c). N_{cc} versus mass % of fine powder

(Modification of saturated model)

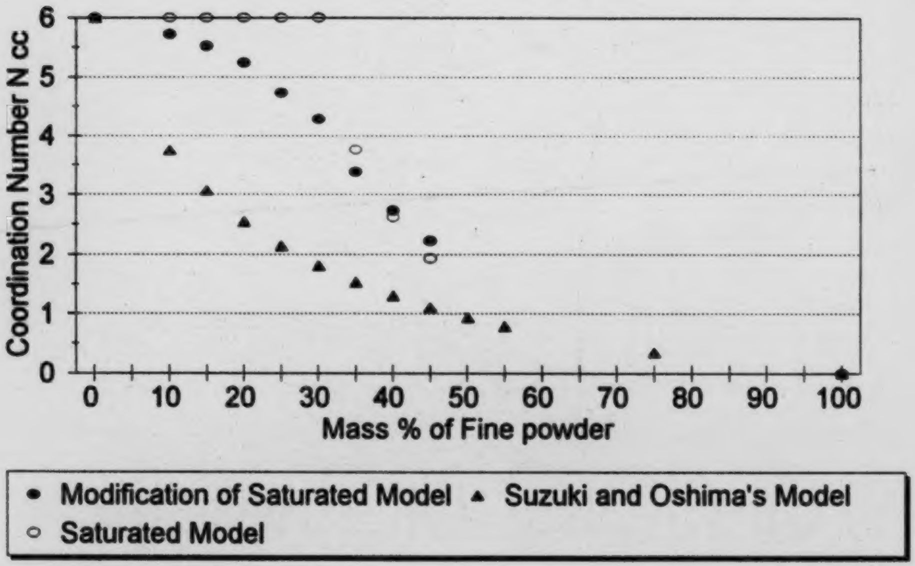

Figure 5-7 (d). N_{cc} versus mass % of fine powder

(For different models)

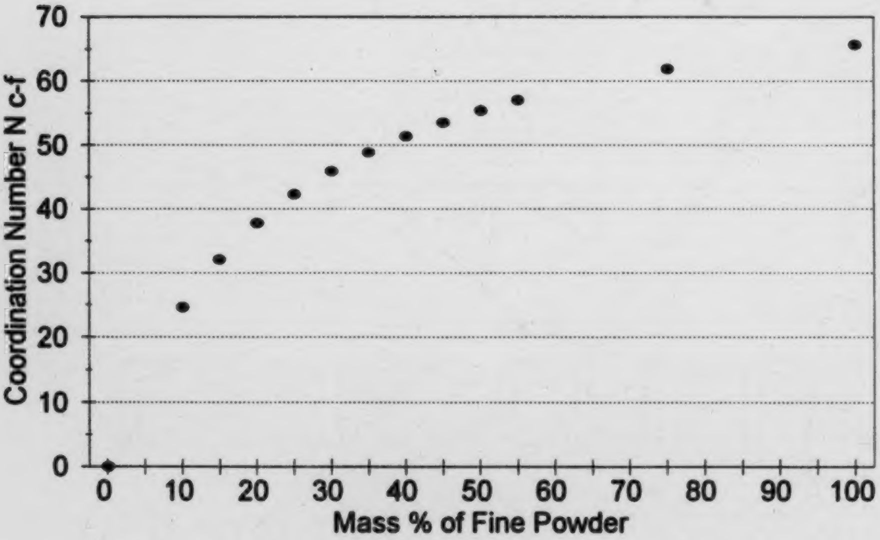

Figure 5-8. N_{cf} versus mass % of fine powder

(Based on Suzuki and Oshima's model)

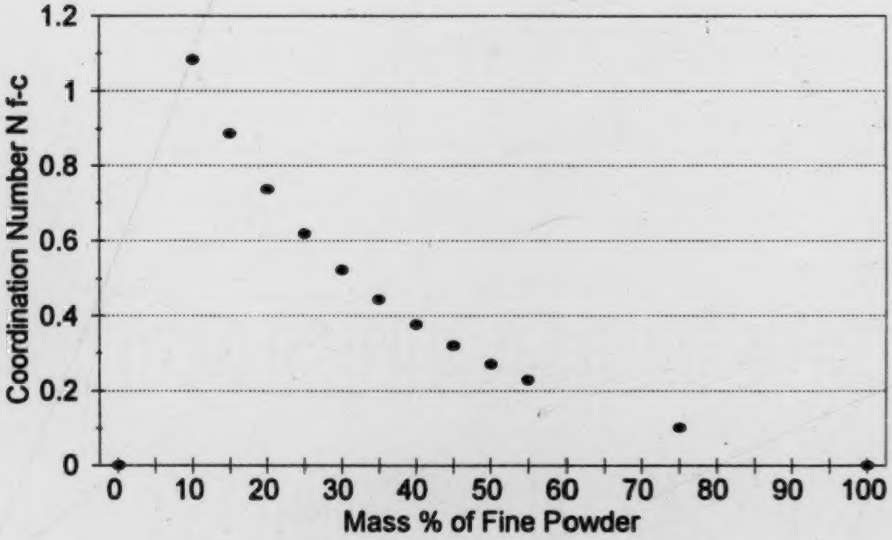

Figure 5-9. N_{fc} versus mass % of fine powder

(Based on Suzuki and Oshima's model)

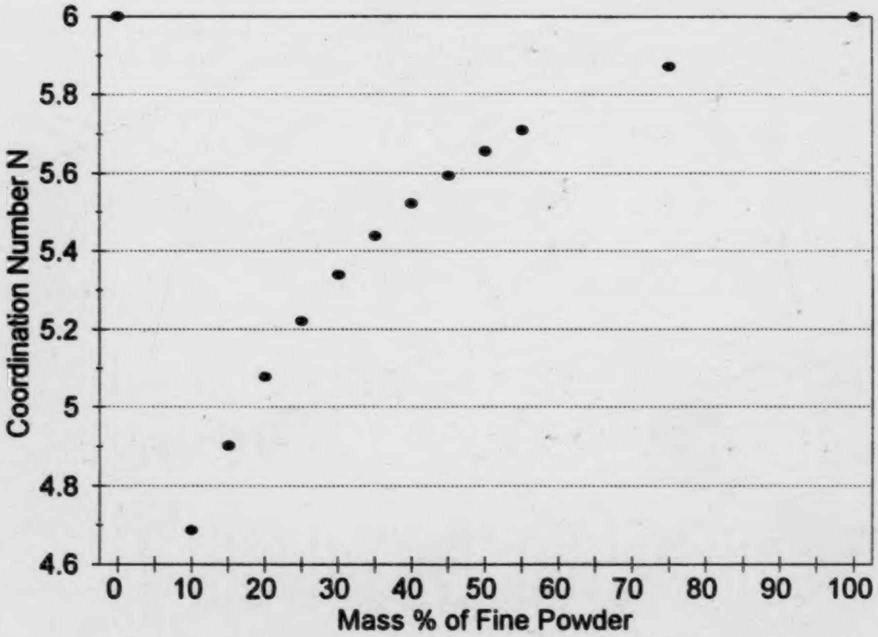

Figure 5-10 (a). N versus mass % of fine powder

(Based on Suzuki and Oshima's model)

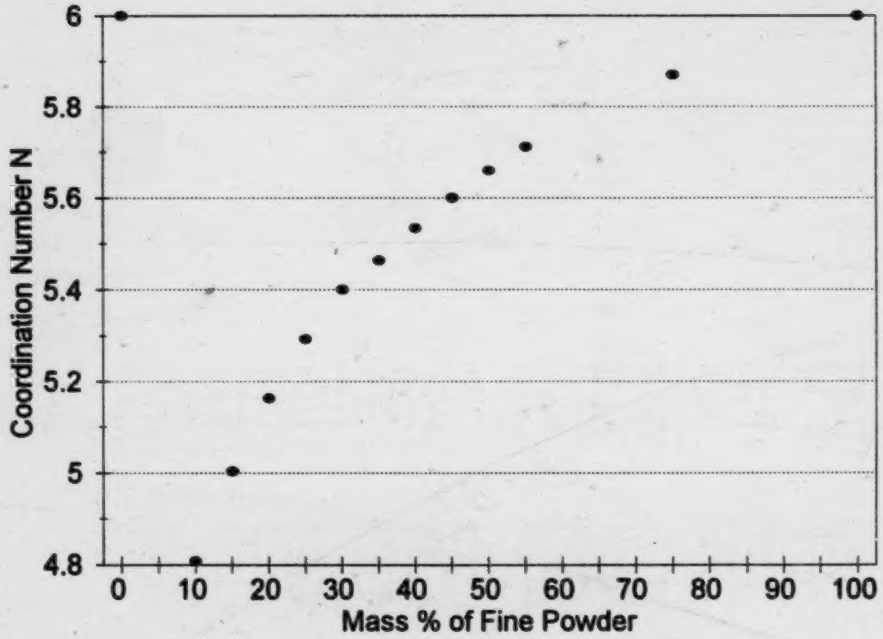

Figure 5-10 (b). N versus mass % of fine powder

(Based on Saturated model)

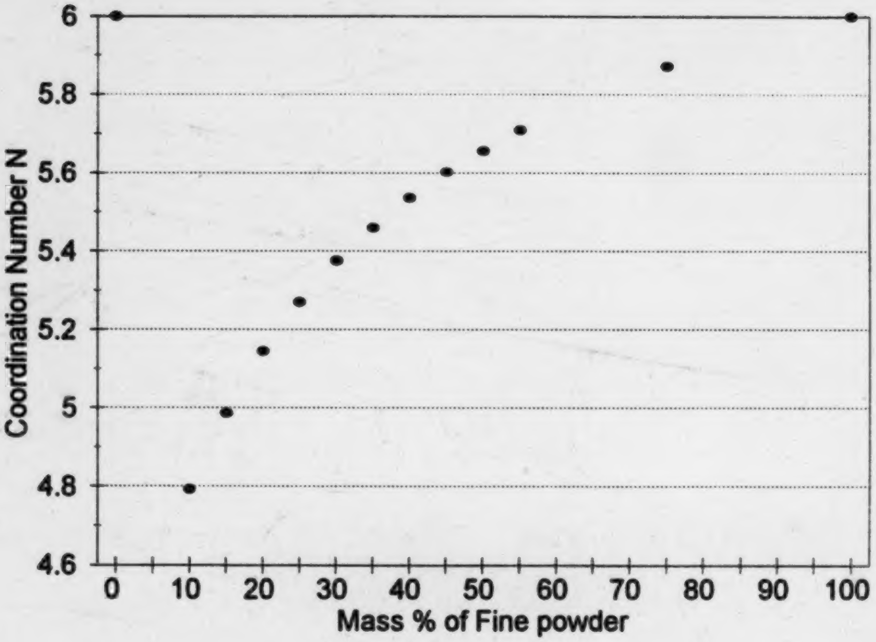

Figure 5-10 (c). N versus mass % of fine powder

(Modification of Saturated model)

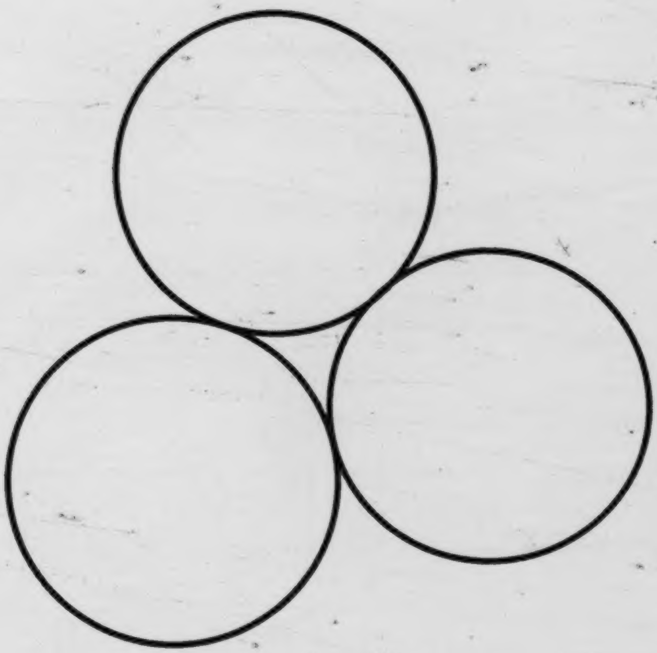

Figure 5-11 (a). The scheme of pure coarse particle packing

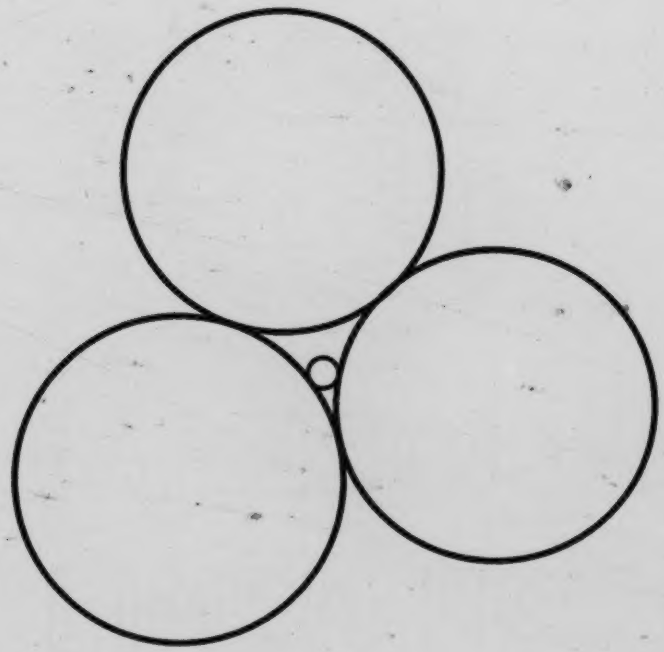

Figure 5-11 (b). The scheme of coarse particle packing with one fine particle in the void (size ratio 1:10)

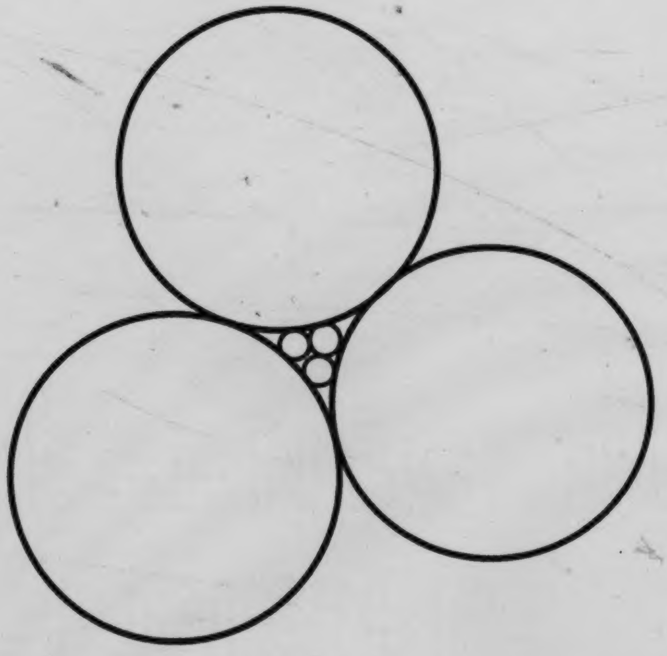

Figure 5-11 (c). The scheme of coarse particle packing with three fine particle in the void (size ratio 1:10)

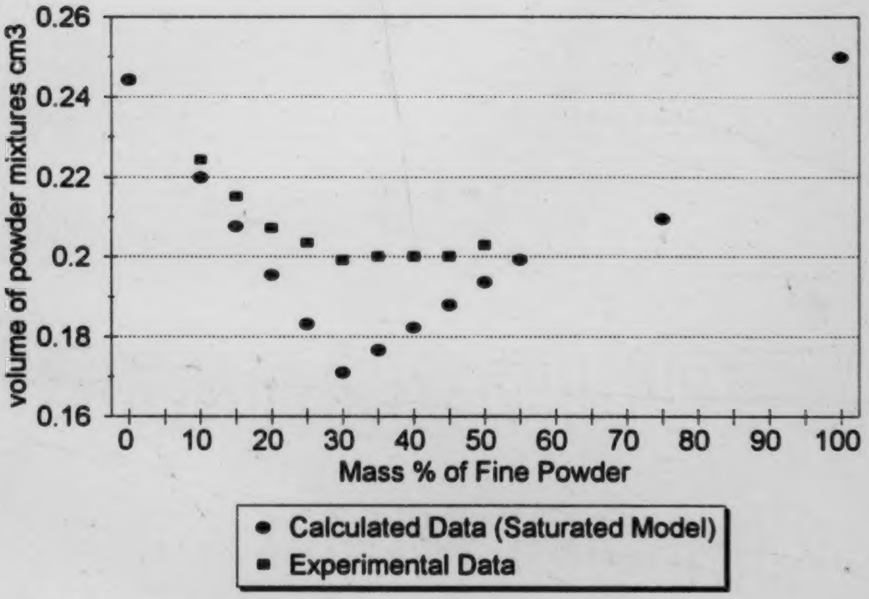

Figure 5-12. Volume versus mass % of fine powder

(total mass of powders is 1 gram)

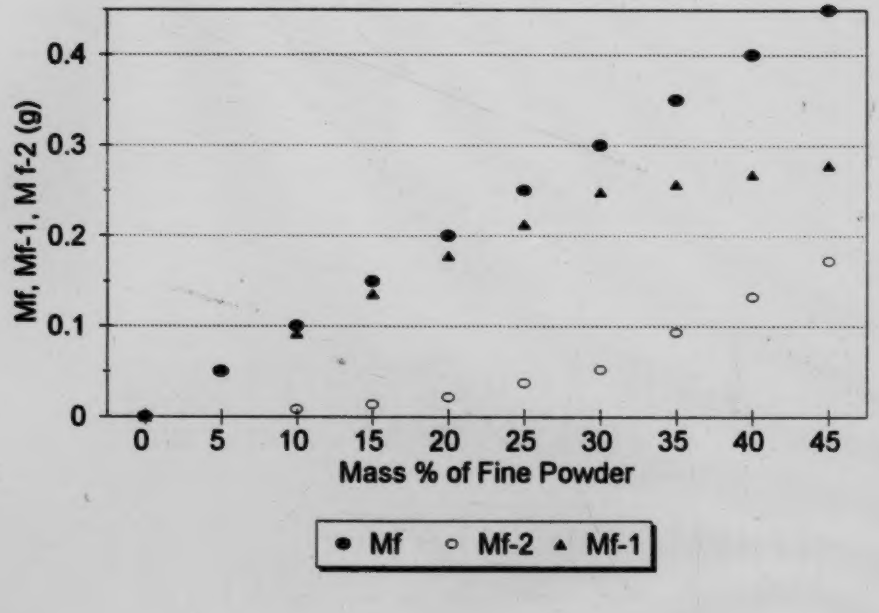

Figure 5-13. M_f , M_{f-1} , M_{f-2} versus mass % of fine powder

(total mass of powders is 1 gram)

CHAPTER 6.

Discussion: The Influence Of Network Structure On The Compaction Of Bimodal Powder Distributions

6.1. Discussion

In Chapter Five, close random packing in bimodal powder distributions was discussed and a new model was developed to calculate the coarse-coarse contact number. This model is expected to be useful if the coarse - fine particle size ratio is in the range 3 to 10. The network structure of the coarse powders in the close random packed bimodal powder distributions can be determined based on the calculation of coarse-coarse contact number. If the coarse-coarse contact number is larger than 4 (mass % of coarse powder > 70), an infinite three dimensional coarse powder network exists in the bimodal powder distribution. Because of the strength of this network, it is believed that its formation has a significant effect on the compaction. Since the powder densification processes all start from particle packing, the influence of network structure on the compaction of close random packed bimodal powder distributions will be discussed based on the concepts in Chapter Five and the experimental results described in Chapter Four.

One of the most important aspects of compaction is described by the equation giving the relationship between green density and the applied external pressure. According to Shapiro, the general compaction equation can be expressed by the following equation [Shapiro, 1994]:

$$\ln(\varepsilon/\varepsilon_0) = A - B\,P_{ext.} \qquad (6\text{-}1)$$

where $P_{ext.}$ is the applied external pressure, ε is the fractional porosity at $P_{ext.}$, ε_0 is the apparent fractional porosity at zero external pressure and equal to (1-fractional apparent density), B is a proportionality constant that reflects the fundamental material deformation behavior and A accounts for rearrangement during compaction [German, 1994; German, 1984].

As discussed in Chapter Four, two sizes (coarse and fine) of 17-4PH stainless steel powder were chosen for the experimental test. Different mass fractions of the coarse and the fine powder were weighed. After mixing in the ball mill, the sample fractional apparent densities ($1-\varepsilon_0$) were measured according to MPIF 04. Equal samples were weighed out and compacted with a single acting die press machine using a pressure of 689.5 MPa ($P_{ext.}$). After pressing, the sample green densities ($1-\varepsilon$) were measured according to MPIF 42.

Using $\Delta\varepsilon/\varepsilon_0$ to represent the compactibility, the present experiment produced the compactibility - mass fraction curve shown as Figure 6-1 , where ε_0 was chosen as relative tap density (ε_0 =1- relative tap density) and $\Delta\varepsilon$ was calculated from relative tap density and relative green density [Chen, *et al.*, 1996]. $\Delta\varepsilon/\varepsilon_0$ and $\varepsilon/\varepsilon_0$ changed with coarse-fine powder mass fraction when the applied external pressure and the pressurization conditions were constant. This meant that ($\varepsilon/\varepsilon_0$) varied with the distribution and hence the constants in Equation (6-1) also varied with powder distribution. The effective pressure was defined as the average load per unit solid cross-section area. The effective pressure on the powder distributions also varied with powder distribution composition at constant applied external pressure because density varied with powder distribution composition.

At the beginning of a compaction, the powder has a density approximately equal to the apparent density. Voids exist between the particles, and with vibration, a higher density can be achieved which is the tap density. After compaction, the green density is achieved. The apparent density, tap density and green density for different powder distributions in these tests are shown in Figure 6-2. It is noted that the peaks are not sharp mainly for three reasons: the coarse to fine size ratio is not infinitely large, there is a broad size distribution in bimodal powder distribution instead of two monosize mixture and the powder's shape is not spherical. The densification starts from apparent density and the first 5 to 10 percent decrease in porosity (increase in density) can be attributed to rearrangement [German, 1994]. The density change by rearrangement is dependent on the powder characteristics. Based on these tests, density changes during vibration (the difference between the apparent density and tap density) are shown in Figure 6-3. The fractional density changes by rearrangement during vibration are

11.5%±2.5 percent increase across the whole range of coarse-fine powder composition. It is reasonable for us to assume that the density change by rearrangement during compaction is closely related to the difference between the apparent and tap density. When the relative tap density (ε_0 = 1- relative tap density) is used in Equation (6-1) instead of apparent density, it can be assumed that A in Equation (6-1) is approximately constant in coarse-fine powder distributions.

Compaction involves both particle repacking (rearrangement) and deformation mechanisms. Rearrangement have been discussed (A in Equation (6-1)) above. Deformation mechanisms (B in Equation (6-1)) are more complicated. There are many factors which influence the deformation of powders distributions. Two important factors influencing the deformation of powder are the internal friction between the powders and the friction between the powder and the die wall. The intrinsic characteristics of a powder affect the pressure-density relations in a compact. They include material properties such as hardness, work (strain) hardening rate, density of powder distributions, surface area, surface state, chemical bonding between particles, chemical composition of powders, oxygen content and crystallographic microstructure of powders [Strijbos, *et al.* 1977; Bocchini, *et al.* 1991; German, 1994 and Oldenburg, 1996]. Equally important are the extrinsic factors associated with powder size, powder shape, the type and amount of lubrication, the mode of compaction, the velocity of the press, and the roughness of the die [Dangerfield, *et al.* 1977; Gethin, *et al.* 1994 and German, 1994]. Some of the factors were constants in these tests. They are chemical composition of the powders, microstructure of the powders, the type and amount of lubrication, the mode of compaction, the velocity of the press, and the roughness of the die. Other factors changed with changes in coarse-fine composition.

The fundamental material properties which influence the deformation of the powder compact are directly related to the properties of pure coarse and pure fine powder. It is reasonable to assume that the influence of the fundamental material properties on the deformation of the powders are proportional to coarse-fine powder composition:

$$f_{mate.} = C^*W_c + D^*W_f \tag{6-2}$$

where f $_{mate.}$ is defined as a materials property factor which is the total effect of fundamental material behavior on deformation, C and D are the constants which represent the material properties of pure coarse powder and pure fine powder respectively, W_c is the mass per cent coarse powder and W_f is the mass per cent fine powder. Basically, the smaller particles are more difficult to press because of larger interparticle friction and particle-wall friction. In Figure 6-1, the compactibility of the 100% pure coarse powder is higher than the compactibility of the 100% fine powder. If the materials property factor (f $_{mate.}$) were the only factor which affected the compactibility of a distribution of coarse-fine powder, the compactibility curve would follow the straight dotted line in Figure 6-1. According to these experimental data (Figure 6-1), the compactibility of powder distributions are below the dotted line. Other factors also affect the deformation of the powder distributions.

The density is thought to be an important factor affecting the fundamental compaction behavior of powder distributions in this situation. Its effect on the solid cross-section area resisting external pressure determines the effective pressure on powder distributions. When Equation (6-1) is applied to the relationship between density and pressure during the compaction of mono-size or narrowly distributed powder, there is a one-to-one relationship between applied pressure and effective pressure. So it is reasonable to use applied external pressure instead of using effective pressure in the compaction of mono-size or narrowly distributed powder. As mentioned above, the effective pressure varies with composition of coarse-fine powder distribution since the solid cross-section area (density) varies with the composition. In order to study the relationship between density and pressure during the compaction of the powder distribution, effective pressure needs to be used in Equation (6-1). For the same external pressure, the effective pressure decreases as the fractional density of powder distribution increases because the solid cross-section area, which supports the load, increases. According to the test results, the tap densities increase to a maximum value around 30% fine + 70% coarse powders and then decrease more slowly with the addition of further fine powders to the powder distributions (Figure 6-2). With the increase of the fine powder composition from 0%, the compactibility would decrease to the lowest value at 30% fine powders then increase with the addition of the fine powders until 100% fine powders. The above argument does not match the test results shown in Figure 6-1, over the range of 30% ~ 55% fine powder, the compactibility continues to decrease. There are two major factors (the solid cross-sectional area and the material factor) that together account for the general shape of the compactibility curve. The compactibility decreases due to increase of the fine powder and the compactibility increases due to decrease of the density when the per cent of fine powder increase from 30% to 55%. Combined the material factor and the density factor effect, the compactibility decreases slightly over the range of 30% ~ 55% fine powder. Considering the effect of density factor and material factor, the calculated compactibility versus coarse-fine composition curve is shown in Figure 6-4 (Calculation procedure is in the appendix). Now the trends are similar between the calculated and experimental curves. The difference between the experimental curve and the calculated curve is that the compactibility data in the calculated curve is lower than those in the experimental curve. This can be explained by the network structure factor.

Because the coarse-fine powder size ratio is larger than 5:1, the packing network structure is believed to be another factor which influences the compactibility or value of $\varepsilon/\varepsilon_0$ by changing the effective solid cross-section area. As discussed in Chapter Five, there are fine powders which are in the voids of coarse powder network. There are not part of the fine particle network and are screened by the coarse powder network and thereby prevented from supporting the pressure, at least initially. During compaction, the density of the powder distributions (discussed under density factor) as well as the amount of fine powder which is in the voids of the coarse powder network and does not support the pressure is changing. The network structure's influence on compaction is limited to the coarse powder network because the fine powder network does not screen coarse powder and does not influence the effective solid cross-section area. The influence of network structure in powder distributions will be discussed and calculated under network structure factor ($f_{stru.}$). Because both density factor ($f_{den.}$) and network structure factor ($f_{stru.}$) influence the solid cross-section area, the factor $f_{den.} * f_{stru.} * P_{ext}$ indicates the effective pressure on powder distribution. The network structure factor would be 1 if there were no network structure influence. Considering the network structure factor, the effective solid cross-section area is smaller than solid cross-section area so the effective pressure and compactibility are higher. This is the reason that the compactibility curve which is calculated without considering the network structure factor ($f_{stru.} = 1$) is lower than the experimental curve.

In summary, the difference between the compaction of mono-sized or narrowly distributed powder and the compaction of coarse-fine powder distributions is that the effective solid cross-section area (which influences the effective pressure) and materials properties vary with coarse-fine composition while these factors are constants in mono-sized powder. So the different compaction behaviors of the powder distributions is caused by different packing density, network structure and different material factors. The density factor ($f_{den.}$), network structure factor ($f_{stru.}$) and material factors ($f_{mate.}$) can be evaluated by modifying Equation (6-1). The "constant" B in Equation (6-1) is replaced by $f_{mate.}\, f_{den.}\, f_{stru.}$:

$$\ln(\varepsilon/\varepsilon_0) = A - f_{mate.} f_{den.} f_{stru.} P_{ext.} \qquad (6\text{-}3)$$

where $f_{den.}\, f_{stru.}\, P_{ext.}$ is the effective pressure on powder distribution.

In the Appendix 6-A, the factors $f_{mate.}$, $f_{den.}$ and $f_{stru.}$are calculated. Based on the experimental data, the following equation is obtained (Appendix 6-A):

$$\ln(\varepsilon/\varepsilon_0)=1.815045-f_{stru.}[3.66031*W_c+3.211357*W_f)]/(1/F_{tap}+1/F_{green}) \qquad (6\text{-}4)$$

Equation (6-4) indicates the relationship between the compactibility in powder distributions and $f_{stru.}$ as the distribution is varied. Substituting all the known parameters

W_c, W_f, F_{tap}, F_{green}, ε, and ε_0 into Equation (6-4) at different composition points, the structure factor $f_{stru.}$ at different points were calculated and are shown in Figure 6-5. The higher value of the $f_{stru.}$ means that the value of $\ln(\varepsilon/\varepsilon_0)$ is smaller so the bimodal powder distribution is compressed more easily. In this case, more fine powders in the voids of coarse powder network are screened by coarse powders and prevented from supporting the pressure. Figure 6-5 suggests that there is indeed a fraction of the fine powder which does not support the pressure in the region of $0\% < X < 30\%$ (i.e. wt % of fine powder < 30%). At the point of 70% coarse + 30% fine powder, the value of the $f_{stru.}$ decreases sharply. This indicates that the network structure of powder distribution changes at this point with the gradual disappearance of the coarse network. In the region from 30% to 45% of fine powder, the values of the $f_{stru.}$ are very low. But there still is a small amount of fine powder which does not support the pressure because there is still the remnants of the infinite coarse network which can screen some fine powders from supporting the pressure. Around the point of 50% fine + 50% coarse powders, the value of the $f_{stru.}$ drops to 1. This represents the disappearance of the infinite coarse network. The above results approximately agree with the percolation theory as developed in Chapter 5 and the results of the coordination number calculation in which the microstructure of powder distribution is divided into three regions in the same way: $0\% < X < 30\%$ (pure infinite coarse powder network), $30\% < X < 45\%$ (coexistence of infinite fine and infinite coarse powder network) and $45\% < X < 100\%$ (pure infinite fine powder network).

Based on percolation theory, the finite network starts to form when the contact number is two and the complete connectivity of an infinite network occurs when the contact number is four. When the coarse -fine powder distribution composition is at the point of 30% fine + 70% coarse, the coarse-coarse contact number is four (calculated in Chapter five). According to Figure 6-5, at the same point of 30% fine + 70% coarse powder, the value of the $f_{stru.}$ decreases sharply. The network structure factor influences the effective pressure obviously when the percent mass of coarse powder is larger than 70% (coarse-coarse contact number is larger than 4). When there is only one contact, particle can move freely around the contact point without restriction. There is restriction along a line if there are two contacts and there is restriction in a plane if there are three contacts. A particle becomes restricted in three dimension only if there are four or more contacts. From Figure 6-5, it is noted that there are clear divisions among the three coarse-fine composition regions that are indicated by the different value levels of $f_{stru.}$. This result reflects the fact that the network structure in bimodal powder distributions changes with changes of the coarse-fine composition. This indicates that when a particle becomes restricted in three dimension it must deform on compaction. It can be found from Figure 6-5 that the values of $f_{stru.}$ remain very low for all the coarse-fine compositions (< 1.05). It indicates that the materials properties and density factor are the major influences in the compaction of powder distributions and the network structure factor is used to modify the solid cross-section area in order to more accurately describe the relationship between the green density and the applied external pressure.

Based on Artz's model [Artz, 1982] and the contact number in bimodal powder distribution (random packing) calculated using the modified saturated model (Chapter Five), the contact numbers of powder distribution after compaction were calculated. The calculated results are shown in Figure 6-6 (Coarse-Coarse Contact Number versus Mass % of Fine Powder), Figure 6-7 (Fine-Fine Contact Number versus Mass % of Fine Powder), Figure 6-8 (Coarse-Fine Contact Number versus Mass % of Fine Powder), Figure 6-9 (Fine-Coarse Contact Number versus Mass % of Fine Powder), and Figure 6-10 (Average coordination Number versus Mass % of Fine Powder).

In order to compare the changes of network microstructure during compaction, the coordination number N_{cc} before compaction is also shown in Figure 6-6. Comparing the change of coordination number N_{cc} during compaction, it is found that after compaction the N_{cc} increases but the threshold of change of network does not change very much. The X_f is around 30% fine powder and X_c is around 45% fine powder. The above results could be used as a starting point for any future sintering discussion.

Even though the pore structure is the more important factor in powder sintering especially in intermediate and final stage of sintering, the particle-particle contact number is believed to determine the densification rate in the initial stage of sintering. In powder distributions, there are three different powder contacts, coarse-coarse particle contact, coarse-fine (fine-coarse) particle contact and fine-fine particle contact. The contribution to the densification rate of the powder compact is different for each type of contact. The reason for this is that the geometry configurations of different type of contacts are different. According to these experimental results (Figure 4-14 in Chapter Four), specific volume change of bimodal distributions stays approximately constant when the fine powder mass fraction changes from 0% to 30%. On the other hand, at mass fractions rich in fine particles, the specific volume change decreases as coarse particles are added. The shrinkage during sintering increases with an increasing amount of fine powder. The possible influence of the coarse powder network structure on sintering is a topic left for future work.

6.2. References

Arzt, E., "The Influence of an Increasing Particle Coordination on the Densification of Spherical Powders," Acta Metall. Vol. 30, pp. 1883-1890, 1982.

Bocchini, G.F. , "Powder and Mix Properties, Tooling and Innovative Presses, Suitable to Avoid Cracks," Advances in Powder Metallurgy - 1991, Compiled by L.F. Pease III and R.J. Sansoucy, Metal Powder Industries Federation, Princeton, New Jersey, Vol. 1, pp. 59-88, 1991.

Chen, X.L., **Eadie**, R.L., **Ghosh**, D.S. and **Roemer**, G., "Improving P/M Parts Made with Conventional Processing by Bimodal Powder Mixtures," Advances in Powder Metallurgy & Particulate Materials - 1996, Compiled by T.M. Cadle and K.S. Narasimhan, Metal Powder Industries Federation, Princeton, New Jersey, Vol. 1, pp. 3-3 -- 3-26, 1996.

Dangerfield, C.J. and **Coleman**, D.S. , "Friction Studies in the Compaction and Ejection of Metal Powders -- Lubricant Systems," Journal of Powder & Bulk Solid Technology, Vol. 1, No. 1, pp. 36-41, 1977.

German, R.M., Powder Metallurgy Science, Metal Powder Industries Federation, Princeton, NJ, 1984.

German, R.M., Powder Metallurgy Science, Metal Powder Industries Federation, Princeton, NJ, pp. 220-221, 1994.

Gethin, D.T., **Tran,** V.T. , **Lewis,** R.W. **and Ariffin,** A.K. , International Journal of Powder Metallurgy, Vol.30, No.4, pp.385-398, 1994.

Oldenburg, M. , "A Friction Model for Iron Powder Pressing Based on a Tribological Approach," Advances in Powder Metallurgy & Particulate Materials - 1996, Compiled by **T.M. Cadle** and **K.S. Narasimhan,** Metal Powder Industries Federation, Princeton, New Jersey, Vol. 2, pp. 7-329 -- 7-340, 1996.

Shapiro, I., "Compaction of Powders XI. Application of the General Equation to Both Metal Powders and Ceramic Powders", Advances in Powder Metallurgy & Particulate Materials - 1994, Compiled by C. Lall and A.J. Neupaver, Metal Powder Industries Federation, New Jersey, Vol. 3, pp. 41-56, 1994.

Strijbos, M., "Friction Between a Powder Compact and a Metal Wall", Journal of Powder & Bulk Solid Technology, Vol. 1, No. 1, pp. 83-88, 1977.

Suzuki, M. and **Oshima,** T., "Coordination Number of a Multiple Component Randomly Packed Bed of Spheres with Size Distribution," Powder Technology, Vol. 44, pp. 213-218, 1985.

6.3. Appendix

The general compaction equation can be expressed by the following equation [Shapiro, 1994]:

$$\ln(\varepsilon/\varepsilon_0) = A - B\,P_{ext.} \qquad \text{[A-1]}$$

The difference between the compaction of mono-sized or narrowly distributed powder and the compaction of coarse-fine powder distributions is that the effective solid cross-section area (which influences the effective pressure) and materials properties vary with coarse-fine composition while these factors are constants in mono-sized powder. Because of this and based on the discussion in this chapter, Equation [A-1] is modified to:

$$\ln(\varepsilon/\varepsilon_0) = A - f_{mate.}\,f_{den.}\,f_{stru.}\,P_{ext.} \qquad \text{[A-2]}$$

The fundamental material properties which influence the deformation of the powder compact are directly related to properties of pure coarse and pure fine powder :

$$f_{mate.} = C{*}W_c + D{*}W_f \qquad \text{[A-3]}$$

The density factor reflects the solid cross-section resisting external pressure and is inversely proportional to the solid cross-section since the higher the solid cross-section, the lower the effective pressure:

$$f_{den.} \propto 1/A_{eff} \qquad \text{[A-4]}$$

Where A_{eff} is the solid cross-section area (without the network structure effect which will be explained later) for supporting the pressure.

In definition [A-4], A_{eff} is proportional to the relative density $F_{rel.}$ so the equation can be rewritten as:

$$f_{den.} = E / F_{rel.} \qquad [A\text{-}5]$$

where E is a constant. Since the $F_{rel.}$ is changing during compaction, it is chosen as the average value:

$$f_{den.} = 1/2*(E / F_{tap} + E/F_{green}) \qquad [A\text{-}6]$$

where F_{tap} is the tap density (relative density) and F_{green} is the green density (relative density).

Combining Equations [A-2]; [A-3] and [A-6], Equation [A-7] is obtained :

$$ln(\varepsilon/\varepsilon_0)=A-f_{stru.}(G*W_c+ H*W_f)/ (1/F_{tap} +1/F_{green}) \qquad [A\text{-}7]$$

where A , G (= $0.5ECP_{ext.}$) and J (=$0.5EDP_{ext.}$) are constants.

In Equation [A-7], the network structure factor can be discussed in terms of percolation theory. Based on percolation theory, there are three possible different network structures in coarse-fine powder distributions (pure coarse powder infinite network, coexistence of coarse and fine powder infinite networks, pure fine powder infinite network) depending on the composition of the distributions. The network structure and compaction behavior change around the percolation thresholds. The value of the network structure factor is related to the composition of the distributions and changes obviously around the percolation points. In the compaction of coarse-fine powder distributions, the major concern is a coarse powder network because the coarse powder network can screen fine powders from supporting the load, but the fine powder network can not screen coarse powders.

At the point 25% coarse + 75% fine powder distribution, the numbers of coarse-coarse contact both in close random packed and compacted conditions are lower than 1, so there is not an infinite coarse particle network in the powder distributions according to Chapter Five. SEM examination of a compacted 25% coarse + 75% fine powder distribution sample also shows that the individual coarse particles are randomly distributed in an infinite fine particle network. Even though there is infinite fine powder network, the fine powder is not screened by coarse powders and prevented from supporting the pressure. So, the structure factor ($f_{stru.}$) is 1 at point of 25% coarse + 75% fine powder distribution , as well as at 100% coarse powder and 100% fine powder. That the structure factor is equal to 1 means that all the solid cross-section support the pressure and there is a not screen effect. The experimental test data F_{tap}, F_{green} ($\varepsilon = 1 - F_{green}$ and $\varepsilon_0 = 1 - F_{tap}$) at the above three points and $f_{stru.} = 1$ are substituted into Equation [A-7]:

$$-0.92676 = A - 0.749064G \qquad [A-8]$$

$$-0.61722 = A - 0.731817(0.25G+0.75H) \qquad [A-9]$$

$$-0.70799 = A - 0.785656H \qquad [A-10]$$

The above equation set is solved and the results of the coefficients are listed below:

$A = 1.815045$, $G = 3.66031$, $H = 3.211357$

So, Equation [A-7] can be written as:

$$ln(\varepsilon/\varepsilon_0)=1.815045-f_{stru.}[3.66031*W_c+3.211357*W_f)]/(1/F_{tap}+1/F_{green}) \qquad [A-11]$$

Equation [A-11] describes the relationship between the compactibility and the coarse-fine composition in these bimodal powder distribution compaction tests.

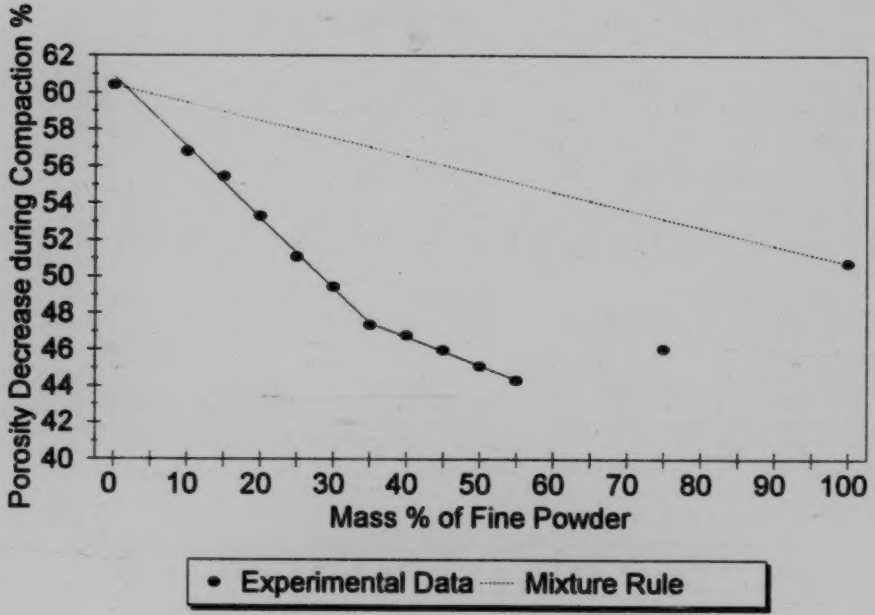

Figure 6-1. Compactibility versus mass % of Fine Powder

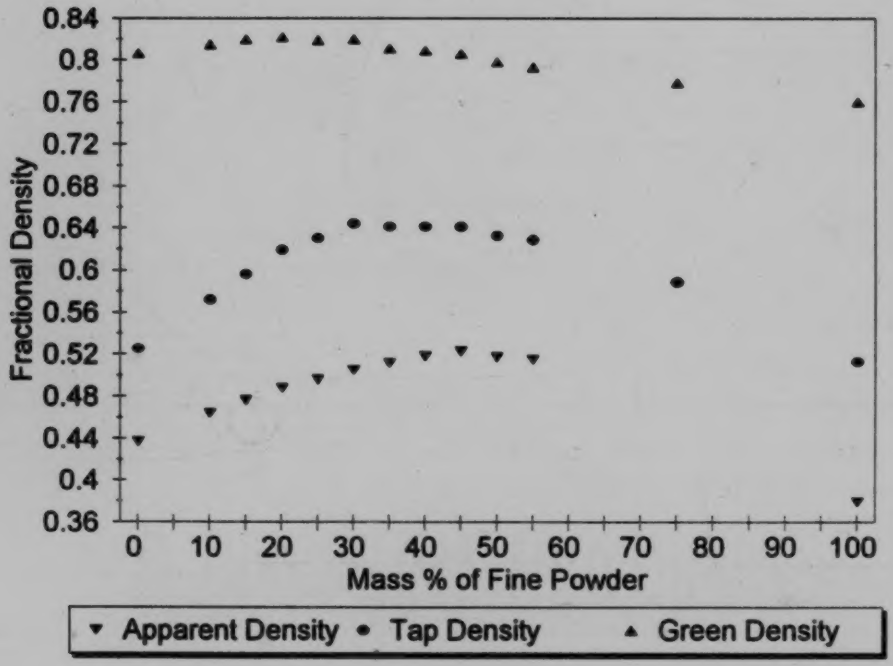

Figure 6-2. Apparent, Tap and Green Densities versus mass % of fine Powder

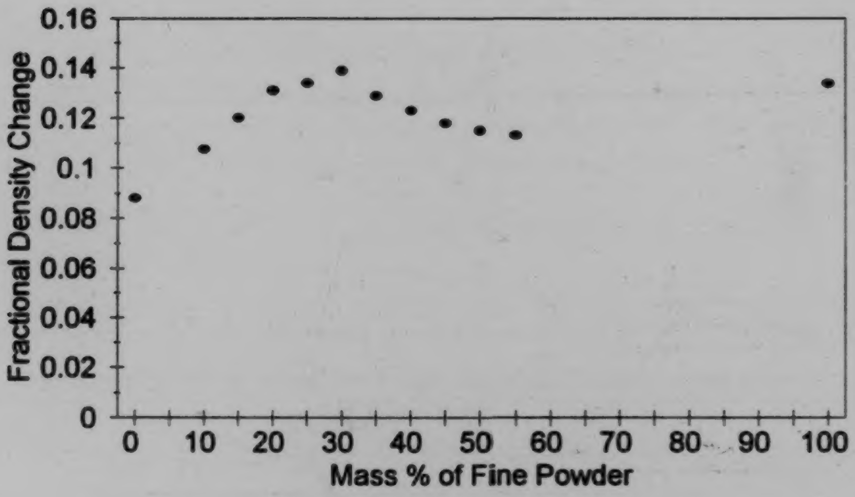

Figure 6-3. Density Change by Rearrangement versus mass % of Fine Powder

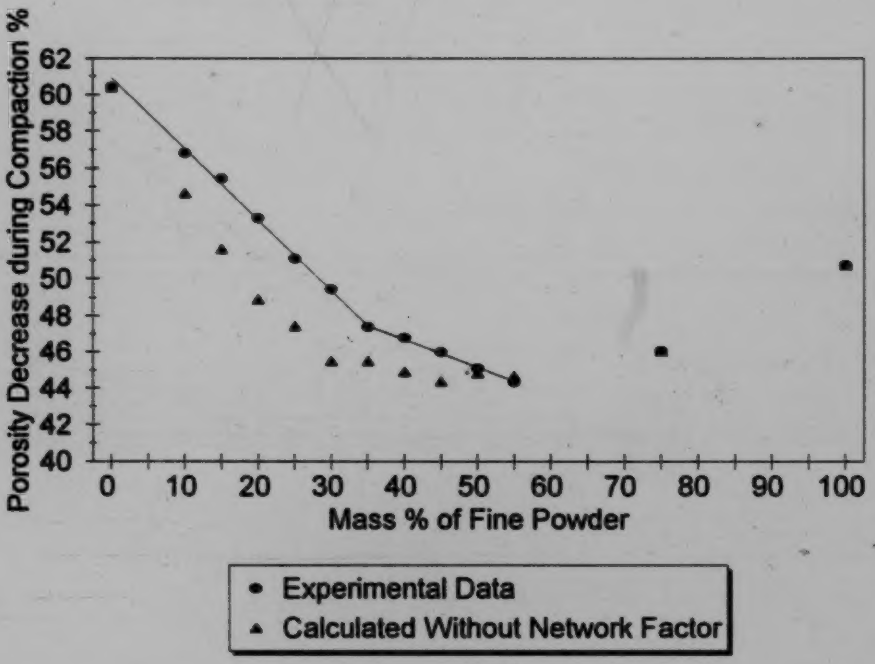

Figure 6-4. Compactibility versus mass % of Fine Powder

(Calculation Without Structure Factor)

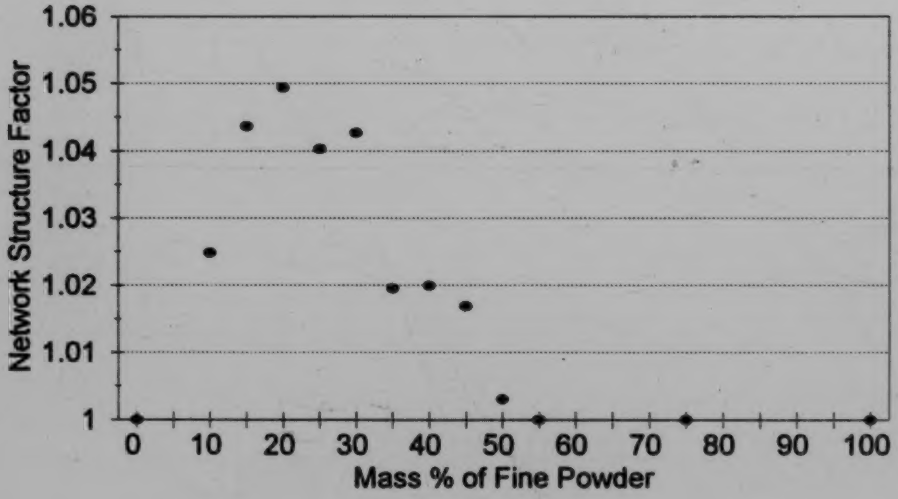

Figure 6-5. Network Structure Factor (Structure Influence in Compaction)

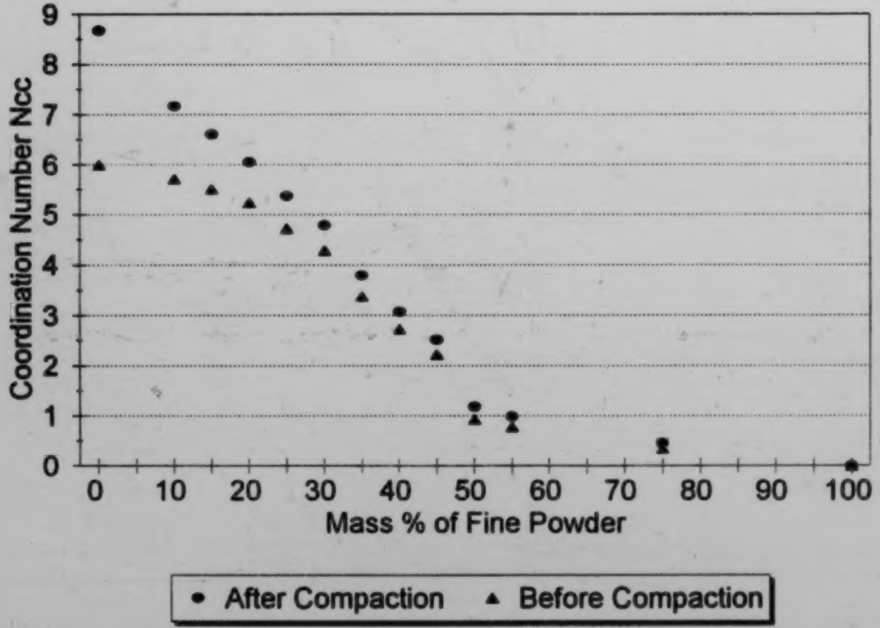

Figure 6-6. N_{cc} versus mass % of Fine Powder (Before and After Compaction)

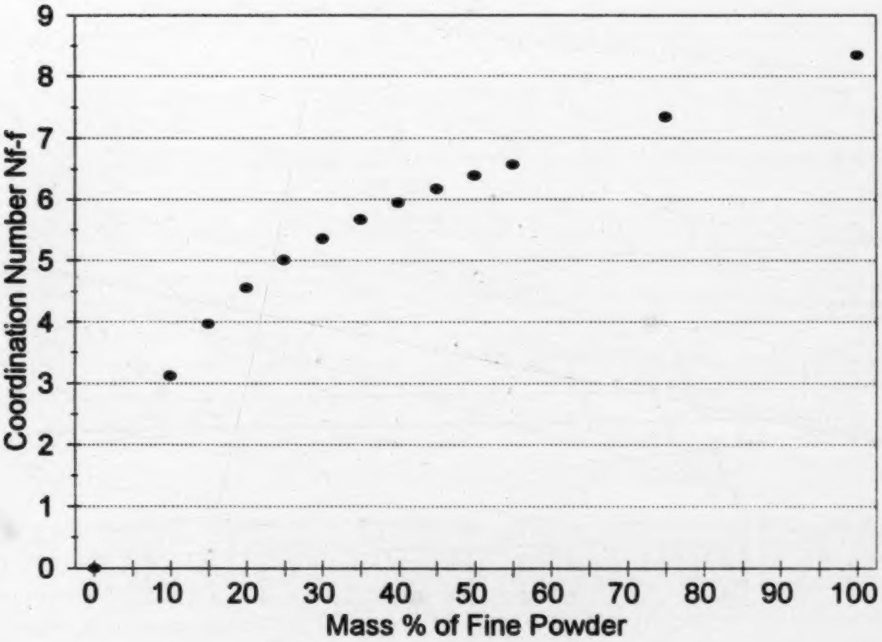

Figure 6-7. N_{ff} versus mass % of Fine Powder (After Compaction)

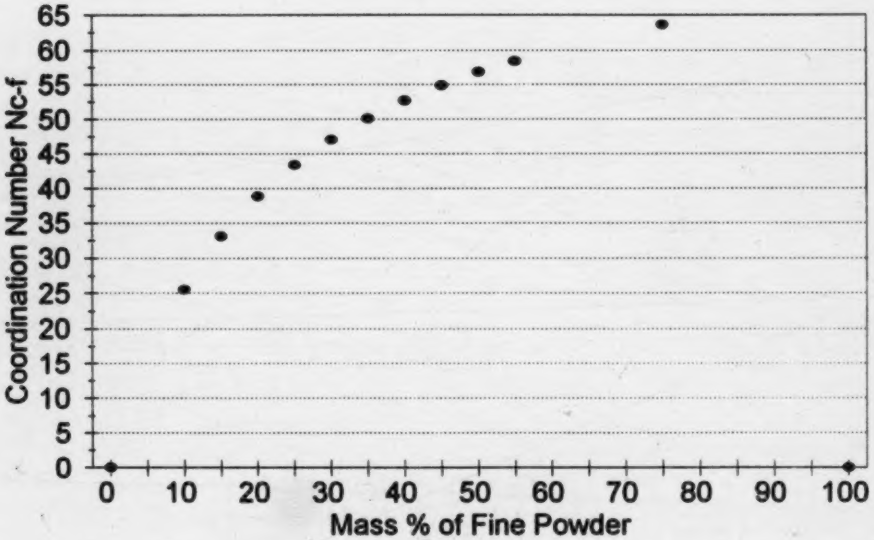

Figure 6-8. N_{cf} versus mass % of Fine Powder (After Compaction)

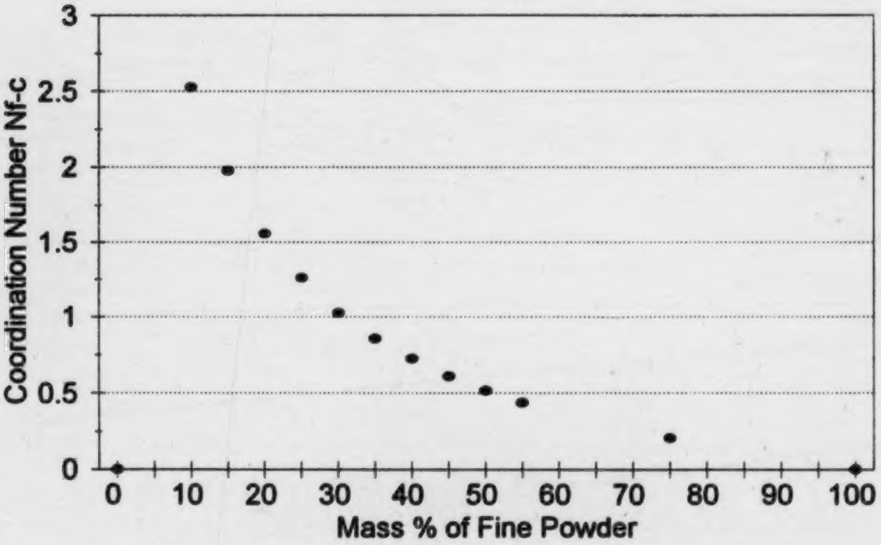

Figure 6-9. N_{fc} versus mass % of Fine Powder (After Compaction)

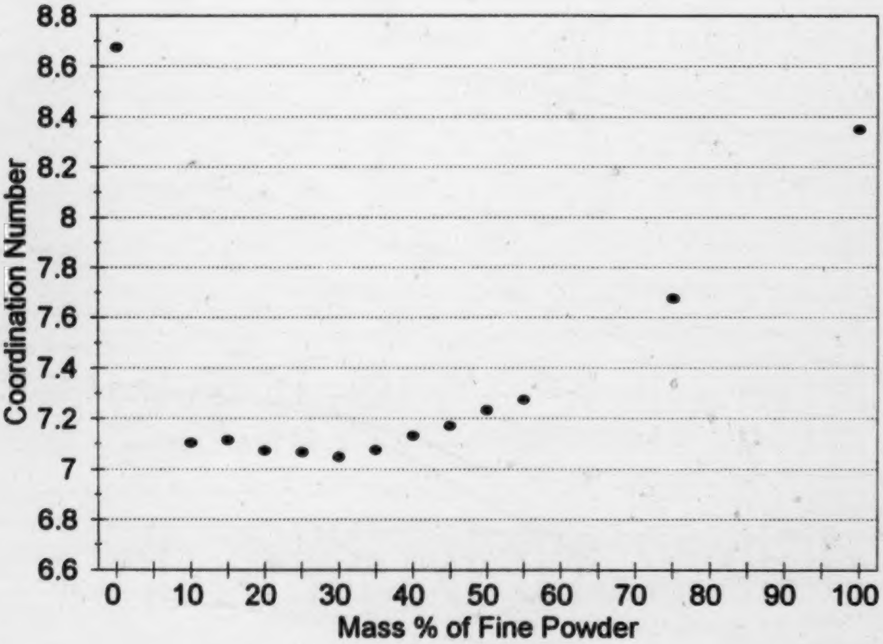

Figure 6-10. Coordination Number N versus mass % of Fine Powder (After Compaction)

CHAPTER 7.

Summary And Conclusions

7.1. Experimental Results

Very high sintered densities (97.7% relative density) and excellent mechanical properties (comparable to wrought products) were achieved by using the conventional P/M processes of single compaction and single sintering. The powders were the bimodal distributions of two size ranges of precipitation hardening stainless steel powders. Both coarse and fine powders had log-normal size distributions. The medians of the two sizes were in the ratio of about 5:1. A 2% increase of final density was achieved by adding only 25% fine powders and the final density of the bimodal powders reached the same value as 100% fine powders. This offers an effective way to get high performance P/M products. Using bimodal powders has practical significance in reducing cost and achieving better dimensional control (lower shrinkage) with a high final density.

As first shown by Furnas [Furnas, 1931], bimodal powder distributions improve the packing density because the fine powder will fill in the voids between the coarse powders. The technique has been applied to ceramics and refractoriness. However, it is not often used in traditional metal powder compaction and sintering. From these experimental tests, it was found that by using bimodal powder distributions, the final density could be improved in cases of high sintering temperatures and long sintering times if the ratio of the medians of the two sizes is larger than 5:1 and the fine powder accounts for about 25% of the total weight.

7.2. Theoretical Models

7.2.1. Packing Models

The factor which has proven to be very significant to the behaviour of the packing of two components is the question of whether the components are interconnected with one another or not. If the particles are interconnected, they form a network. When a network is formed then the component is said to percolate the structure [Stauffer, 1985]. Previous bimodal particle models treated coarse and fine particle in the distribution packing as the same and did not consider networks of large particles. The percolation concept was used in order to get a better understanding of the packing of bimodal particle packing. According to the saturated model of German [German, 1989], when coarse powders form an infinite coarse powder network, the pores between the coarse powders can be filled with fine particles to the extent of the tap density of the fine powder before the coarse powder is affected. The fine powders which are in the voids of the coarse powder do not influence the packing of the coarse powders. This concept was used to modify existing bimodal powder packing models.

A new model (modified saturated model) for coordination number in bimodal packing was developed and presented based on the percolation points. It is concluded that the structures that arise in the bimodal distributions lie somewhere between the random structure proposed by Suzuki and Oshima [Suzuki and Oshima, 1985] and the ideal saturated structure proposed by German [German, 1989]. Examining the Suzuki and Oshima model which is a random model and comparing it to the experimental observations, it was found that Suzuki and Oshima's model underestimated the coarse-coarse contact number N_{c-c}. From the calculation based on the ideal saturated model, the coarse infinite network started to lose complete connectivity at around X = 35% and disappeared at X= 45%. It was assumed in the ideal saturated model that all the fine powder were in the voids of the coarse powder if there is enough void space. This would violate entropy considerations. Since the ideal saturated microstructure was used in this model, the coarse-coarse contact numbers were overestimated. The packing structure can not be perfect so the saturated model was modified. According to the modified saturated model, the coarse infinite network started to lose complete connectivity at around X = 30% and disappeared at X= 45%. The results of the modified saturated model were more reasonable than Suzuki and Oshima's model in the case of high powder size ratio ($D_c/D_f > 3$) and gave better agreement with experimental observations and predicted the percolation thresholds. From the experimental results it can be concluded that reality lies between the ideal saturated structure and the random structure - "a modified saturated structure" or "a modified random structure".

The proposed model is useful if the coarse - fine particle size ratio is in the range 3 to 10.

The microstructure (network) of the close random packed bimodal powder distributions could be determined based on the calculation of coarse-coarse contact number. If the coarse-coarse contact number is larger than 4, an infinite rigid coarse powder network exists in the bimodal powder distribution. Since the powder densification processes all start from particle packing, the influence of microstructure on the compaction and sintering of close random packed bimodal powder distributions can be discussed based on this model. The random packing and the important role of the fine particles, which fill in the voids of the infinite coarse particle network, are emphasized. It describes the real packing situation in powder metallurgy processing. Using coordination number and percolation it has been shown that a bridge can be established between packing density, microstructure and leading eventually to processing behaviour and macroscopic properties.

7.2.2. Compaction Models

One of the most important aspects of compaction is described by the equation giving the relationship between the compactibility and the applied external pressure. According to Shapiro, there is a linear relationship between the compactibility and external pressure in monosized or narrowly distributed powder compaction [Shapiro, 1994]. In the compaction of powder distributions, the constants in Shapiro's model change over the range of distributions, which suggests fundamental changes in compaction behaviour. The modifications are proposed based on percolation concepts to explain this behavior. The difference between the compaction of mono-sized or narrowly distributed powder and the compaction of coarse-fine powder distributions is that the effective solid cross-section area (which influences the effective pressure) and materials properties vary with coarse-fine composition while these factors are constants in certain mono-sized powders. Combining the material factor and the density factor, the general shape of the calculated compactibility versus coarse-fine composition curve is similar to the experimental curve.

In order to improve the model, the fundamental factors which influence the packing behaviour in powder distributions and some ideas about networks which are embodied in the percolation concept were considered. Because the coarse-fine powder size ratio is larger than 5:1, the packing network structure would be another factor which influences the compactibility by changing the "effective" solid cross-section area. There are fine powders which are in the voids of coarse powder network. There are not part of the fine particle network and are screened by the coarse powder network; thereby they are prevented from supporting the pressure, at least initially. During compaction, the density of the powder distributions (discussed under density factor) as well as the amount of fine powder which is in the voids of the coarse powder network and does not support the pressure is changing. The network structure's influence on compaction is limited to the coarse powder network because the fine powder network does not screen coarse powder and does not influence the effective solid cross-section area. The influence of network structure in powder distributions is accounted for with the network structure factor ($f_{stru.}$). Because both density factor ($f_{den.}$) and network structure factor ($f_{stru.}$) influence the solid cross-section area, the product $f_{den.} * f_{stru.} * P_{ext.}$ describes the effective pressure on powder distributions. The network structure factor has been used to modify the solid cross-section area to more accurately depict the relationship between the compactibility and the applied external pressure.

According to this modified compaction model, the network factors were evaluated and it was found that there are clear divisions among the three coarse-fine composition regions that are indicated by different values of $f_{stru.}$. This result reflects the fact that the microstructure in bimodal powder distributions changes with changes of the coarse-fine composition. It supports the idea that there is a fraction of the fine powder which does not support the pressure in the region of 0%< X < 30% (i.e. wt % of fine powder < 30%). At the point of 70% coarse + 30% fine powder, the value of the $f_{stru.}$ decreases sharply. This indicates that the network structure of powder distribution changes at this point with the gradual disappearance of the coarse network. In the region of wt % of fine powder from 30% to 45%, the values of the $f_{stru.}$ are very low since there is an infinite fine powder network which supports the pressure. But there still is a small amount of fine powder which does not support the pressure because there is still an infinite coarse network which can screen some fine powders from supporting the pressure. Around the point of 50% fine + 50% coarse powders, the value of the $f_{stru.}$ drops to 1. This represents the disappearance of the infinite coarse network. The above results agree with the percolation theory and the results of the coordination calculation in which the microstructure of powder distribution is divided into three regions in the same way: 0% < X < 30% (pure infinite coarse powder network), 30% < X < 45% (coexistence of infinite fine and infinite coarse powder network) and 45 % < X < 100% (pure infinite fine powder network).

7.2.3. Sintering Models

It is the surface curvature that provides the driving force for sintering. Grain boundary diffusion, surface diffusion and lattice diffusion from the grain boundary are the mechanisms that usually contribute to sintering - with the lattice diffusion dominating at the highest temperatures and largest neck sizes. The sintering of powder size distributions is more complicated since the geometry of the distribution is more complicated than that of the monosized or narrowly distributed powders. To be able to properly account for the geometry, the surface curvature factor in the sintering model needed to be in a more accurate form. In the present experimental test situation -- high deformation before sintering (high pressure and metal powders), high sintering temperature and near-full density, lattice diffusion is the major focus.

A new method has been presented to determine the lattice diffusion contribution in sintering. The two-sphere model for monosized powder to determine the lattice diffusion contribution in sintering is considered. Based on Eadie and Weatherly's model [Eadie and Weatherly, 1975], two new solutions have been developed and presented, an upper limit solution with surface curvature at a maximum all along the neck and a more accurate solution in which the form of the surface curvature at the neck can be varied as appropriate. This analysis differs from previous ones in that the surface curvature is treated in a more quantitative way. The model also establishes with more rigour the approximations used previously for the construction of sintering diagrams. When interaction between the lattice diffusion and grain boundary diffusion is considered, the solution is called the coupled solution. The coupled solution is more accurate than the uncoupled solution but it can not tell the relative contribution of the lattice diffusion and grain boundary diffusion. It is clear that in the region where lattice diffusion is most significant i.e. $x/a > 0.3$ and homologous

T > 0.8 the uncoupled solution is quite close to the coupled solution (within 10%). This suggests that the new equations can be confidently used in the construction of sintering maps.

7.3. Future Work

The packing and the compaction of bimodal powder distributions were studied in some detail in this work. Some experimental tests on bimodal powder distribution sintering have been done. The future work should be focused on theoretical studies of bimodal powder distribution sintering. The newly developed two-sphere monosized powder sintering model which treats the curvature in a more accurate way needs to be extended to powder distributions. In order to study the sintering of the powder distribution, more experimental tests need to be conducted. Among the necessary tests, shrinkage rate during the sintering is one of the most important. More attention needs to be focused on the fine-fine network in bimodal powder distribution packing in future work. The coarse-coarse network in the packing and the compaction of bimodal powder distribution were studied because of the important screening influence of the coarse-coarse network on the compaction of powder distributions. In sintering of powder distributions, the influence of the fine-fine powder network should be more important since the surface curvatures are higher. The coarse network likely is also important because of its strength to resist sintering forces.

7.4. References

Eadie, R.L. and **Weatherly**, G.C., "Solutions for the Shrinkage Rate in the Intermediate Stage of Sintering," Scripta Metallurgica et Materialia, 1975, Vol.9, p 285.

Furnas, C.C., "Grading Aggregates I - Mathematical Relations for Beds of Broken Solids", Ind. Eng. Chem., Vol. 23, pp. 1052-1058, 1931.

German, R.M., "Particle Packing Characteristics," Metal Powder Industries Federation, Princeton, New Jersey, 1989.

Shapiro, I., "Compaction of Powders XI. Application of the General Equation to Both Metal Powders and Ceramic Powders", Advances in Powder Metallurgy & Particulate Materials - 1994, Compiled by C. Lall and A.J. Neupaver, Metal Powder Industries Federation, New Jersey, Vol. 3, 1994, pp. 41-56.

Stauffer, D., "Introduction to Percolation Theory", Taylor and Francis, London, 1985.

Suzuki, M. and **Oshima**, T., "Coordination Number of a Multiple Component Randomly Packed Bed of Spheres with Size Distribution," Powder Technology, Vol. 44, pp. 213-218, 1985.